

# Design and simulation of a vertical dynamics control system within an advanced simulation environment

---

**Berljavac, Paolo**

**Master's thesis / Diplomski rad**

**2021**

*Degree Grantor / Ustanova koja je dodijelila akademski / stručni stupanj:* **University of Zagreb, Faculty of Mechanical Engineering and Naval Architecture / Sveučilište u Zagrebu, Fakultet strojarstva i brodogradnje**

*Permanent link / Trajna poveznica:* <https://urn.nsk.hr/urn:nbn:hr:235:078784>

*Rights / Prava:* [In copyright / Zaštićeno autorskim pravom.](#)

*Download date / Datum preuzimanja:* **2024-05-10**

*Repository / Repozitorij:*

[Repository of Faculty of Mechanical Engineering and Naval Architecture University of Zagreb](#)



UNIVERSITY OF ZAGREB  
FACULTY OF MECHANICAL ENGINEERING AND NAVAL  
ARCHITECTURE

# **MASTER'S THESIS**

**Paolo Berljavac**

Zagreb, 2021.

UNIVERSITY OF ZAGREB  
FACULTY OF MECHANICAL ENGINEERING AND NAVAL  
ARCHITECTURE

**DESIGN AND SIMULATION OF A  
VERTICAL DYNAMICS  
CONTROL SYSTEM WITHIN AN  
ADVANCED SIMULATION  
ENVIRONMENT**

Mentor:  
Prof. dr. sc. Joško Deur, dipl. ing.

Student:  
Paolo Berljavac

Zagreb, 2021.

## **IZJAVA**

Izjavljujem da sam ovaj rad izradio samostalno koristeći stečena znanja tijekom studija i navedenu literaturu.

Paolo Berljavac

## **STATEMENT**

I declare that I have done this study using knowledge and skills gained during my University studies and using specified scientific literature.

Paolo Berljavac

## **ZAHVALA**

Ovim se putem zahvaljujem prof. dr. sc. Jošku Deuru i mag. ing. mech. Ivanu Cvoku na kontinuiranom usmjeravanju, uloženom vremenu i savjetima koji su omogućili uspješnu izradu diplomskog rada.

Veliko hvala mr. sc. Nikoli Naranči zbog podrške i dane mogućnosti za izradu diplomskog rada u suradnji s tvrtkom AVL-AST d.o.o. te hvala kolegama iz ureda za podršku pri izradi rada. Zahvaljujem se Dipl.-Ing. Mariu Teitzeru i Dipl.-Ing. Stefanu Kellneru iz tvrtke AVL List GmbH za stručne rasprave dane savjete tokom izrade rada.

Od srca sam zahvalan svojim roditeljima, sestri te prijateljima za pruženu podršku tokom studija.

Paolo Berljavac

## **ACKNOWLEDGMENTS**

I would like to thank prof. dr. sc. Joško Deur and mag. ing. mech. Ivan Cvok for the continuous guidance, invested time and suggestions which allowed for a successful master thesis.

A big thank you to mr. sc. Nikola Naranča for the support he provided and the opportunity to write my thesis in collaboration with AVL-AST d.o.o. and thank you to my office colleagues for the given support. Thank you to Dipl.-Ing. Mario Teitzer and Dipl.-Ing. Stefan Kellner from AVL List GmbH for the technical discussions and given suggestions throughout the thesis study.

I am most sincerely thankful to my parents, sister and friends for supporting me throughout my faculty studies.

Paolo Berljavac



SVEUČILIŠTE U ZAGREBU  
FAKULTET STROJARSTVA I BRODOGRADNJE



Središnje povjerenstvo za završne i diplomske ispite  
Povjerenstvo za diplomske ispite studija strojarstva za smjerove:

Procesno-energetski, konstrukcijski, inženjersko modeliranje i računalne simulacije i brodstrojarski

|  |        |
|--|--------|
| Sveučilište u Zagrebu<br>Fakultet strojarstva i brodogradnje |        |
| Datum  | Prilog |
| Klasa: 602 - 04 / 21 - 6 / 1                                 |        |
| Ur.broj: 15 - 1703 - 21 -                                    |        |

## DIPLOMSKI ZADATAK

Student: **Paolo Berljavac**

JMBAG: 0035203668

Naslov rada na hrvatskom jeziku: **Sinteza i simulacija sustava upravljanja vertikalnom dinamikom vozila u naprednom simulacijskom okruženju**

Naslov rada na engleskom jeziku: **Design and simulation of a vertical dynamics control system within an advanced simulation environment**

Opis zadatka:

Semi-active and active vehicle suspensions greatly improve ride comfort and handling performance of a passenger vehicle compared to the passive suspensions. Besides control system design, the level of performance improvement is affected by hardware design and available sensor measurements. As the market prices of semi-active and active suspension actuators, sensors and control units decrease, the implementation feasibility potential increases. The focus of the thesis is on the development of a practical control law for active and semi-active suspension system, including implementation and verification of the control system within advanced simulation environment AVL VSM. To this end, the main tasks of the thesis are as follows:

1. Develop a control-oriented vertical vehicle dynamics model in AVL VSM environment.
2. Implement an optimal control system for active and semi-active suspensions based on Linear Quadratic Regulator (LQR) for MATLAB/Simulink-AVL VSM co-simulation.
3. Design a practical feedback control law for semi-active and active suspension, which relies on available vertical dynamics sensor suite.
4. Optimize the performance of practical feedback control law using the control-oriented vertical vehicle dynamics model.
5. Analyse the ride comfort and vehicle handling performance of the implemented control system based on characteristic vertical and lateral vehicle dynamics test procedures simulated within AVL VSM.

The literature used should be revealed through the list of references and any eventually received assistance/support should be acknowledged.

Zadatak zadan:

Datum predaje rada:

Predviđeni datumi obrane:


6. svibnja 2021.


8. srpnja 2021.

12. – 16. srpnja 2021.

Zadatak zadao:

Predsjednik Povjerenstva:

  
prof. dr. sc. Joško Deur

  
Prof. dr. sc. Tanja Jurčević Lulić

## CONTENT

|   |    |
|---|----|
| 1. INTRODUCTION.....  | 1  |
| 2. SUSPENSION SYSTEM REQUIREMENTS .....                                 | 3  |
| 2.1. Comfort.....   | 3  |
| 2.2. Road holding.....  | 4  |
| 2.3. Mechanical constraints .....                                       | 5  |
| 2.4. Key performance indicators.....                                    | 5  |
| 3. ADVANCED SUSPENSION SYSTEMS .....                                    | 7  |
| 3.1. Historical development.....  | 9  |
| 3.2. State-of-the-art suspension systems.....                           | 11 |
| 3.2.1. MagneRide .....  | 11 |
| 3.2.2. Predictive Active Suspension [18] .....                          | 12 |
| 3.2.3. E-Active Body Control (Mercedes-Benz).....                       | 13 |
| 3.3. Current control system developments .....                          | 14 |
| 3.3.1. Model predictive control .....                                   | 14 |
| 3.3.2. Fuzzy logic .....  | 14 |
| 4. FULLY-ACTIVE CONTROL SYSTEM DESIGN.....                              | 15 |
| 4.1. Design requirements .....  | 15 |
| 4.2. Quarter vehicle model .....  | 16 |
| 4.3. Optimal control [24] .....   | 18 |
| 4.4. Reduced-order control law .....                                    | 19 |
| 4.5. Control system parameter optimization.....                         | 21 |
| 4.6. System response comparison for a two degree-of-freedom model ..... | 22 |
| 5. SEMI-ACTIVE CONTROL SYSTEM DESIGN .....                              | 24 |
| 5.1. Clipped-optimal LQR control.....                                   | 24 |
| 5.2. Skyhook suspension control .....                                   | 24 |
| 6. CO-SIMULATION ENVIRONMENT .....                                      | 27 |
| 6.1. Simulation tools.....  | 27 |
| 6.1.1. AVL VSM™ .....   | 27 |
| 6.1.2. MatLab® / Simulink® .....  | 29 |
| 6.1.3. Full vehicle simulation model .....                              | 30 |
| 6.2. Controller implementation.....                                     | 30 |
| 6.2.1. Fully-active suspension controller .....                         | 30 |
| 6.2.2. Semi-active suspension controller.....                           | 31 |
| 7. SIMULATION RESULTS.....  | 32 |
| 7.1. Vertical dynamics test procedures .....                            | 32 |

|          |  |    |
|----------|--|----|
| 7.1.1.   | Sine bump.....   | 32 |
| 7.1.2.   | Sine sweep.....  | 36 |
| 7.2.     | Lateral dynamics test procedures .....                         | 41 |
| 7.2.1.   | Lane change with road roughness (ISO 3888-1).....              | 41 |
| 7.2.2.   | Hockenheim short lap time simulation with road roughness ..... | 46 |
| 7.3.     | Robustness analysis .....                                      | 50 |
| 7.3.1.   | Actuator dynamics.....   | 51 |
| 7.3.1.1. | Actuator lag time constant .....                               | 51 |
| 7.3.1.2. | Actuator force gradient .....                                  | 52 |
| 7.3.2.   | Axle load change uncertainty .....                             | 52 |
| 7.3.3.   | Measurement noise and offset.....                              | 53 |
| 8.       | CONCLUSION .....   | 56 |



## LIST OF FIGURES

|   |    |
|---|----|
| Figure 1. Approximated human perception of vertical acceleration in frequency domain [1] ..   | 4  |
| Figure 2. Static and dynamic wheel vertical load [1].....   | 4  |
| Figure 3. Conventional spring stiffness characteristic with respect to deflection including end stops [2] .....   | 5  |
| Figure 4. Road-holding versus comfort trade-off of a passive suspension system (solid line) and the optimal boundary (dashed line) [2] .....                      | 6  |
| Figure 5. Suspension classes in terms of control range, bandwidth, power request and control variable [2] .....   | 8  |
| Figure 6. Layout of a continuously variable damper with a controllable valve [12] .....   | 10 |
| Figure 7. Simplified layout of the <i>McLaren</i> hydraulic suspension system, controlled by the <i>McLaren Proactive Chassis Control II</i> [14] .....           | 11 |
| Figure 8. Magnetorheological damper schematic [16].....   | 11 |
| Figure 9. Comparison of <i>MagneRide</i> damping characteristic, conventional damper, and a valve-based variable damper [17] .....                                | 12 |
| Figure 10. <i>Audi A8</i> (2018) Active suspension front axle system components [19] .....  | 13 |
| Figure 11. <i>Mercedes-Benz GLE</i> Slow-active suspension system components [20] .....   | 14 |
| Figure 12. Two degree-of-freedom quarter vehicle model [3].....   | 17 |
| Figure 13. <i>Skyhook</i> principle schematic [27] .....  | 24 |
| Figure 14. Damping force range of the continuously controllable damper [2].....   | 25 |
| Figure 15. Co-simulation setup .....  | 27 |
| Figure 16. Vertical dynamics full vehicle model (7 DOF) [29].....   | 27 |
| Figure 17. Main front suspension kinematic features as functions of steering wheel angle and wheel travel: <i>camber</i> angle (a) and <i>toe</i> angle (b) ..... | 28 |
| Figure 18. Layout of the sensor, fully-active suspension controller and actuator dynamics <i>Simulink</i> <sup>®</sup> model.....                                 | 30 |
| Figure 19. Layout of the sensor, semi-active suspension controller and actuator dynamics <i>Simulink</i> <sup>®</sup> model.....                                  | 31 |
| Figure 20. Time responses of comfort-oriented fully-active suspension controllers and passive suspension for <i>sine bump</i> road excitation .....               | 33 |
| Figure 21. Time responses of comfort-oriented semi-active suspension controllers and passive suspension for <i>sine bump</i> road .....                           | 35 |
| Figure 22. Vehicle response (a, b, c) in time domain for a passive suspension in a <i>sine sweep</i> (d) test procedure.....                                      | 37 |
| Figure 23. Frequency response amplification of comfort-oriented fully-active and semi-active suspension controllers and passive suspension .....                  | 38 |
| Figure 24. Lane change ISO 3888-1 test stage layout [30].....   | 41 |
| Figure 25. Lane change ISO 3888-1 test stage layout.....  | 42 |
| Figure 26. Time responses of handling-oriented fully-active controllers and passive suspension for <i>lane change</i> procedure.....                              | 43 |
| Figure 27. Time responses of handling-oriented semi-active controllers and passive suspension for <i>lane change</i> procedure.....                               | 45 |
| Figure 28. <i>Hockenheim Short</i> track – Analysed track corner in Figures 29 and 30, circled in red .....   | 46 |
| Figure 29. Time responses of handling-oriented fully-active suspension controllers and passive suspension for <i>Hockenheim short</i> lap time simulation.....    | 47 |
| Figure 30. Time responses of handling-oriented semi-active suspension controllers and passive suspension for <i>Hockenheim short</i> lap time simulation.....     | 49 |
| Figure 31. Signal noise in dependence of noise power .....  | 54 |

## LIST OF TABLES

|   |    |
|---|----|
| Table 1. Quarter vehicle model vehicle parameters .....   | 17 |
| Table 2. Optimal controller state variables .....   | 19 |
| Table 3. Reduced-order controller state variables.....  | 20 |
| Table 4. Vehicle setups and corresponding feedback gains for optimal (LQR) and reduced-order controller (ROC) .....                         | 22 |
| Table 5. <i>Sine sweep</i> procedure KPIs of passive suspension, linear quadratic regulator (LQR) and reduced-order controller (ROC) .....  | 23 |
| Table 6. KPI comparison of fully-active suspension controllers and passive suspension for <i>sine bump</i> excitation .....                 | 34 |
| Table 7. KPI comparison of semi-active suspension controllers and passive suspension for <i>sine bump</i> procedure .....                   | 36 |
| Table 8. KPI comparison of fully-active suspension controllers and passive suspension for <i>sine sweep</i> excitation .....                | 39 |
| Table 9. KPI comparison of semi-active suspension controllers and passive suspension for <i>sine sweep</i> excitation .....                 | 40 |
| Table 10. KPI comparison of fully-active suspension controllers and passive suspension for <i>lane change</i> procedure .....               | 44 |
| Table 11. KPI comparison of semi-active suspension controllers and passive suspension for <i>lane change</i> procedure .....                | 46 |
| Table 12. KPI comparison of fully-active suspension controllers and passive suspension for <i>Hockenheim short lap time</i> procedure.....  | 48 |
| Table 13. KPI comparison of semi-active suspension controllers and passive suspension for a <i>Hockenheim short lap time</i> procedure..... | 50 |
| Table 14. FAS ROC <i>E-ABC</i> performance for varying actuator bandwidth .....   | 51 |
| Table 15. FAS ROC <i>E-ABC</i> performance for varying actuator force gradient limit .....  | 52 |
| Table 16. FAS ROC <i>E-ABC</i> performance for varying rear axle load .....   | 53 |
| Table 17. FAS ROC <i>E-ABC</i> performance for varying measurement signal noise power .....   | 54 |
| Table 18. FAS ROC <i>E-ABC</i> performance for varying measurement signal offset.....   | 55 |

## LIST OF SYMBOLS

| Symbol          | Unit    | Description  |
|-----------------|---------|--|
| $a_{rms}$       | $m/s^2$ | Acceleration RMS value                                     |
| $a_{y,d}$       | $m/s^2$ | Demand lateral acceleration                                |
| $a_{y,m}$       | $m/s^2$ | Measured lateral acceleration                              |
| <b>A</b>        | —       | State-space dynamic system state matrix                    |
| $b_{min}$       | $Ns/m$  | Minimum controllable damper damping value                  |
| $b_{max}$       | $Ns/m$  | Maximum controllable damper damping value                  |
| $b_s$           | $Ns/m$  | Suspension damping   |
| $b_{sky}$       | $Ns/m$  | Skyhook damping  |
| $b_t$           | $Ns/m$  | Tyre vertical damping                                      |
| <b>B</b>        | —       | State-space dynamic system input matrix                    |
| $f$             | Hz      | Excitation frequency                                       |
| $f_{BW}$        | Hz      | Frequency bandwidth  |
| $f_{dyn,max}$   | N       | Wheel maximum dynamic vertical load                        |
| $f_{LPF}$       | Hz      | Low-pass filter cut-off frequency                          |
| $f_{static}$    | N       | Wheel static vertical load                                 |
| $f_{wheel}$     | N       | Wheel vertical load  |
| $g$             | $m/s^2$ | Gravitational vertical acceleration                        |
| $G_{cont.}(s)$  | —       | Continuous transfer function                               |
| $G_{discr.}(s)$ | —       | Discrete transfer function                                 |
| <b>K</b>        | —       | Controller gain vector                                     |
| $k_s$           | $N/m$   | Suspension spring stiffness                                |
| $k_t$           | $N/m$   | Tyre vertical stiffness                                    |
| $K_{LPF}$       | —       | Low-pass filter amplification                              |
| $K_p$           | —       | Nondimensional human discomfort perception                 |
| $m_s$           | kg      | Quarter vehicle sprung mass                                |
| $m_u$           | kg      | Quarter vehicle unsprung mass                              |
| $n$             | —       | Number of data samples                                     |
| <b>N</b>        | —       | Mixed variable penalization matrix                         |
| <b>P</b>        | —       | Unique solution to the discrete algebraic Riccati equation |
| <b>Q</b>        | —       | State variable penalization weighing matrix                |
| <b>R</b>        | —       | Control variable penalization weighing matrix              |

|                 |                  |   |
|-----------------|------------------|---|
| $s$             | —                | Continuous transfer function variable                   |
| $t$             | s                | Time  |
| $T_{LPF}$       | s                | Discrete input signal sample time                       |
| $T_s$           | s                | Discrete input signal sample time                       |
| $U$             | N                | Actuator force  |
| $u_k$           | —                | $k$ -indexed data step control vector                   |
| $v_{rel}$       | m/s              | Body and wheel relative vertical speed                  |
| $x_1$           | m                | Tyre deflection state variable                          |
| $x_2$           | m/s              | Vertical unsprung mass speed state variable             |
| $x_3$           | m                | Suspension deflection state variable                    |
| $x_4$           | m/s              | Vertical sprung mass speed state variable               |
| $x_5$           | m/s <sup>2</sup> | Vertical unsprung mass acceleration state variable      |
| $x_6$           | m/s <sup>2</sup> | Vertical sprung mass acceleration state variable        |
| $x_{1,i}$       | m                | Vertical tyre deflection at $i$ -th data sample         |
| $x_{3,i}$       | m                | Vertical suspension deflection at $i$ -th data sample   |
| $\dot{x}_4$     | m/s <sup>2</sup> | Vertical chassis acceleration                           |
| $\dot{x}_{4,i}$ | m/s <sup>2</sup> | Vertical chassis acceleration at $i$ -th data sample    |
| $x_k$           | —                | $k$ -indexed data step state vector                     |
| $x_{k+1}$       | —                | $(k + 1)$ -indexed data step state vector               |
| $z$             | —                | Discrete transfer function variable                     |
| $z_r$           | m                | Quarter vehicle road profile vertical height            |
| $z_s$           | m                | Quarter vehicle sprung mass vertical position           |
| $z_u$           | m                | Quarter vehicle unsprung mass vertical position         |
| $\dot{z}$       | m/s              | Vertical chassis speed                                  |
| $\dot{z}_{def}$ | m/s              | Vertical suspension deflection speed                    |
| $\dot{z}_r$     | m/s              | Quarter vehicle road profile vertical speed             |
| $\dot{z}_s$     | m/s              | Quarter vehicle sprung mass vertical speed              |
| $\dot{z}_u$     | m/s              | Quarter vehicle unsprung mass vertical speed            |
| $\ddot{z}_r$    | m/s <sup>2</sup> | Quarter vehicle road profile vertical acceleration      |
| $\ddot{z}_s$    | m/s <sup>2</sup> | Quarter vehicle sprung mass vertical acceleration       |
| $\ddot{z}_u$    | m/s <sup>2</sup> | Quarter vehicle unsprung mass vertical accel.           |
| $\alpha$        | —                | <i>SH-Linear</i> suspension controller tuning parameter |
| $\mu_{x_3}$     | m                | Mean suspension deflection                              |
| $\mu_{x_1}$     | m                | Mean tyre deflection                                    |

|                    |                |   |
|--------------------|----------------|---|
| $\mu_{\ddot{x}_4}$ | $\text{m/s}^2$ | Mean chassis vertical acceleration        |
| $\zeta$            | —              | Single mass damping ratio                 |
| $\zeta_{min}$      | —              | Minimum controllable damper damping ratio |
| $\zeta_{max}$      | —              | Maximum controllable damper damping ratio |

## LIST OF ABBREVIATIONS

| Abbreviation     | Description                                      |
|------------------|--|
| AA               | Anti-aliasing                                    |
| <i>ABC</i>       | <i>Active Body Control</i>                       |
| A/D              | Analog-to-digital                                |
| BEV              | Battery electric vehicle                         |
| <i>COBYLA</i>    | Constrained optimization by linear approximation |
| C-O              | Clipped-optimal                                  |
| DOF              | Degrees-of-freedom                               |
| <i>E-ABC</i>     | <i>E-Active Body Control</i>                     |
| e-MPC            | Explicit model predictive control                |
| FAS              | Fully-active suspension                          |
| i-MPC            | Implicit model predictive control                |
| KPI              | Key performance indicator                        |
| LPF              | Low-pass filter                                  |
| LQR              | Linear quadratic regulator                       |
| <i>MBC</i>       | <i>Magic Body Control</i>                        |
| ODE              | Ordinary differential equation                   |
| <i>PAS</i>       | <i>Predictive Active Suspension</i>              |
| ROC              | Reduced-order controller                         |
| SAS              | Semi-active suspension                           |
| <i>SH-2</i>      | <i>Skyhook-2 states</i> logic                    |
| <i>SH-Linear</i> | <i>Skyhook-Linear</i> logic                      |
| SUV              | Sports utility vehicle                           |
| ZOH              | Zero-order hold                                  |

## SAŽETAK

U ovom je radu prikazana sinteza aktivnih i polu-aktivnih ovjesa putničkih vozila, njihova implementacija u napredno simulacijsko okruženje te usporedna analiza performansi sustava upravljanja. U radu su uspoređeni pasivni ovjes, optimalni aktivni i polu-aktivni ovjes temeljeni na primjeni linearnog kvadratnog regulatora, aktivni ovjes s regulatorom reduciranog reda, te polu-aktivni ovjes sa *Skyhook* upravljanjem. Potonji aktivni i polu-aktivni ovjes koriste ograničen broj senzora koji su najčešće dostupni na putničkom vozilu.

Usporedna analiza temelji se na primjeni karakterističnih procedura vertikalne dinamike vozila poput ceste oblika poluvala sinusoide (engl. *sine bump*), ceste s promjenjivom frekvencijom vala sinusoide (engl. *sine sweep*) te procedura bočne dinamike vozila – promjena trake (engl. *lane change*) i simulacija brzog kruga trkaće staze *Hockenheim short* (engl. *lap time simulation*).

Osim usporedne analize različitih upravljanja, provedena je analiza robustnosti regulatora s obzirom na dinamiku aktuatora poput ograničenja gradijenta sile te brzine odziva na performanse upravljanja u navedenim procedurama. Ispitivanje robustnosti regulatora prošireno je na slučajeve promijenjenog statičkog opterećenja osovine vozila te unos šuma (engl. *noise*) i odstupanja (engl. *offset*) u mjerene signale.

Primjena regulatora reduciranog reda te polu-aktivnog ovjesa sa *Skyhook* upravljanjem dovodi do značajnih poboljšanja komforta u testnim procedurama vertikalne dinamike u usporedbi s pasivnim ovjesom. Performanse optimalnih regulatora aktivnog te polu-aktivnog ovjesa su neznatno bolje od odgovarajućih regulatora reduciranog reda te polu-aktivnog ovjesa sa *Skyhook* upravljanjem. Usporedna analiza regulatora, temeljenih na četvrtinskom modelu vozila te primijenjenih na puni model vozila, u vidu bočne dinamike je pokazala prihvatljiva poboljšanja po pitanju stabilnosti i neznatne razlike u vidu upravljivosti vozila te se upućuje na primjenu regulatora dizajniranog na temelju modela cijelog vozila u svrhu poboljšanja tih indeksa performansi.

Ključne riječi: upravljački sustavi, komfor, upravljivost, dinamika vozila, aktivni ovjes.

## SUMMARY

This thesis presents the design of a fully-active and a semi-active suspension control system, their implementation in an advanced simulation environment and a comparative performance analysis. The comparative analysis includes a passive suspension, optimal fully- and semi-active suspensions based on a linear quadratic regulator, a reduced-order control of fully-active suspension and a *Skyhook* control of semi-active suspension. The reduced-order and *Skyhook* controllers require a limited sensor suite, which is frequently implemented on high-end passenger vehicles. This gives an insight into how practical controllers compare to benchmark optimal controllers.

The controller performance is analyzed in two vertical dynamics test procedures - *sine bump* and *sine sweep* and two lateral dynamics test procedures – *lane change* (ISO 3888-1) and *Hockenheim short track lap time* simulation.

Furthermore, a robustness analysis is carried out with respect to actuator dynamics in terms of force gradient limitation and actuator bandwidth. The robustness analysis is extended to the case of included parameter uncertainties such as rear axle static load change and the addition of noise and offset to feedback loop measurement signals.

The reduced-order fully-active suspension controller and *Skyhook* semi-active suspension controller resulted in significant improvements in terms of comfort in typical vertical dynamics test procedures compared to a passive suspension. The optimal fully- and semi-active suspension controller provide only slightly better results than the practical controllers with respect to most metrics. The comparative analysis of controllers, based on a quarter car model and implemented on the full vehicle model, in lateral dynamics test procedures showed acceptable improvements in terms of vehicle stability and negligible handling improvements. This indicates that a full vehicle model-based controller design would be more appropriate for greater handling metric improvements.

Key words: control system design, comfort, handling, vehicle dynamics, active suspension.



## PROŠIRENI SAŽETAK

Veliki dio istraživanja u području upravljanja aktivnim ovjesom temeljen je na primjeni četvrtinskih modela vozila i optimalnog upravljanja – koje često u povratnoj vezi koristi signale koji se ne mogu mjeriti ili se teško estimiraju. Zbog slabe primjenjivosti takvih sustava, cilj ovog rada je sintetizirati upravljački zakon koji koristi mjerljive ili signale koji se mogu jednostavnije estimirati. Također je cilj performanse takvog upravljačkog sustava usporediti s pasivnim ovjesom te optimalnim regulatorom na temelju simulacijskog modela cijelog vozila.

U ovome je radu prikazana sinteza aktivnih i polu-aktivnih ovjesa putničkih vozila, implementacija u napredno simulacijsko okruženje te usporedna analiza performansi upravljanja. U radu su uspoređeni aktivni ovjes s linearnim kvadratnim regulatorom (engl. *optimal controller*), polu-aktivni ovjes s linearnim kvadratnim regulatorom (engl. *clipped-optimal controller*), aktivni ovjes s regulatorom reduciranog reda (engl. *reduced-order controller*), polu-aktivni ovjes sa *Skyhook* upravljanjem te pasivni ovjes. Pritom je posvećena pažnja primjeni upravljačkih sustava koji koriste ograničen broj senzora najčešće dostupnih na putničkom vozilu.

Rad se sastoji od 8 poglavlja:

### 1) Uvod

Opisan je utjecaj parametara vozila na zahtjeve postavljene na ovjes. Prikazana je usporedba aktivnih i pasivnih ovjesa, te su navedene prednosti i nedostaci primjene aktivnih ovjesa, uključujući implementacijske aspekte. Dana je motivacija za sintezom regulatora koji će omogućiti jednostavnu implementaciju uz uobičajeno dostupne senzore.

### 2) Zahtjevi sustava ovjesa

Prikazana je poveznica između zahtjeva postavljenih na sustav ovjesa vozila te statističkih mjera koje kvantificiraju performanse ovjesa. Navedeni su ključni indeksi performansi koji se u nastavku rada koriste pri usporednoj analizi performansi sustava upravljanja aktivnim ovjesom.

### 3) Napredni upravljački sustavi ovjesa

Navedena je podjela upravljanih sustava ovjesa koje proizvođači vozila koriste kako bi zadovoljili sve veće kriterije kojima se osigurava bolje iskustvo vozača i putnika vozila. Kroz osvrt na brzinu upravljanja te potrošnju energije takvih sustava dan je uvid u prednosti karakterističnih izvedbi, trenutno stanje tehnike i ograničenja koja određeni tip vozila predstavlja. Također, prikazani su i smjerovi istraživanja sustava upravljanja aktivnim ovjesom.

### 4) Dizajn aktivnog sustava upravljanja

Postavljeni su izrazi za statističke veličine koje kvantificiraju performanse upravljanog ovjesa. Navedene su pretpostavke te jednadžbe koje opisuju linearni četvrtinski model vozila koji se koristi u sintezi optimalnog regulatora i regulatora reduciranog reda. Prikazani su rezultati optimizacijske procedure kojom su određena pojačanja regulatora reduciranog reda. Konačno je i usporedno analiziran odziv u vidu *sine sweep* procedure za dizajnirane regulatore, optimalne regulatore te pasivni ovjes.

## 5) Dizajn polu-aktivnog sustava upravljanja

Prikazana je teoretska podloga *Skyhook* upravljačke logike te dizajn *Skyhook-Linear* regulatora polu-aktivnog ovjesa. Određen je raspon prigušenja koji će se koristiti u simulacijskom modelu pri usporednoj analizi performansi regulatora sustava ovjesa.

## 6) Ko-simulacijsko okruženje

Opisan je simulacijski softver *AVL VSM™* te *MatLab®/Simulink®*, koji se koriste za implementaciju dizajniranih regulatora u simulacijski model cijelog vozila. Navedeni su utjecaji koje parametrizacija vozila može imati na odziv u pogledu vertikalne dinamike. Osvrt na dizajn aktivnog i polu-aktivnog regulatora u *Simulink®*-u daje uvid u korištene tehnike za opis dinamike senzora i aktuatora.

## 7) Pregled rezultata simulacija

Provedena je usporedna analiza kojom je prikazan potencijal prethodno navedenih regulatora temeljenih na četvrtinskom modelu vozila s obzirom na poboljšanje performansi vertikalne i bočne dinamike cijelog vozila.

Analiza robusnosti je provedena s obzirom na dinamiku aktuatora po pitanju vremenske konstante aktuatora te maksimalnog gradijenta sile. Utjecaj nesigurnosti parametara analiziran je s obzirom na dodatno vertikalno opterećenje stražnje osovine, dodatak šuma te odstupanja u signal povratne veze.

## 8) Zaključak

Navedeni su zaključci koji proizlaze iz usporedne analize regulatora te analize robusnosti. Predloženo je nekoliko pristupa koji bi mogli rezultirati boljim performansama za analizirane testne procedure. Konačno, prikazani su trenutni pravci razvoja upravljačkih sustava u području aktivnih ovjesa.

# 1. INTRODUCTION

Since the beginning of road vehicle development, primitive suspensions were used to provide “cushion” between road and chassis. At first, they were introduced as rigid axles with longitudinal leaf-springs which support the chassis. Multi-leaf steel spring pack designs were implemented later on, to provide additional damping. With the invention of the pneumatic tyre at the end of the 19<sup>th</sup> century, additional ride comfort improvements were possible. The road irregularities cause vertical movement of the tyre contact patch, which are also transmitted to the unsprung and sprung masses of the vehicle. Vertical vibrations caused by force transmission from the unsprung to sprung mass are perceived by passengers and affect their comfort. Generally, it is preferred to reduce the vibration transmission from unsprung mass to sprung mass and seat to improve ride comfort.

Passengers perceive vertical oscillations as physical vibrations in frequencies up to 30 Hz (ride range), while higher frequencies (above 100 Hz) are audibly perceptible. The frequency range between 30 Hz and 100 Hz, referred to as harshness, is a transition range from the ride to the noise range. Vertical vehicle dynamics is typically focused on primary and secondary ride (up to 30 Hz), which encompass the sprung and unsprung mass natural frequencies [1].

Handling became important with motorized vehicles running at higher speeds. A vehicle running at a certain speed through a bend of a certain curvature will experience centrifugal force on the body. This force is mainly reacted through the tyre contact patch, as to provide the lateral acceleration and yaw rate which the driver demands through his inputs. Other than having the ability to manoeuvre the vehicle at an acceptable speed along a curvy road, handling also plays an important role in passenger safety – the vehicle needs to have acceptable braking performance and lateral grip, so it can stop in a short-enough distance or manoeuvre around unexpected obstacles. Even though the general chassis layout, total mass, weight distribution, suspension system type and tyre choice have a large influence on the vehicle’s longitudinal and lateral dynamics, it is important to maintain vertical tyre load as it directly impacts the tyre’s tangential forces. Therefore, reducing vertical tyre load oscillations with respect to road irregularities by properly tuning or controlling the suspension is needed to maintain safety and improve handling [2].

Generally, an independent passive suspension will provide greater passenger comfort for lower suspension damping, as it will provide better filtering of road irregularities. High suspension damping will result in lower resonant peaks of tyre deflection, while causing a deterioration of passenger comfort. This poses the passive suspension development with a trade-off between ride comfort and handling [2].

By equipping the vehicle with controllable dampers or force sources (actuators), the driver can select whether his current priority is better comfort or road-holding. The former is called semi-active suspension, and they are able to continuously control the dissipative, damping forces. The latter, fully-active suspension can generate active force, which enables better control compared to semi-active systems that only generate dissipative forces.

Active suspension control strategies are commonly based on linear quadratic control [3], *SkyHook* logic [2] and model predictive control [4]. More advanced chassis control systems can distinguish regular driving from dynamic events based on measured signals which define the vehicle state and driver inputs [5].

A typically applied Linear Quadratic Regulator (LQR) for active suspension system based on a two degree-of-freedom quarter vehicle model is presented in [3]. The LQR applied to linear

system results in optimal control law. The limiting factor for the optimal controller is that it uses the tyre deflection as feedback, which is a signal that is not practically measurable by the currently available sensor suite. An explored solution is to build an observer coupled with tyre belt accelerometer measurements within a Kalman filter, as shown in [6]. The requirement of tyre deflection sensors is not typical on production vehicles, and measurement robustness cannot yet be guaranteed.

Therefore, there is a need to develop a controller which is based on measurable signals. Suspension deflection sensors, commonly referred to as “ride height” sensors, are available on each wheel in high-end vehicles which feature an advanced suspension system. Vertical chassis acceleration for each vehicle corner can be calculated from a vertical acceleration measurement, roll and pitch angular accelerations in the vehicle center of gravity. Another way of calculating the mentioned values is by mounting three vertical acceleration sensors positioned longitudinally and laterally relative to each other within the chassis.

This thesis will focus on the design of a control system based on the common sensor suite and compare its performance to the theoretical, optimal controller and a passive suspension using a full vehicle model simulation environment.

## 2. SUSPENSION SYSTEM REQUIREMENTS

This chapter describes suspension system design requirements and the metrics for their evaluation. The design requirements depend on the type and application of the vehicle for which the controller is designed. For example, an executive sedan suspension system must provide a high level of passenger comfort for most typical road conditions and driver inputs. On the other hand, a race car suspension system must provide great performance in terms of road-holding with little variation depending on the fuel load, racetrack and tyre temperature etc. Adequate functional safety must be insured in case a sensor or system component fails.

### 2.1. Comfort

Passenger comfort has more aspects than the suspension system can provide. Other supporting systems beside chassis suspension include the seat design regarding ergonomics and disturbance transmittance from the chassis to the passenger, as well as audible noise damping. As described in chapter 36. of [1], the passenger tends to disregard all other positive features of the vehicle in case there exists one issue which causes discomfort. Therefore, passenger comfort is determined by the combination of subsystem properties including the tyres, springs, dampers, bushings, body mass and stiffness, steering, pedal assembly component stiffness etc. The vehicle must be designed to provide good performance in all aspects of comfort.

In suspension system design, the goal is to minimize the influence of road disturbance on the chassis movement. According to the standard ISO 2631, the nondimensional human discomfort perception  $K$ , can be roughly estimated as a function of the RMS of chassis vertical acceleration and the excitation frequency. This relationship was found through extensive ergonomic investigations as described in [1].

As shown in Figure 1, vibrations in the range of 4 to 8 Hz are perceived as most disturbing to the passengers. Exposing passengers to high levels of disturbance for a prolonged time can influence mental performance or even cause physical health issues. The human perception of comfort drops off linearly for higher frequencies, which are also rarely excited with high acceleration amplitudes. Therefore, the goal is to attenuate primarily low-frequency vibrations, up to 20 Hz. Larger lumped masses of the vehicle tend to have their natural frequencies in this range. The passenger vehicle sprung mass (chassis) has its natural frequency typically around 1 Hz, while the unsprung mass (the wheel assembly) typically resonates at around 10 Hz. Therefore, the frequency response in this thesis is analysed in the range of up to 20 Hz.

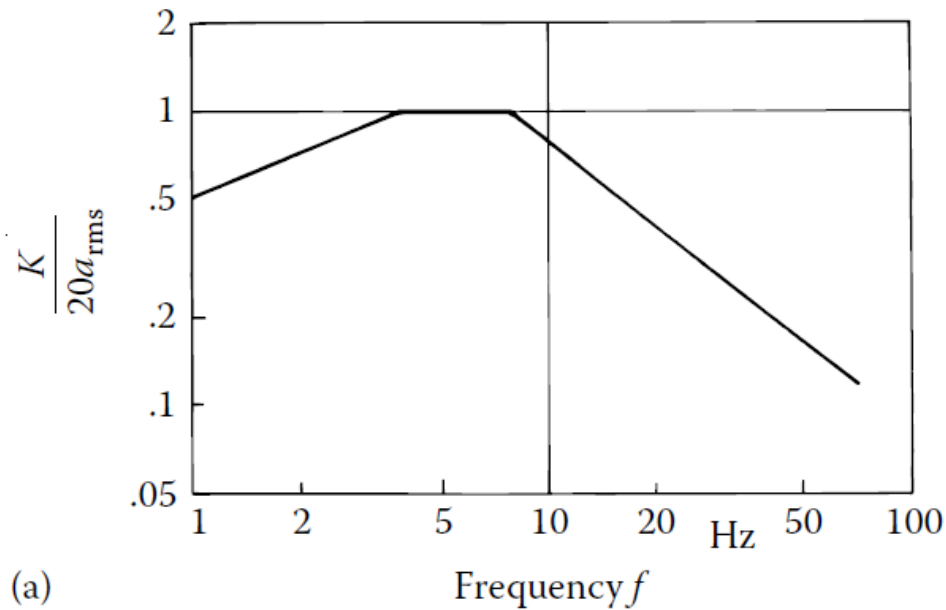


Figure 1. Approximated human perception of vertical acceleration in frequency domain [1]

## 2.2. Road holding

A safety aspect of ride is maintaining the contact between the tyre contact patch and road. This is of concern as most forces which influence horizontal body movement come from the contact patches, and they can only act on the vehicle if the tyre is in contact with the road. Maintaining contact of the tyre with the road is particularly important to provide adequate braking potential during emergency braking situations or lateral acceleration potential when the driver has to manoeuvre around an obstacle or bend.

The pneumatic tyre has the property of relaxation, which means that for a change in longitudinal slip ratio or lateral slip angle, a longitudinal or lateral force change will occur with a delay in comparison to a steady-state case. During driving over road irregularities, the tyre vertical load oscillation (illustrated in Figure 2), may lead to unfulfilled steady-state friction force potential. This is more pronounced for a larger oscillation amplitude or frequency.

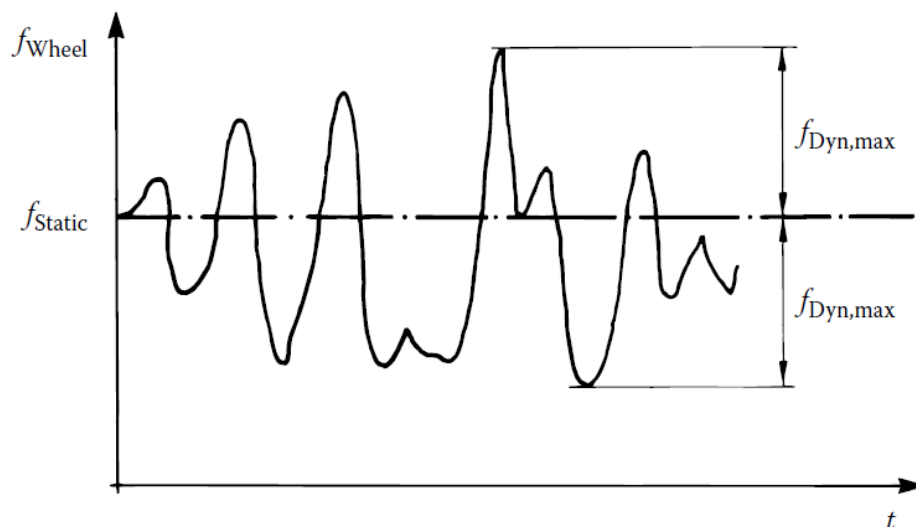


Figure 2. Static and dynamic wheel vertical load [1]

## 2.3. Mechanical constraints

As with any mechanical system, physical constraints with respect to forces and travel must be respected to keep the system operative. In the case of a suspension system, the bump and rebound stops (end stops) are used to increase the suspension stiffness near the limit of suspension travel or prevent binding of suspension components (Figure 3). End stop actuation causes an abrupt vertical chassis acceleration peak, which translates to comfort deterioration. If a linear model is used to describe the suspension system, it is necessary to keep the suspension stroke within the travel limits during regular driving conditions. A typical road car suspension has a total wheel travel of 140 mm, while a SUV has a total wheel travel around or greater than 200 mm.

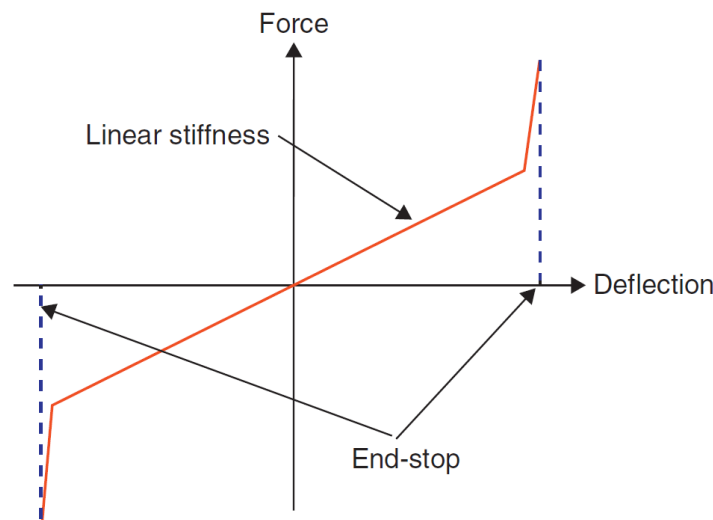


Figure 3. Conventional spring stiffness characteristic with respect to deflection including end stops [2]

## 2.4. Key performance indicators

General suspension system requirements described in the previous subsection need to be quantified for suspension control system design and performance analysis. To this end, for each requirement – comfort, road-holding and suspension travel limit, a key performance indicator (KPI) is defined.

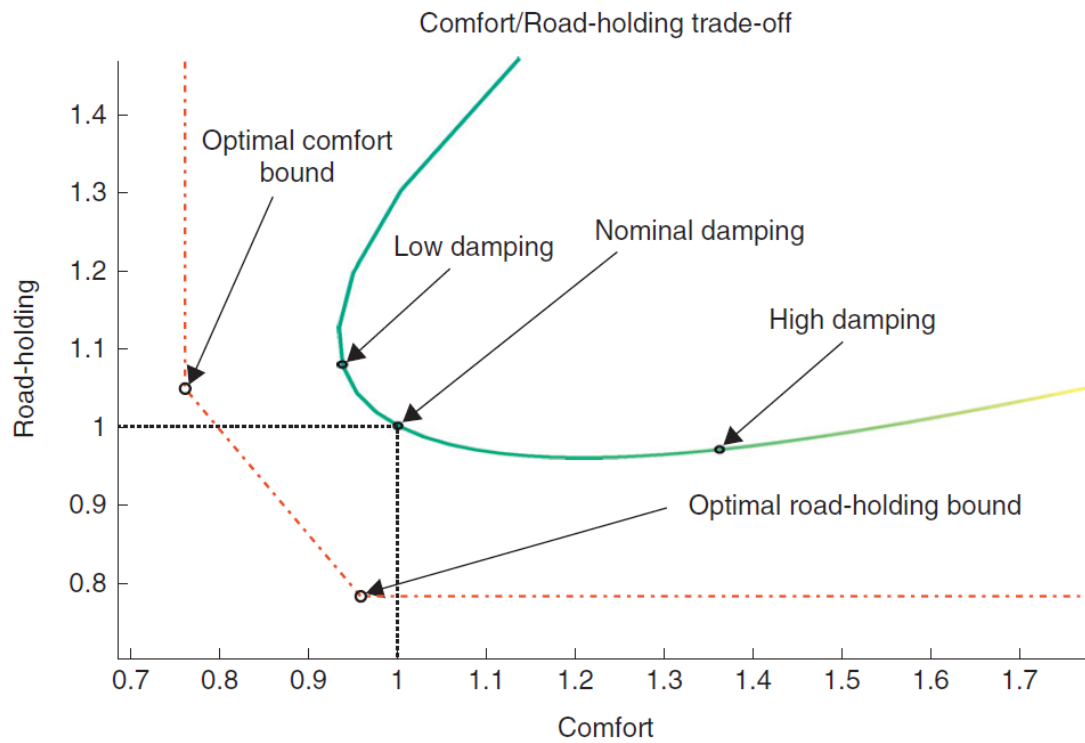
Ride comfort performance metrics are typically based on chassis (sprung mass) acceleration signals [2], or alternatively jerk. One of the most common metrics, also considered as ride comfort KPI here, is the variance of vertical, pitch and roll accelerations.

Tyre vertical load or deflection (assuming linear tyre vertical stiffness) are commonly used to define the handling performance of a vehicle [2]. In this thesis, the road holding KPI is defined as the variance of the tyre deflection.

The suspension deflection variance is regularly used to quantify the suspension deflection oscillations in vertical test procedures [2]. Minimized suspension deflection is preferred to keep the wheel travel within limits. Generally, lower suspension spring stiffness will cause larger suspension deflections and lower suspension damping will cause prolonged oscillation of the suspension deflection.

The defined KPIs are generally conflicting [2]. For example, Figure 4 illustrates the trade-off between road-holding and comfort for passive suspension with different damping setups. KPI

values for a single passive suspension setup define a point on the solid line. For a single setup of an optimal active suspension, the KPI values form a point on the red dashed line.



**Figure 4. Road-holding versus comfort trade-off of a passive suspension system (solid line) and the optimal boundary (dashed line) [2]**



### 3. ADVANCED SUSPENSION SYSTEMS

Vehicle manufacturers are faced with an increasing number of customers demanding vehicles with superior passenger comfort and handling. Initially the chassis development focused on new suspension layouts (from the leaf spring solid axle to an independent suspension) which provided decoupling of same-axle wheels, better tyre-road interaction, and better vehicle balance. After improvements provided by purely mechanical systems started plateauing, advanced controllable systems had to be developed and implemented to aid in further comfort and road-holding improvement on high-end vehicles.

The general breakdown of advanced suspension system types in terms of bandwidth and control range is presented in Figure 5. A passive suspension has fixed spring and damping characteristics, while an adaptive suspension will have continuously controllable or switchable dampers which can produce dissipative forces in a certain damping range with limited bandwidth (up to 5 Hz). Semi-active suspensions feature a wider bandwidth of damping control in relation to an adaptive setup. Adaptive and semi-active suspensions spend minor power as they produce only dissipative forces. The power that they do require is used to control the damping by controlling valves, orifices or electromagnets.

A load levelling suspension controls the axle or wheel static force, while having constant spring and damper characteristics. Load levelling suspensions usually feature an air compressor (in the case of an air suspension) or a hydraulic pump (for a hydraulic suspension) to control the wheel load using slow actuation. During additional axle loading or a load transfer scenario, the fluid is pumped to compensate the dynamic forces which are acting on the wheel, which requires more power to drive the compressor/pump. In regular driving scenarios, there is no power demand from load-levelling suspension systems.

Higher consumption systems, like slow-active and fully-active suspensions use the actuator force as the control variable. Even though slow-active and fully-active systems are continuously operating, passenger vehicle implementations of such systems always feature passive springs, used to lower the power consumption by providing static load support. Additionally, passive or adaptive dampers are used to filter the high frequency dynamic forces which are above the actuator bandwidth.

Typically, the bandwidth of slow-active suspension is around 5 Hz and the power request range from 1 to 5 kW. A fully-active suspension setup is equipped with a higher bandwidth system, which can control secondary ride range irregularities as well, which leads to an increase in power request by up to 10 kW. The introduction of 48 V low-voltage systems into passenger vehicles has provided the possibility to use electric motors of adequate power as actuators in the suspension system. In some designs, electric motors are used to power hydraulic pumps which drive hydraulically-actuated systems.

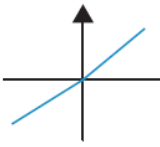
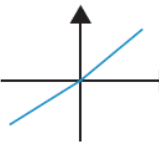
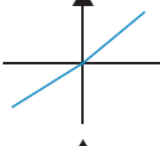
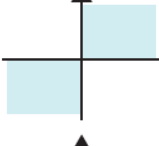
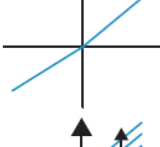

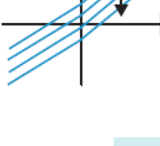

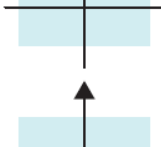

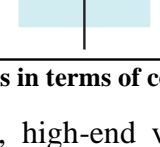
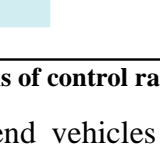
| System class  | Control range (spring)  | Control range (damper)  | Control bandwidth | Power request | Control variable    |
|---------------|---|---|-------------------|---------------|---------------------|
| Passive       |    |    | -                 | -             | -                   |
| Adaptive      |    |    | 1-5 Hz            | 10-20 W       | $c$ (damping ratio) |
| Semi-active   |    |    | 30-40 Hz          | 10-20 W       | $c$ (damping ratio) |
| Load leveling |    |    | 0.1-1 Hz          | 100-200 W     | $W$ (static load)   |
| Slow active   |   |   | 1-5 Hz            | 1-5 kW        | $F$ (force)         |
| Fully active  |  |  | 20-30 Hz          | 5-10 kW       | $F$ (force)         |

Figure 5. Suspension classes in terms of control range, bandwidth, power request and control variable [2]

In recent developments, high-end vehicles commonly feature adaptive suspensions, load-leveling suspensions or their combinations. Adaptive dampers give the possibility to manage the trade-off between comfort and road-holding, as they provide better road irregularity filtering, but also a stiffer (sportier) ride on demand. Load-leveling suspensions are not as good in road irregularity filtering due to their low bandwidth, but provide additional comfort in terms of body motion control in additional loading or load transfer scenarios. They also require controllable static force components e.g. air springs, hydraulic cylinders or movable spring perches. High-end vehicles like the Tesla Model S feature a “highway” driving mode, in which the ride height is lowered to provide less air resistance and reduce drivetrain power consumption. A few manufacturers are also implementing slow-active systems equipped with road preview, with an actuator bandwidth of up to 6 Hz - supporting only primary ride control. Slow-active systems available in production vehicles generally feature road preview.

Improved performance for both conflicting criteria (comfort and road-holding) can be achieved by using a semi-active suspension controller to continuously control the suspension damping force. The control law can be based on e.g. full- or reduced-state feedback. As the damper is a purely dissipative system element, the resulting demand force must be limited to only act opposite to the damper velocity. A different approach to semi-active controller design is to use a switching, e.g. *Skyhook 2-states* or continuous, e.g. *Skyhook Linear* controller logic, both presented in [2]. The performance of a continuous semi-active suspension controller with *Skyhook Linear* logic will be evaluated in this thesis.

As with an advanced semi-active system, the fully-active suspension actuator force can be controlled by an advanced controller. An advantage of semi-active systems is that they stabilize the system response due to the purely dissipative nature of the damper forces. This does not have to be the case with a fully-active system, as high controller gains can cause the system to respond in a destabilizing manner in certain scenarios. This has to be taken into consideration in the design of a such controller through the implementation of adequate functional safety.

The full capabilities of a fully-active suspension system are utilized by “road-preview”, i.e. by scanning the oncoming road, e.g. via a stereo camera. Road preview information enables the controller to act proactively by preparing the suspension for oncoming road irregularities. For example, in a bump scenario the oncoming wheel will be unloaded moments before impacting the bump, to reduce the influence on the wheel and chassis vertical acceleration disturbance. The theoretical background of a quarter vehicle road preview optimal controller is presented in [3]. An explicit model predictive control (abbr. e-MPC) design of a decentralized suspension controller is presented in [7]. The control optimization is conducted offline and the actuator setup becomes a function of the oncoming road data. This contrasts implicit model predictive control (abbr. i-MPC) designs, in which the oncoming road data is used as an input for online optimization of the actuator response. Therefore, an e-MPC implementation results in faster calculation of the next actuator setup step with hardware of equal computing power, compared to an i-MPC implementation.

### 3.1. Historical development

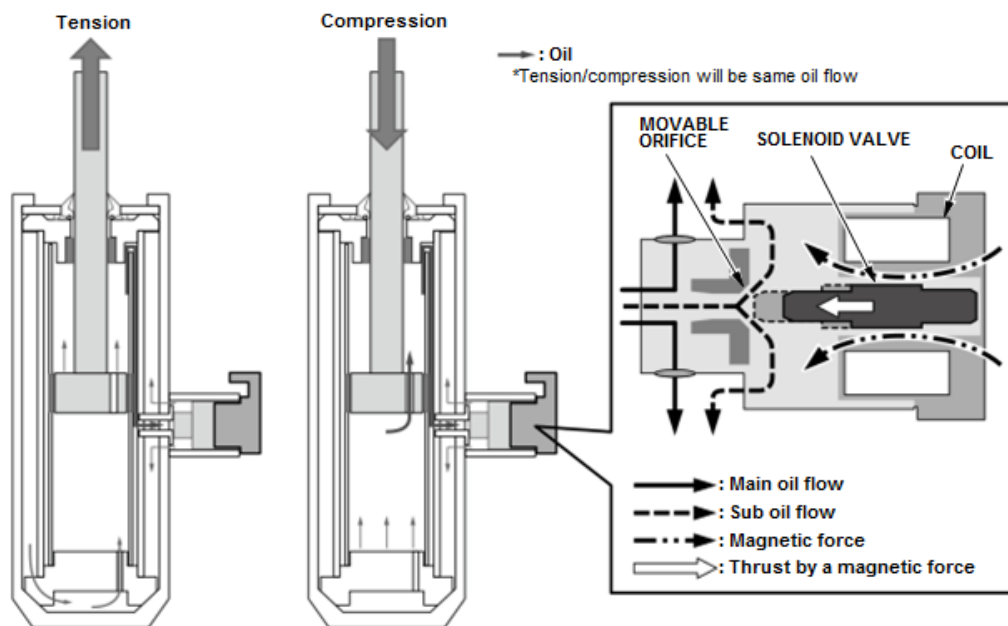
Even though research of active suspension control started in the 1980s, a combination of high component prices, high energy consumption, system weight and bad performance due to slow actuator control kept the control systems from being implemented on a production passenger vehicle for about 20 years. As the price of actuators, sensors and control units decreased, the implementation of an active or semi-active control system became more feasible.

Ford's BBAS (Broad-Bandwidth Active Suspension) prototype and research [8] showed the necessary power demand was too large for state-of-the-art actuators in the early 1990's, as it would mean that system components would be heavy and large in volume. The research also showed that the actuator dynamics did not provide good enough performance improvement in secondary ride (above 5 Hz).

A notable application of an active suspension system was on the *Williams* F1 race car *FW14B* in the early 1990's, which dominated the F1 championship until active chassis control systems were ruled-out due to safety concerns. The hydraulic active suspension system was mainly used to counteract body movement due to inertial forces, which in turn results with more consistent aerodynamic efficiency, as the oscillation of chassis distance from the ground is minimized. Although the details of the control logic are a well-kept secret, it is known that the system was reactive to the current driving condition and specially tuned for each circuit it was raced on [9].

Since the 1960-s, *Mercedes-Benz* used pneumatic and hydro-pneumatic suspensions in production cars to provide a superior level of comfort in comparison with the competition. They were initially purely passive systems. After a few active suspension prototypes in the 1990-s, *Mercedes-Benz* introduced its first production vehicle active suspension system, named *Active Body Control* (abbr. *ABC*) on its *CL500* model (1999.). The system was hydraulically actuated and featured changeable driving modes which was used to manage the trade-off between comfort and road-holding. The suspension system controller featured a sample time of 10 ms and a hydraulic actuator to provide filtering of lower frequency excitations, as the bandwidth is in the range of the sprung mass natural frequency. This means that high-frequency road

disturbance filtering is not possible. Instead, the passive spring and damper are used to provide high frequency excitation filtering. The active system also effectively counteracts body movement due to inertial forces, which means that roll and pitch angle amplitudes due to vehicle accelerations are reduced [10]. The ABC has since gone through a few design iterations. Some high-end models are now equipped with a semi-active *AirMatic* suspension, which uses air springs (with load levelling capabilities and a 50 ms response time) and adaptive dampers (Figure 6) for road irregularity filtering. Other models use an updated *ABC* system, which replaces the air spring with a hydraulic cylinder (with load levelling capability as well) [11]. Since the 2013 model, the *S-Class* is offered with a fully-active suspension system named *Magic Body Control* (abbr. *MBC*) which uses road preview to proactively react to oncoming road irregularities via electronic actuators [10].



**Figure 6. Layout of a continuously variable damper with a controllable valve [12]**

Even though *Citroën* equipped the *DS* with a fully hydraulic suspension system as early as the 1950's, the advancement in sensor and control system technology allowed for *McLaren* to develop a hydraulic suspension system which provides better road-holding as well as comfort. The *McLaren Proactive Chassis Control II* uses hydraulic cylinders mounted on each chassis corner (Figure 7). The individual hydraulic cylinders are interconnected by tubes. The system controls the suspension by limiting the flow of hydraulic fluid between the wheels in dynamic scenarios. The system is equipped with hydraulic pumps which can also produce active forces. This system is used to counteract load transfer induced body movement and to keep the lateral balance of the vehicle during cornering [13] while maintaining a soft ride in regular driving conditions - when road irregularity filtering is most important.

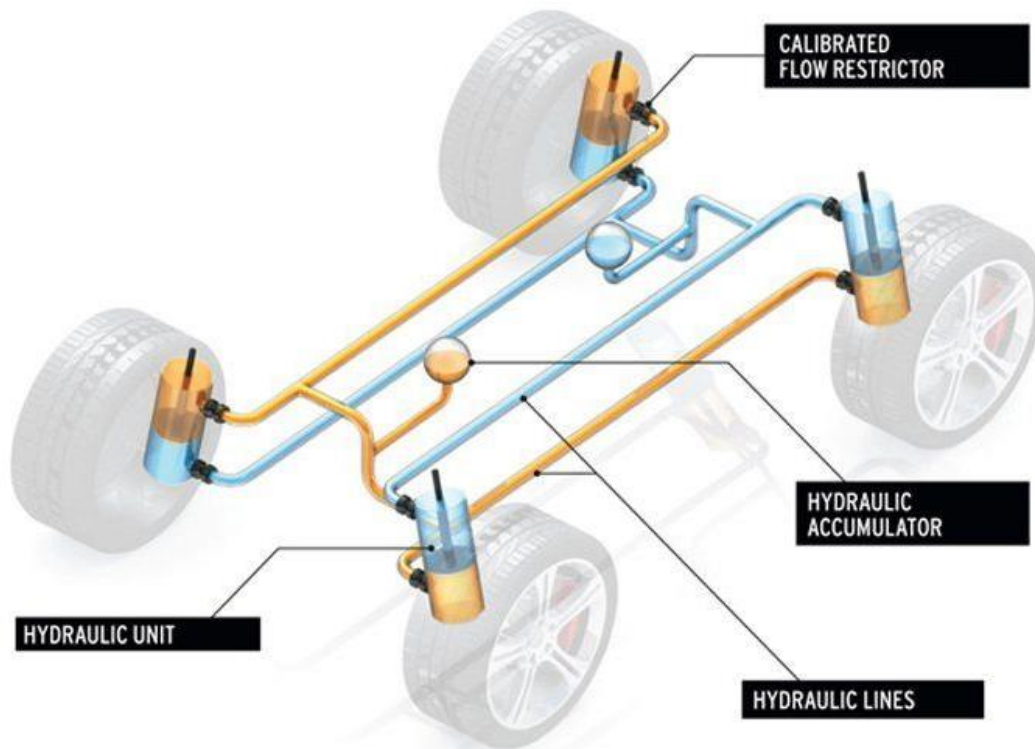


Figure 7. Simplified layout of the *McLaren* hydraulic suspension system, controlled by the *McLaren Proactive Chassis Control II* [14]

## 3.2. State-of-the-art suspension systems

This subchapter presents a few popular choices of advanced suspension systems in high-end production vehicles.

### 3.2.1. *MagneRide*

Adaptive magnetorheological dampers developed by *Delphi Automotive* corporation are used in a wide range of high-end vehicles. The *MagneRide* actuator control system controls current flow through electromagnets to change the viscosity of the magnetorheological fluid. The fluid contains ferromagnetic particles which “align” in the presence of an electromagnetic field and therefore resist fluid motion to a larger degree, effectively increasing the damping coefficient. The adaptive *MagneRide* dampers (Figure 8) are most frequently mounted parallel to a conventional or air spring. The control system is implemented in suspensions of vehicles such as the *Ford Mustang*, *Chevrolet Corvette*, *Ferrari LaFerrari* and *Lamborghini Aventador*, various *Cadillac* models and some *Audi* models [15].

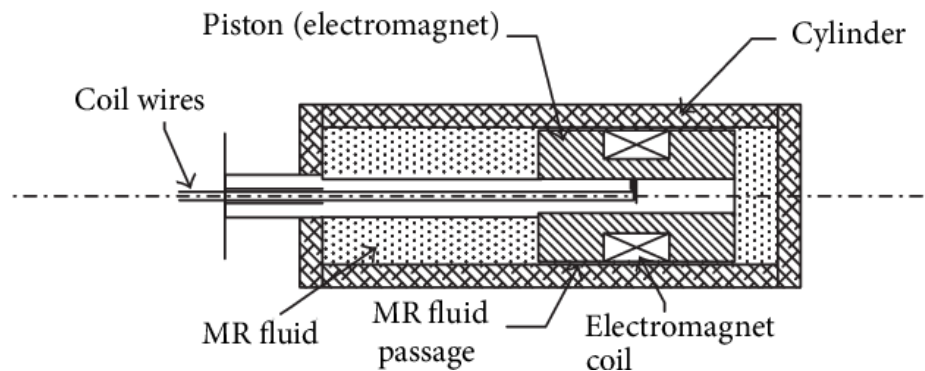


Figure 8. Magnetorheological damper schematic [16]

The system is used to continuously control the damping, i.e., change damping characteristics, as illustrated in Figure 9, of the suspension shock absorber to provide improvements in road-holding and comfort. The driver can choose between different driving modes which will influence the control system logic so that road-holding or passenger comfort is prioritized. Generally, larger damping values provide better road-holding in comparison to low damping and the opposite is true for passenger comfort.

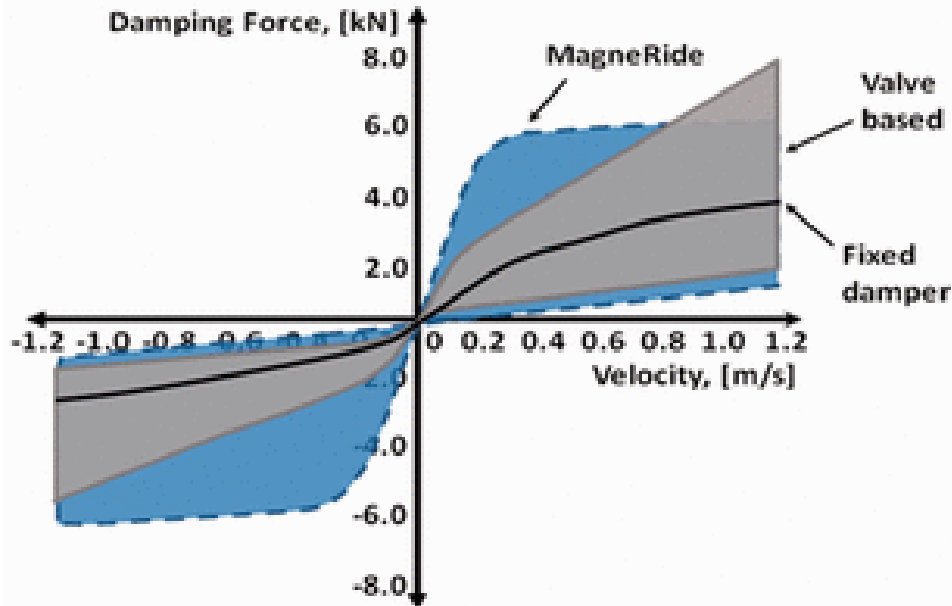


Figure 9. Comparison of *MagneRide* damping characteristic, conventional damper, and a valve-based variable damper [17]

### 3.2.2. Predictive Active Suspension [18]

Audi offered advanced suspension systems in the past. The sports coupe model, *Audi R8*, is offered with an adaptive suspension system which features magnetorheological dampers since 2006. The luxury sedan A8 was offered with a self-levelling air suspension system and continuous damper control in its 2<sup>nd</sup> generation since 2002.

The 4<sup>th</sup> generation *Audi A8* (2018) is offered with a slow-active suspension which features road preview. Each wheel corner features an electric motor connected to the suspension linkage via a strain wave transmission and link. As shown in Figure 10, the electric motor is connected to the strain wave transmission via a rubber belt, due to packaging constraints. The transmission output forces are transferred to the wheel via a link which connects to the suspension wishbones. They cause vertical wheel load increase or decrease, depending on the operation mode. Additionally, the electric motor can operate as a generator and recuperate the energy back into the 48V battery.

The A8 *Predictive Active Suspension* features advanced capabilities, for example the *Pre sense 360* in the event of an impending high-speed side impact will raise the chassis by up to 80 mm on the side of the impact, so that the sill takes the brunt of the impact instead of the door. This minimizes the cabin deformation, as the chassis absorbs a greater amount of kinetic energy, which in turn protects the passengers. During door handle operation, the *Elevated entry* feature causes the chassis to rapidly rise by 50 mm to provide greater comfort for the passenger during getting in or out of the vehicle.

The active system features a 2 kW electric actuator for every wheel, which produces forces up to 3,7 kN at the wheel using an advanced reduction system. The maximum force gradient is 16 kN/s and the actuator bandwidth is 6 Hz. From the consumption standpoint, the system consumes up to 60 W in a city environment and up to 250 W on rough roads. The low power consumption is possible due to the vehicle static weight being supported by air springs. The controller calculates the next actuation step every 5 ms, using road preview data up to 20 m ahead of the vehicle with a resolution of 3 to 16 cm.

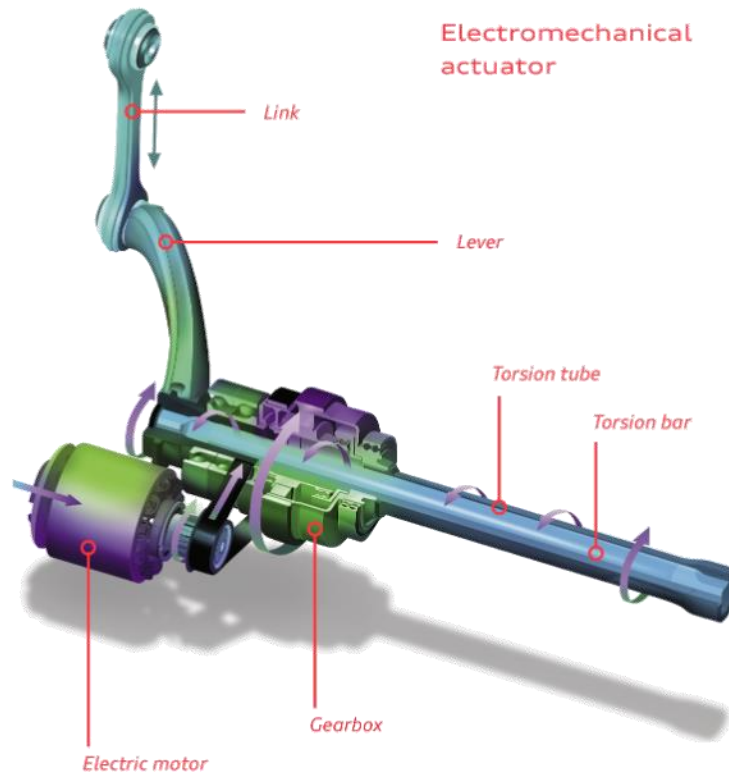


Figure 10. Audi A8 (2018) Active suspension front axle system components [19]

### 3.2.3. E-Active Body Control (Mercedes-Benz)

The most recent development from *Mercedes-Benz*, implemented on the *GLE* (2018) model, is a slow-active suspension system. The *E-ABC* features air springs and adjustable dampers - which are connected to an electric pump and hydraulic accumulators, as shown in Figure 11. The electric pump enables the use of the damper as a hydraulic cylinder, as it can alter the damper force and position in a relatively fast manner (bandwidth up to 5 Hz). The air spring carries the static vehicle load and is used for load-levelling. The active system can produce vertical forces up to 7 kN at the wheels, with a dynamic response of up to 24 kN/s. Power consumption is 150 W on average, but the system can require up to 13 kW in extreme events. On higher excitation frequencies, the response is dominated by the mechanical properties of the passive system. The *E-ABC* differs from the *MBC* due to it featuring a design in which the hydraulic system is pressurized by an electric pump mounted on the chassis [20].



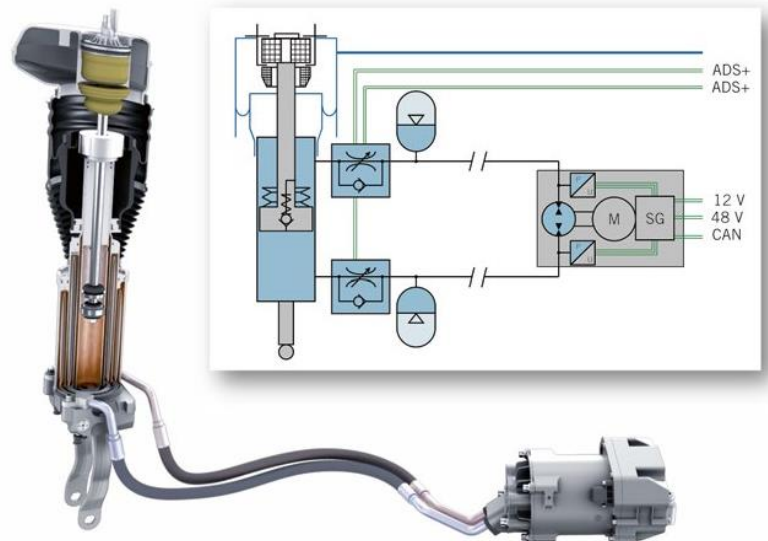


Figure 11. Mercedes-Benz GLE Slow-active suspension system components [20]

### 3.3. Current control system developments

#### 3.3.1. Model predictive control

Due to the increasing performance of vehicle computers and recent findings regarding optimization algorithms, the application of model predictive control (abbr. MPC) is being investigated. MPC relies on optimizing the response of a dynamical model which represents the controlled system. The optimization of control trajectories is carried out on a finite horizon – called the prediction horizon. The control variables are set to the optimized values of the first prediction step, which corresponds to the current time step of the controller, while the optimization is carried out for the next time step. Therefore, fast real-time optimization is required for small sample times used in active suspension controllers to improve the suspension performance [17].

In [21], new road height profile generation methods are presented. The active suspension control combines feedforward disturbance compensation (calculated from the road preview signal) with a feedback loop without preview and preview model predictive control.

An approach including semi-active suspension optimal control, known model parameters and full-state feedback is presented in [22], which gives better performance than *Skyhook* and clipped-optimal LQR approaches in a series of test-cases.

#### 3.3.2. Fuzzy logic

*Fuzzy logic* system output is defined as a combination of the input variables and rules prescribed to them. By weighing the rules, the effect of rules on the output can be varied. The weighing factors can be static (constant) or dynamic (dependent on other rules). This gives possibility for weighing factor optimization to improve the system response. *Fuzzy logic* makes way for the design of a control system based on a limited sensor suite and can be used to implement functional safety in the event of measurement sensor failure. Due to these capabilities, it has become a popular approach for control of nonlinear systems with parameter uncertainties [17].

In [23] it was shown that a *fuzzy logic* controller equipped with a limited sensor suite can achieve performance close to the theoretical optimum defined by the clipped-optimal LQR controller.



## 4. FULLY-ACTIVE CONTROL SYSTEM DESIGN

In this chapter, a fully-active suspension controller design is presented. Two different controllers are considered: an optimal controller and a reduced-order controller. The optimal controller uses full state feedback, which may not be available in the vehicle and thus requires estimation. The reduced-order controller relies on available sensor suite signals and presents a practical controller. The design of both controllers is based on a two degree-of-freedom quarter car model.

### 4.1. Design requirements

The KPIs are defined as variances of physical quantities which correlate with suspension design requirements. The variance statistical quantity is defined as the average squared deviation of the mean value of a given vector. The variance can be calculated also by squaring the standard deviation.

The ride comfort KPI is defined as variance of sprung mass acceleration (see Figure 12):

$$Var(\dot{x}_4) = \frac{1}{n} \sum_{i=1}^n (\dot{x}_{4,i} - \mu_{\dot{x}_4})^2, \quad (4.1)$$

where  $\dot{x}_{4,i}$  is the sprung mass acceleration.  $\mu_{\dot{x}_4}$  is the mean value of the sprung mass acceleration, and is calculated:

$$\mu_{\dot{x}_4} = \frac{1}{n} \sum_{i=1}^n \dot{x}_{4,i}. \quad (4.2)$$

As the model is built in a simulation environment, the tyre deflection ( $x_1$ ) can be used as a road-holding KPI and part of the cost function as well.

The road-holding KPI is defined as variance of tyre deflection:

$$Var(x_1) = \frac{1}{n} \sum_{i=1}^n (x_{1,i} - \mu_{x_1})^2, \quad (4.3)$$

where  $x_{1,i}$  is the tyre deflection value for the data index  $i$ .  $\mu_{x_1}$  is the mean value of the tyre deflection, and is calculated:

$$\mu_{x_1} = \frac{1}{n} \sum_{i=1}^n x_{1,i}. \quad (4.4)$$

The suspension deflection (travel) constraint KPI is defined as variance of suspension deflection  $x_3$ :

$$Var(x_3) = \frac{1}{n} \sum_{i=1}^n (x_{3,i} - \mu_{x_3})^2, \quad (4.5)$$

where  $x_{3,i}$  is the suspension deflection value for the data index  $i$ .  $\mu_{x_3}$  is the mean value of the suspension deflection, and is calculated:

$$\mu_{x_3} = \frac{1}{n} \sum_{i=1}^n x_{3,i}. \quad (4.6)$$

Smaller values of the defined KPIs ( $Var(\dot{x}_4)$ ,  $Var(x_1)$  and  $Var(x_3)$ ) result in better suspension system performance.

## 4.2. Quarter vehicle model

The two degree of freedom vehicle model, shown in Figure 12, is most frequently used to describe quarter vehicle assembly vertical dynamics. It gives an accurate and simple approximation of vertical vibrations for the range of excitation frequencies up to 30 Hz. For higher excitation frequencies, the vibrational response is affected by the suspension bushings and structural properties of the vehicle components. As it provides a solid base for primary and secondary ride analyses, the two degree-of-freedom quarter vehicle model is used in this thesis to model and tune a quarter vehicle suspension controller, which is later implemented into a full-vehicle simulation model (Chapter 6).

The linearized model used in this thesis allows for model-based control system design and analysis. Generally, vehicle parameters are rarely constant, and there are additional components not included in the two degree-of-freedom quarter vehicle model such as end stops, anti-roll bars and suspension bushings which cause nonlinearities in the kinematics of the wheel movement, ride stiffness and damping characteristics. Therefore, it is of importance that the unmodelled components have a small or insignificant influence on the response in regular driving conditions.

Assumptions introduced by the implementation of a simplified and linearized quarter vehicle model are:

- constant spring stiffness and linear damper characteristics,
- constant tyre stiffness and damping value,
- bump stops, rebound stops, suspension bushings and their effects on suspension vibrational, stiffness and damping properties are not modelled,
- suspension kinematics are disregarded, including the suspension actuation motion ratio,
- anti-roll bars coupling the opposite wheels are not modelled.

The basic two degree-of-freedom model includes a fully-active suspension actuator that acts between the spring and unsprung mass with a force  $U$ , which is positive when compressive.

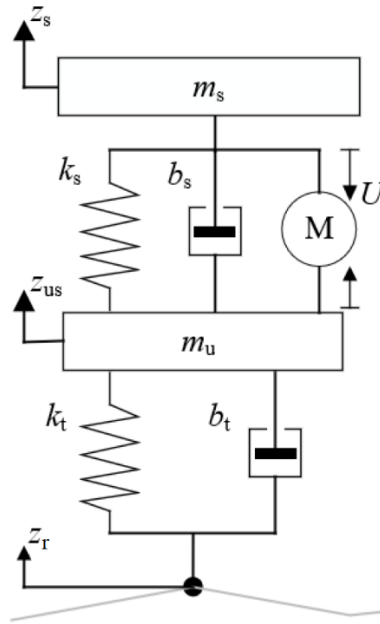


Figure 12. Two degree-of-freedom quarter vehicle model [3]

The two degree-of-freedom dynamic model is described by the following vertical balance equations of the sprung and unsprung masses:

$$m_u \ddot{z}_u = -k_t(z_u - z_r) - b_t(\dot{z}_u - \dot{z}_r) + k_s(z_s - z_u) + b_s(\dot{z}_s - \dot{z}_u) + U - m_u g, \quad (4.7)$$

$$m_s \ddot{z}_s = -k_s(z_s - z_u) - b_s(\dot{z}_s - \dot{z}_u) - U - m_s g, \quad (4.8)$$

where  $z_r$ ,  $z_u$  and  $z_s$  are the vertical positions of the road profile, unsprung mass and sprung mass.  $\dot{z}_r$ ,  $\dot{z}_u$  and  $\dot{z}_s$  are the vertical speeds of the road profile, unsprung mass and sprung mass.  $\ddot{z}_u$  and  $\ddot{z}_s$  are the vertical accelerations of the unsprung mass and sprung mass. Vehicle model parameters used for analyses in this thesis are given in Table 1. They reflect a fully-electric sports utility vehicle (BEV SUV).

Table 1. Quarter vehicle model vehicle parameters

| Symbol | Parameter name              | Value  | Unit |
|--------|-----------------------------|--------|------|
| $m_s$  | Sprung mass                 | 621,75 | kg   |
| $m_u$  | Unsprung mass               | 45     | kg   |
| $k_s$  | Suspension spring stiffness | 31000  | N/m  |
| $b_s$  | Suspension damping          | 1830   | Ns/m |
| $k_t$  | Tyre vertical stiffness     | 426970 | N/m  |
| $b_t$  | Tyre vertical damping       | 0      | Ns/m |

### 4.3. Optimal control [24]

The prerequisites for optimal control theory are that the system dynamics can be accurately described by a set of ordinary differential equations. Its goal is to control a dynamic system in a way which minimizes the cost function, typically defined in quadratic form. This gives a linear quadratic problem and a linear quadratic regulator.

The application of a linear quadratic regulator is possible when all state variables are measured or estimated. The design of a linear quadratic regulator is based on the state-space representation of system dynamics and quadratic cost function which sets the trade-off between different criteria.

Consider a discrete-time linear system:

$$x_{k+1} = \mathbf{A}x_k + \mathbf{B}u_k, \quad (4.9)$$

where  $u_k$  is the  $k$ -indexed step input vector,  $x_k$  is the  $k$ -indexed step state vector,  $x_{k+1}$  is the  $(k+1)$ -indexed step state vector,  $\mathbf{A}$  is the state matrix and  $\mathbf{B}$  is the input matrix.

The optimal state feedback control law for system (4.9):

$$u_k = -\mathbf{K}x_k, \quad (4.10)$$

is obtained by minimizing the linear quadratic cost function defined as [24]:

$$J = \sum_{k=0}^{\infty} (x_k^T \mathbf{Q}x_k + u_k^T \mathbf{R}u_k + 2x_k^T \mathbf{N}u_k), \quad (4.11)$$

where  $\mathbf{Q}$  is the positive-semidefinite symmetric weighing matrix which penalizes the state variables,  $\mathbf{R}$  is the positive-definite weighing matrix which penalizes the control variables,  $\mathbf{N}$  is the weighing matrix which penalizes combinations of state variables and control variables.

The controller gain vector is calculated as:

$$\mathbf{K} = (\mathbf{R} + \mathbf{B}^T \mathbf{P} \mathbf{B})^{-1} (\mathbf{B}^T \mathbf{P} \mathbf{A} + \mathbf{N}^T), \quad (4.112)$$

where  $\mathbf{P}$  is the unique, positively-definite solution of the discrete algebraic Riccati equation:

$$\mathbf{P} = \mathbf{A}^T \mathbf{P} \mathbf{A} - (\mathbf{A}^T \mathbf{P} \mathbf{B} + \mathbf{N})(\mathbf{R} + \mathbf{B}^T \mathbf{P} \mathbf{B})^{-1} (\mathbf{B}^T \mathbf{P} \mathbf{A} + \mathbf{N}^T) + \mathbf{Q}. \quad (4.123)$$

For design of active suspension optimal controller, the quarter vehicle model given by (4.7) and (4.8) is transformed to the state-space representation as follows:

$$\begin{bmatrix} \dot{x}_1 \\ \dot{x}_2 \\ \dot{x}_3 \\ \dot{x}_4 \end{bmatrix} = \begin{bmatrix} 0 & 1 & 0 & 0 \\ -\frac{k_t}{m_u} & -\frac{b_s + b_t}{m_u} & \frac{k_s}{m_u} & \frac{b_s}{m_u} \\ 0 & -1 & 0 & 1 \\ 0 & \frac{b_s}{m_s} & -\frac{k_s}{m_s} & -\frac{b_s}{m_s} \end{bmatrix} \begin{bmatrix} x_1 \\ x_2 \\ x_3 \\ x_4 \end{bmatrix} + \begin{bmatrix} 0 \\ \frac{1}{m_u} \\ 0 \\ -\frac{1}{m_s} \end{bmatrix} U + \begin{bmatrix} -1 \\ \frac{b_t}{m_u} \\ 0 \\ 0 \end{bmatrix} w, \quad (4.134)$$

where the state variables  $x_1, x_2, x_3, x_4$  are presented in Table 2. The control input is defined as  $U$  (actuator force) and the disturbance vector  $w$  is ground velocity for which  $w = \dot{z}_r$  holds.

Table 2. Optimal controller state variables

| Symbol | State variable name          | Equivalent    | Unit |
|--------|------------------------------|---------------|------|
| $x_1$  | Tyre deflection              | $(z_u - z_r)$ | m    |
| $x_2$  | Unsprung mass vertical speed | $\dot{z}_u$   | m/s  |
| $x_3$  | Suspension deflection        | $(z_s - z_u)$ | m    |
| $x_4$  | Sprung mass vertical speed   | $\dot{z}_s$   | m/s  |

The linear quadratic cost function for active suspension control system design is given as:

$$\min[PI = E(r_1 \cdot x_1^2 + r_2 \cdot x_3^2 + \dot{x}_4^2)]. \quad (4.145)$$

and contains the KPIs which represent the design requirements set on the suspension control system as described in chapter 4.1. The tyre deflection variance and suspension deflection variance are weighted by factors  $r_1$  and  $r_2$ . The weighing factors can be coupled by setting a constant ratio between the weighing factors. In [3], it was concluded that a ratio of tyre deflection to suspension deflection penalization  $r_1/r_2 = 10$  gives a good trade-off between the two criteria. This means that the suspension performance can be set by changing only the tyre deflection weighing factor  $r_1$ .

#### 4.4. Reduced-order control law

The reduced-order controller design is based on more practical state feedback, relying solely on measurable state variables.

Looking into optimal controller state variables (Table 2), tyre deflection ( $x_1$ ) is hard to measure or estimate due to the tyre rotation, as the part of the tyre which is in contact with the ground changes constantly. Also, the tyre contact patch is flexible in more than one dimension in relation to the rim, which leads to the tyre carcass deflection being three-dimensional. The vertical sprung and unsprung mass speeds ( $x_2$  and  $x_4$ ) can be estimated from vertical chassis acceleration and suspension deflection, but a problem arises as the calculation requires an integration of the measured vertical chassis acceleration signal which is prone to “drift” or error accumulation due to measurement noise. Suspension deflection ( $x_3$ ) can be directly measured by using a linear or rotational potentiometer on each suspension strut.

Based on the available sensor suite, which commonly features a vertical chassis acceleration ( $\dot{x}_4$ ) sensor and suspension deflection ( $x_3$ ) sensor for each vehicle corner, the vertical wheel acceleration ( $\dot{x}_2$ ) is estimated as follows:

$$x_5 = \dot{x}_2 = \frac{d^2 z_s}{dt^2} - \frac{d^2 (z_s - z_u)}{dt^2} = \dot{x}_4 - \ddot{x}_3 \quad (4.156)$$

and can be used within the feedback loop together with the directly measured state variables.

Using the practical state variables in the model, the actuator force is calculated as follows:

$$U = -K_1 \cdot x_3 - K_2 \cdot x_5 - K_3 \cdot x_6. \quad (4.167)$$

Where derivations of the two newly introduced state variables,  $x_5$ , and  $x_6$ , respectively are obtained by first-order lag filtering of unsprung and sprung mass accelerations  $\dot{x}_2$  and  $\dot{x}_4$ :

$$\dot{x}_5 = \frac{\dot{x}_2}{T_s} - \frac{x_5}{T_s}, \quad (4.178)$$

$$\dot{x}_6 = \frac{\dot{x}_4}{T_s} - \frac{x_6}{T_s}. \quad (4.189)$$

where  $T_s$  is the filter time constant set at a small value (0,1 ms in this thesis).

The state-space representation of the extended system is:

$$\begin{bmatrix} \dot{x}_1 \\ \dot{x}_2 \\ \dot{x}_3 \\ \dot{x}_4 \\ \dot{x}_5 \\ \dot{x}_6 \end{bmatrix} = \begin{bmatrix} 0 & 1 & 0 & 0 & 0 & 0 \\ -\frac{k_t}{m_u} & -\frac{b_s+b_t}{m_u} & \frac{k_s}{m_u} & \frac{b_s}{m_u} & 0 & 0 \\ 0 & -1 & 0 & 0 & 0 & 0 \\ 0 & \frac{b_s}{m_s} & -\frac{k_s}{m_s} & -\frac{b_s}{m_s} & 0 & 0 \\ -\frac{k_t}{T_s m_u} & -\frac{b_s+b_t}{T_s m_u} & \frac{k_s}{T_s m_u} & \frac{b_s}{T_s m_u} & -\frac{1}{T_s} & 0 \\ 0 & \frac{b_s}{T_s m_s} & -\frac{k_s}{T_s m_s} & -\frac{b_s}{T_s m_s} & 0 & -\frac{1}{T_s} \end{bmatrix} \begin{bmatrix} x_1 \\ x_2 \\ x_3 \\ x_4 \\ x_5 \\ x_6 \end{bmatrix} + \begin{bmatrix} 0 \\ \frac{1}{m_u} \\ 0 \\ -\frac{1}{m_s} \\ \frac{1}{T_s m_u} \\ -\frac{1}{T_s m_s} \end{bmatrix} U + \begin{bmatrix} -1 \\ \frac{b_t}{m_u} \\ 0 \\ 0 \\ 0 \\ 0 \end{bmatrix} w. \quad (4.20)$$

the state variables of system (4.20) are defined in Table 3.

**Table 3. Reduced-order controller state variables**

| Symbol | State variable name                             | Equivalent    | Unit             |
|--------|---|---------------|------------------|
| $x_1$  | Tyre deflection                                 | $(z_u - z_r)$ | m                |
| $x_2$  | Unsprung mass vertical speed                    | $\dot{z}_u$   | m/s              |
| $x_3$  | Suspension deflection                           | $(z_s - z_u)$ | m                |
| $x_4$  | Sprung mass vertical speed                      | $\dot{z}_s$   | m/s              |
| $x_5$  | Unsprung mass vertical acceleration measurement | $\ddot{z}_u$  | m/s <sup>2</sup> |
| $x_6$  | Sprung mass vertical acceleration measurement   | $\ddot{z}_s$  | m/s <sup>2</sup> |

## 4.5. Control system parameter optimization

The reduced-order controller control law (ROC) gain vector optimization is based on the expanded quarter vehicle model (4.20) using the vehicle parameters defined in Table 1. The *Python* programming language provides a solid base for optimization and dynamic system simulation, due to the availability of packages which include global optimization and ordinary differential equation (abbr. ODE) solvers. An optimization script was designed which includes a two degree-of-freedom dynamic system simulation. The control law is given in equation 4.17. The road profile excitation is a 2 mm sine wave of continuously increasing frequency from 0,1 to 20 Hz, shown in Figure 22 d. Using the *odeint* [25] function, the simulation is solved numerically. With a solving time of circa 5 s for a frequency response analysis, this simulation tool enables a relatively fast optimization of suspension controller gains  $K_1$ ,  $K_2$  and  $K_3$ .

Before the optimization procedure, the design space is explored by iterating the values of the optimization parameters (gain vector components). The response of the two degree-of-freedom model is checked and the combinations of optimization parameters which cause unstable model response are disregarded by limiting the design space by boundary conditions.

For the reduced-order controller gain optimization, the boundary conditions are set to:

$$-5000 \leq K_1 \leq 5000,$$

$$-50 \leq K_2 \leq 50,$$

$$-3500 \leq K_3 \leq 1000.$$

A part of the *SciPy* package for the Python programming language, the optimization algorithm Constrained Optimization by Linear Approximation (*COBYLA*) [26] is used in this thesis for reduced-order controller gain optimization. This optimization algorithm is a derivative-free trust region method that uses linear approximation models of the objective function. The objective function is evaluated at every optimization iteration and used to define a cost function approximation in the area, which leads to the calculation of the next iteration step. The optimization objective function is equivalent to Equation 4.15, with the squared terms being replaced with variances of the signals.

To validate the optimization procedure accuracy, an optimization of the LQR-like control law [3] was performed and results were compared with the algebraic solution (obtained using Eq. 4.11). The comparison resulted in a cost function difference within 0,2 % and individual KPI weighing with differences in similar range, which confirms the accuracy of the given optimization algorithm.

Since an identical cost function and weighing factors are used as in the LQR case, three vehicle setups are optimized for the reduced-order controller (ROC) case: handling-oriented, balanced and comfort-oriented. The vehicle setups differ in tyre deflection weighing factor  $r_1$  as shown in Table 4, with the ratio of tyre-to-suspension deflection fixed to  $r_1/r_2 = 10$ . Table 4 also shows the optimized control vector components.

**Table 4. Vehicle setups and corresponding feedback gains for optimal (LQR) and reduced-order controller (ROC)**

|   | Configuration |                  |                  |                 |                  |                  |                 |
|---|---------------|------------------|------------------|-----------------|------------------|------------------|-----------------|
|   | Passive       | FAS LQR Handling | FAS LQR Balanced | FAS LQR Comfort | FAS ROC Handling | FAS ROC Balanced | FAS ROC Comfort |
| Tyre deflection weighing factor ( $r_1$ )       | N/A           | 80000            | 50000            | 30000           | 80000            | 50000            | 30000           |
| Suspension deflection weighing factor ( $r_2$ ) | N/A           | 8000             | 5000             | 3000            | 8000             | 5000             | 3000            |
| Gain $K_1$                                      | N/A           | 4234,12          | -3009,91         | -6597,38        | 54,27            | 0,65             | 9,32            |
| Gain $K_2$                                      | N/A           | -35,82           | -388,25          | -699,83         | -3,42            | 0,07             | 1,82            |
| Gain $K_3$                                      | N/A           | -24476,70        | -12961,60        | -3123,86        | 0,00             | 11,75            | -490,15         |
| Gain $K_4$                                      | N/A           | -6512,12         | -5532,54         | -4628,21        | N/A              | N/A              | N/A             |

#### 4.6. System response comparison for a two degree-of-freedom model

The KPIs of active suspension controller setups (Table 4) and a passive suspension presented in Table 5 are obtained for a *sine sweep* road height profile (from 0,1 to 20 Hz).

When considering handling-oriented setups, both LQR and ROC achieve road-holding KPI improvement of 2,5% and 10% respectively, compared to the passive suspension. However, these setups result in worse ride comfort, where ROC has 25% increased chassis vertical acceleration compared to the passive suspension. Handling setups also somewhat decrease suspension deflection. Better ride comfort is achieved by comfort-oriented setups. ROC comfort setup has the best ride comfort as it decreases vertical acceleration variance by 25%, at the expense of worsened road-holding, which is also higher compared to LQR case. The “balanced” setups show consistently a worse performance than the passive suspension for the considered procedure. Theoretically, for the stochastic road profile in which the excitation frequency bandwidth is infinite, FAS LQR outperforms the passive suspension in at least one KPI [3]. However, for the limited excitation frequencies considered, the balanced LQR performs worse than the passive suspension in terms of combined KPIs. This indicates that when optimizing the suspension performance for a limited excitation frequency range, the FAS LQR does not necessarily perform better than passive suspension.

This data shows the potential of the FAS ROC in suspension control application, which achieves comparable performance to the optimal FAS LQR.



**Table 5. Sine sweep procedure KPIs of passive suspension, linear quadratic regulator (LQR) and reduced-order controller (ROC)**

| KPI [unit]   | Configuration |                  |                  |                 |                  |                  |                 |
|--|---------------|------------------|------------------|-----------------|------------------|------------------|-----------------|
|  | Passive       | FAS LQR Handling | FAS LQR Balanced | FAS LQR Comfort | FAS ROC Handling | FAS ROC Balanced | FAS ROC Comfort |
| Chassis vertical acceleration variance [ $\text{m}^2/\text{s}^4$ ] | 0,272         | 0,319            | 0,276            | 0,231           | 0,340            | 0,317            | 0,205           |
|  | -             | 17,16%           | 1,22%            | -15,32%         | 24,85%           | 16,20%           | -24,60%         |
| Tyre deflection variance [ $\text{m}^2$ ]                          | 3,9E-06       | 3,8E-06          | 5,0E-06          | 6,8E-06         | 3,5E-06          | 3,8E-06          | 8,2E-06         |
|  | -             | -2,49%           | 29,05%           | 75,53%          | -9,98%           | -2,05%           | 110,78%         |
| Suspension deflection variance [ $\text{m}^2$ ]                    | 5,1E-06       | 4,8E-06          | 6,0E-06          | 7,9E-06         | 5,0E-06          | 5,0E-06          | 9,5E-06         |
|  | -             | -6,64%           | 18,20%           | 54,28%          | -2,17%           | -1,95%           | 86,51%          |

## 5. SEMI-ACTIVE CONTROL SYSTEM DESIGN

This section presents the design of an optimal semi-active suspension control system based on the clipped-optimal approach which is used as a benchmark for a practical semi-active suspension system controller. Then, two practical semi-active suspension control systems based on the *Skyhook* logic are presented.

### 5.1. Clipped-optimal LQR control

The clipped-optimal LQR control is based on the fully-active suspension LQR control law. Due to semi-active systems only being able to generate dissipative forces, the demand damper force must be “clipped” to only include forces acting opposite to the controllable damper compression speed, i.e. to satisfy the damper passivity constraint  $U(x_4 - x_2) \geq 0$  [3].

### 5.2. *Skyhook* suspension control

The *Skyhook* suspension control logic is a semi-active suspension control strategy with the goal of minimizing vertical oscillations of the chassis. Theoretically, this strategy tries to mimic a damper connecting the chassis and sky as shown in Figure 13 [27].

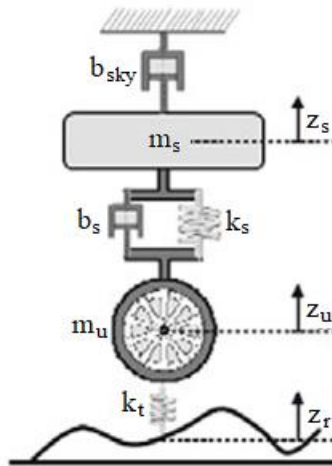


Figure 13. *Skyhook* principle schematic [27]

The implementation of a *Skyhook* damper  $b_{sky}$  is not practically possible, so an equivalent damping value for the suspension damper  $b_s$  is calculated as follows:

$$F_{sky} = b_{sky} \cdot v_{body} = b_s \cdot v_{rel} \quad (5.1)$$

$$b_s = b_{sky} \cdot \frac{v_{body}}{v_{rel}} \quad (5.2)$$

where  $F_{sky}$  is the *Skyhook* damping force,  $b_{sky}$  is the *Skyhook* damping,  $v_{body} = \dot{z}_s$  is the body vertical speed,  $b_s$  is the suspension damping and  $v_{rel} = \dot{z}_s - \dot{z}_u$  is the body and wheel relative vertical speed.

The equivalent suspension damping value calculated by Equation 5.2 varies continuously with the ratio of chassis vertical speed and damper extension speed. A semi-active suspension that closely follows a reference *Skyhook* damping requires a continuously variable controlled damper. However, the required damping value may in some cases be negative or close to 0.

Such low damping values are hard to achieve using any controllable hydraulic-based damper which relies on fluid flow restriction. Therefore, following the logic of Equation 5.2, the damping will be adjusted to a high damping value during wheel and chassis relative opposite-direction travel or low speed same-direction travel. In the case of higher speed same-direction wheel and chassis travel, the damper will be set to a low damping value [27].

In [2], a few semi-active suspension control logic types based on the *Skyhook* principle are presented, which differ in damper controllability and sensor suite requirements. *Skyhook* control strategies generally focus on passenger ride comfort, with limited road-holding improvement capability.

A simple *Skyhook* two-state (*SH-2*) logic is presented [2], which requires two-state adjustable dampers, a vertical chassis speed sensor for each wheel and a vertical suspension deflection sensor. The more advanced *Skyhook-Linear* (*SH-Linear*) logic requires continuously adjustable dampers in combination with the same sensor suite as the *SH-2* logic. The continuously controllable damper is limited in terms of achievable damping values as shown in Figure 14, which range from  $b_{min}$  to  $b_{max}$ .

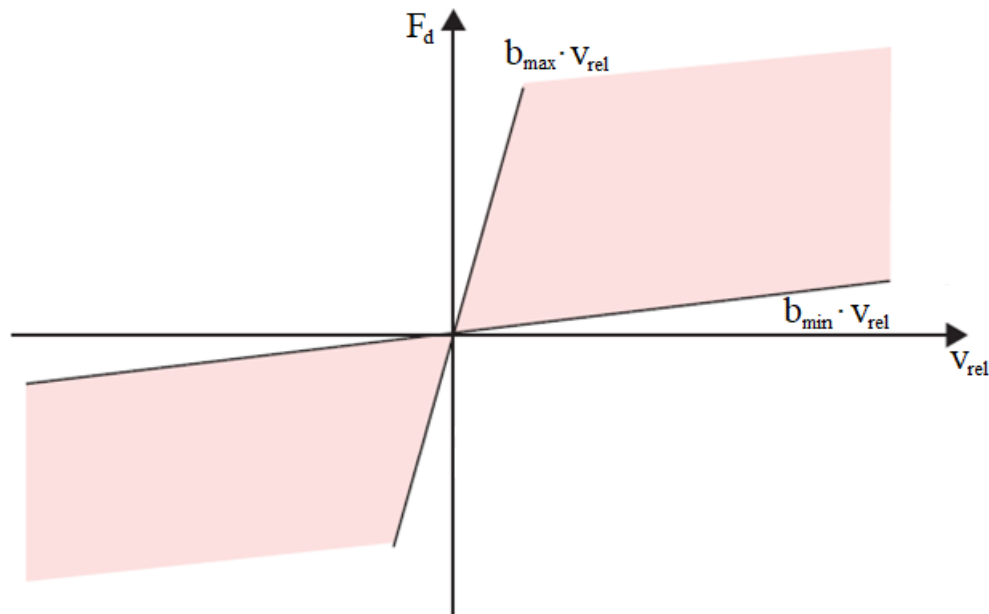


Figure 14. Damping force range of the continuously controllable damper [2]

The *SH-Linear* approach is used in this thesis in the practical semi-active suspension controller design. This controller approximates the *Skyhook* logic within the damping limits that the system can achieve, with a tuning parameter used to manage the trade-off between comfort and handling:

$$b_s = \begin{cases} b_{min} & \text{if } \dot{z}\dot{z}_{def} \leq 0, \\ Sat_{b_s \in [b_{min}, b_{max}]} \left( \frac{\alpha b_{max} \dot{z}_{def} + (1 - \alpha) b_{max} \dot{z}}{\dot{z}_{def}} \right) & \text{if } \dot{z}\dot{z}_{def} > 0. \end{cases} \quad (5.3)$$

The tuning parameter  $\alpha$  (ranging from 0 to 1) has an influence on the higher damping value, which continuously changes depending on the vertical chassis speed and suspension deflection speed. As described in [2], when set to  $\alpha = 0$ , the controller prioritizes passenger comfort due to continuous transition from lower to higher damping values and vice-versa. When setting the tuning parameter closer to 1, the road-holding is prioritized. If the tuning parameter is set to

$\alpha = 1$ , the logic is equivalent to *SH-2*, as the second addend in the calculation of the higher damping value in equation 5.3 is zeroed-out [2].

According to [28], an acceptable range of damping ratio ( $\zeta$ ) for a continuously variable damper is in the range of 0,045 to 0,4.

The suspension damping can be approximated using the following equation which is valid for a single mass system:

$$b_s = \zeta \cdot 2\sqrt{k_s m_s}, \quad (5.4)$$

where  $\zeta$  is the suspension damping ratio.

The damping value lower and upper boundaries are calculated using vehicle parameters given in Table 1.:

$$b_{min} = \zeta_{min} \cdot 2\sqrt{k_s m_s} = 0,045 \cdot 2\sqrt{31000 \cdot 621,75} = 409,17 \text{ Ns/m}, \quad (5.5)$$

$$b_{max} = \zeta_{max} \cdot 2\sqrt{k_s m_s} = 0,4 \cdot 2\sqrt{31000 \cdot 621,75} = 3637,08 \text{ Ns/m}. \quad (5.6)$$

## 6. CO-SIMULATION ENVIRONMENT

The suspension control systems are implemented into an advanced simulation environment, to enable control system verification in a full vehicle vertical dynamics simulation model including lateral dynamics in various ride and handling procedures.

Figure 15 shows the co-simulation setup consisting of *AVL VSM*<sup>TM</sup> and *MatLab*<sup>®</sup>/*Simulink*<sup>®</sup>. The full vehicle simulation model including test procedures is implemented within *AVL VSM*<sup>TM</sup>, while the suspension controller and actuator dynamics are implemented in *Simulink*<sup>®</sup>. Details of each co-simulation component are described in the following subsections.

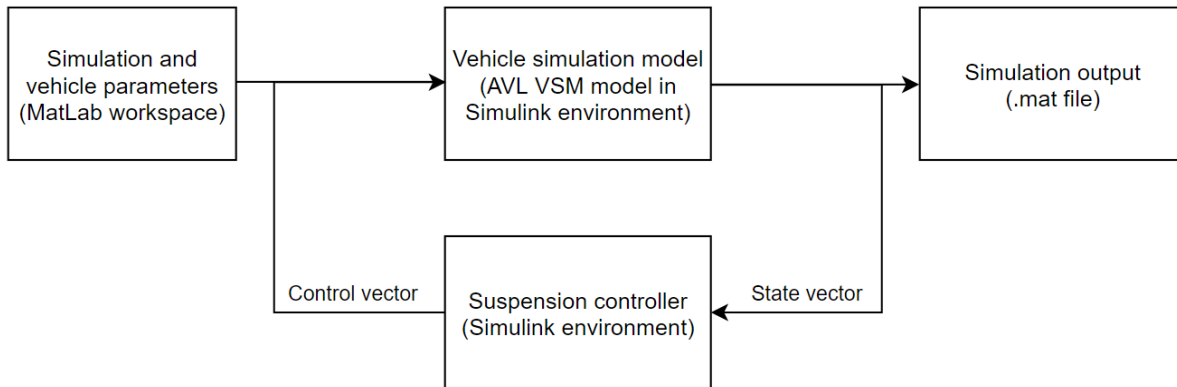


Figure 15. Co-simulation setup

### 6.1. Simulation tools

#### 6.1.1. *AVL VSM*<sup>TM</sup>

*AVL VSM*<sup>TM</sup> provides detailed vehicle model and test procedure modelling capabilities. The software consists of an advanced simulation environment, based on a transient vehicle simulation model. Therefore, vehicle component inertial and damping properties have an influence on the simulation results, which is not the case for steady-state vehicle simulation tools.

Vehicle vertical dynamics are described as a seven degrees-of-freedom vehicle model, illustrated in Figure 16, in which the sprung mass has three degrees of freedom – vertical displacement (heave), roll angular displacement and pitch angular displacement, and the four unsprung masses have a vertical displacement degree-of-freedom each.

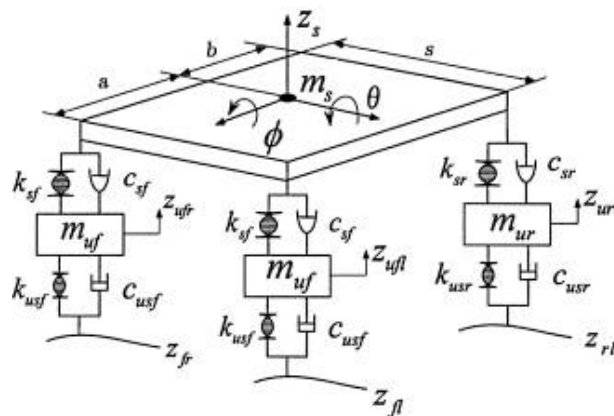
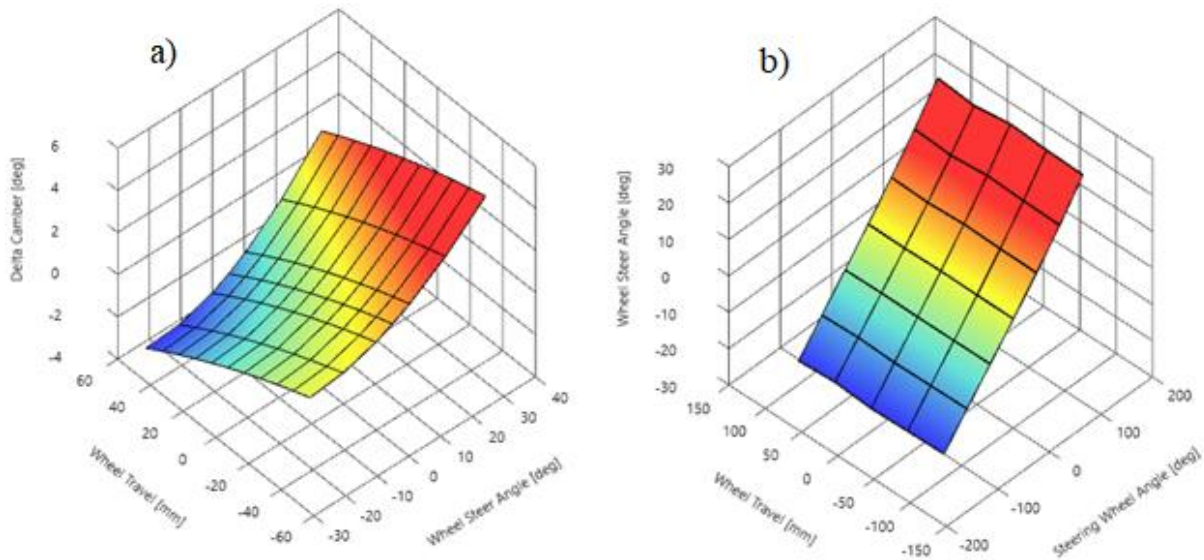


Figure 16. Vertical dynamics full vehicle model (7 DOF) [29]

The *VSM* single-point contact tyre model features advanced *Magic formula* semi-empirical parametrization. It is extensive in terms of longitudinal and lateral dynamics, but regarding vertical dynamics it comes down to the parametrization of vertical tyre stiffness and damping, which are set to constant values. As the quarter vehicle model features constant tyre vertical stiffness and damping values as well, it gives an accurate representation of the tyre model in *VSM* regarding vertical dynamics [30].

Suspension kinematic features in *VSM* are described as maps, obtained from suspension actuation results in a multi-body simulation environment [30]. For the front suspension, which features two degrees of freedom per wheel, vertical travel and front wheel steering rotation, respectively, the following kinematic features must be defined:

- *camber* angle as a function of steering wheel angle and vertical wheel travel, illustrated in Figure 17 a,
- *toe* angle as a function of steering wheel angle and vertical wheel travel, illustrated in Figure 17 b,
- *track* width change as a function of vertical wheel travel,
- *roll center* height as a function of vertical wheel travel,
- *instantaneous center* height as a function of vertical wheel travel,
- *anti-dive* percentage as a function of vertical wheel travel,
- *anti-lift* percentage as a function of vertical wheel travel,
- *caster* angle as a function of vertical wheel travel,
- *kingpin* angle as a function of vertical wheel travel,
- *scrub* radius as a function of vertical wheel travel,
- vertical wheel travel as a function of steering wheel angle (*steer jacking*).



**Figure 17. Main front suspension kinematic features as functions of steering wheel angle and wheel travel: *camber* angle (a) and *toe* angle (b)**

The rear suspension, with only the vertical wheel travel degree of freedom in relation to the chassis, is defined by the following kinematic features as functions of vertical wheel travel:

- *toe* angle
- *camber* angle
- *track* width change,
- *roll center* height,
- *instantaneous center* height,
- *anti-dive* percentage,
- *anti-lift* percentage,

The ride height, static *camber* and *toe* angles are defined as constants for both the front and rear suspension. The front suspension also uses a constant value of *mechanical trail* to calculate the steering wheel torque. The nomenclature regarding suspension kinematics is explained in detail in [27].

The suspension springs stiffness can be set as a constant or displacement-dependent characteristic. The dampers are parametrized by a nonlinear characteristic of damper force with respect to the damper's relative velocity. The anti-roll bar properties are most simply set by defining the anti-roll bar stiffness and damping in relation to wheel travel – keeping in mind that they are only actuated during opposite wheel travel of the same axle. Bump stops and rebound stops are actuated when the suspension travel exceeds defined limits. Their stiffness and damping are set as functions of wheel travel.

In the test procedures the vehicle follows a given path by using the VSM driver model (position, curvature or saturation controlled) and demand longitudinal acceleration or vehicle speed. Alternatively, the accelerator pedal position, brake pressure, steering wheel angle can be defined by the user for each time step or distance section of the track.

The road height profile is set as a function of distance or time of *Manoeuvre designer* type test procedures for each wheel independently. This means that for a realistic response, the vehicle's wheelbase length must be added as a distance (or time at a certain driving speed) offset for the rear wheels. *Stage* and *Circuit* type test procedures have the possibility to use stochastic noise as the road height profile, which is used in *lane change* and *Hockenheim short lap* time simulation test procedures to simulate a realistic road texture.

### 6.1.2. *MatLab*<sup>®</sup> / *Simulink*<sup>®</sup>

As *AVL VSM*<sup>™</sup> offers co-simulation capability with *Simulink*<sup>®</sup>, the vehicle model can be extended to feature custom vehicle control systems. The simulation data signals, which contain vehicle, track, driver and general simulation data, can be directly used within the closed-loop control or to estimate additional state variables. *AVL VSM*<sup>™</sup> features a passive suspension model, therefore the *Simulink*<sup>®</sup> model will be used to extend the functionality of the *VSM* vehicle model by implementing advanced suspension controllers.

External spring and damper forces can be fed back into the *VSM* vehicle model. As advanced suspension systems generally feature regular coil springs, the modelling approach in this case is to use only external dampers as the fully-active suspension active force source with additional passive damping, while in the semi-active suspension case only the controllable damper force is fed into the *VSM* vehicle model.

### 6.1.3. Full vehicle simulation model

With the availability of sprung mass vertical acceleration and suspension deflection measurement signals for each wheel, the unsprung mass vertical acceleration can be estimated by Equation 4.16. The estimated signal is not prone to additional noise and offset, as it is calculated from signals which already contain both artefacts, as well as the sensor anti-aliasing filter.

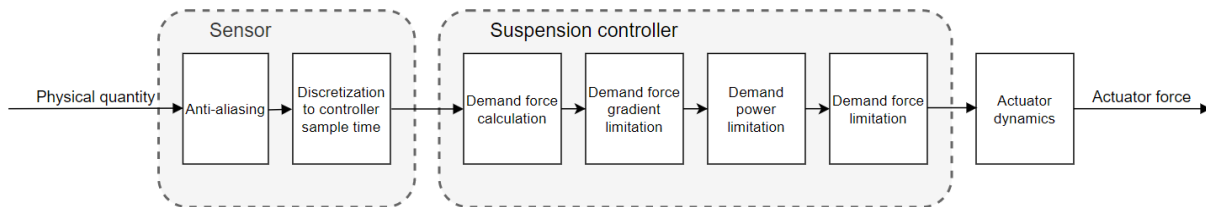
## 6.2. Controller implementation

The general approach in this thesis is equipping vehicle corners with suspension controllers which use its corresponding corner's state variables as feedback. This approach is used in the design of the fully-active optimal and practical controllers (described in Chapter 4), as well as the semi-active clipped-optimal and practical controllers (described in Chapter 5).

### 6.2.1. Fully-active suspension controller

The optimal fully-active suspension controller (Chapter 4.3) is implemented without actuator dynamics in terms of actuator time lag, force or power limitation. This way, the optimal controller serves as a benchmark for any fully-active model-based controller without road preview.

The practical fully-active suspension controller is based on the quarter-car model-based reduced-order controller described in Chapter 4. The measurable signals feature noise and signal offset to test the robustness of the controller. Anti-aliasing filters are implemented on directly measurable signals to model the sensor filtering (Figure 18). The controllers are implemented in discrete-time form with sample time modelled as Zero-order hold.



**Figure 18. Layout of the sensor, fully-active suspension controller and actuator dynamics *Simulink*® model**

Analogue sensor measurements typically contain high-frequency noise which is filtered out using anti-aliasing filters placed before analogue-to-digital conversion. Typically, aliasing occurs due to the digitalization of signals which have a frequency larger than half of the sampled frequency of the digital system. This is referred to as the *Nyquist frequency*. A simple way to implement anti-aliasing is by using a low-pass filter (abbr. LPF). The low-pass filter is therefore implemented with a sample time calculated from the *Nyquist frequency* in relation to the controller [31] – which is 0,005 s.

In continuous time domain, the low-pass filter is defined by the transfer function:

$$G_{Cont.}(s) = \frac{K_{LPF}}{T_{LPF} \cdot s + 1}. \quad (6.1)$$

where  $s$  is the continuous transfer function variable,  $T_{LPF}$  is the lag time constant which defines the cut-off frequency ( $f_{LPF} = \frac{1}{2 \cdot \pi \cdot T_{LPF}}$ ) and it is set to 0,005 and  $K_{LPF}$  is the filter amplification set to 1.



In discrete time domain, the low-pass filter is defined as:

$$G_{Discr.}(z) = K_{LPF} \frac{(T_s/T_{LPF})z^{-1}}{1 + (T_s/T_{LPF} - 1)z^{-1}}. \quad (6.2)$$

where  $z$  is the discrete transfer function variable,  $T_s$  is the simulation sample time set to 0,0005 s [30].

The A/D conversion of measured signals is carried out by using Zero-order hold (abbr. ZOH) blocks. They keep the signal value constant for a pre-defined sample time. In this model the *ZOH* sample time is set to 0,01 s, which corresponds to the suspension controller sample time.

The actuator dynamics are modelled using a discrete first-order lag. The actuator lag time constant is calculated from the actuator bandwidth as  $T_{ACT} = \frac{1}{2 \cdot \pi \cdot f_{BW}}$ . The reduced-order fully-active controller (FAS ROC) has a lag time constant of ~0,032 s (which equals 5 Hz actuator bandwidth). The actuator produces a maximum force of 7 kN, with a maximum gradient of 13 kN and 13 kW power (in alignment with the *E-ABC* system description [20]).

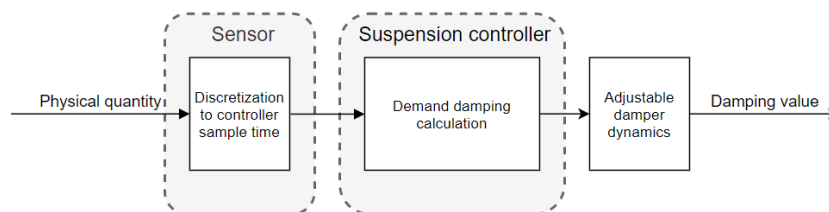
### 6.2.2. Semi-active suspension controller

The clipped-optimal semi-active suspension controller is implemented without actuator dynamics in terms of actuator time lag, force or power limitation and serves as a performance benchmark for semi-active model-based controller without road preview.

The semi-active practical controller operates by using the logic described in Chapter 5. It features independent chassis corner control, which means that measurement signals for the chassis corner are used as inputs into the controller suspension controller, which uses them to calculate the demand damping value (and force) for the individual continuously variable suspension damper.

As with the fully-active practical controller, the A/D conversion is modelled with *ZOH* blocks on the measurement signals, to fit into a realistic digital controller description. For this discretization, a sample time of 10 ms is used.

The high-bandwidth continuously variable dampers are most frequently magnetorheological fluid-based dampers. The semi-active *Skyhook-Linear* controller model (SAS *SH-Lin*) features fluid dynamics modelled using a first-order lag with a time constant of 5 ms (angular frequency of circa 32 Hz). This approximates the gradual transition of damping value that occurs after a change in damper piston magnetic flow and magnetorheological fluid particles alignment. The controllers are implemented in discrete-time form with sample time modelled as Zero-order hold (Figure 19).



**Figure 19.** Layout of the sensor, semi-active suspension controller and actuator dynamics *Simulink*® model

## 7. SIMULATION RESULTS

In this chapter the performance of the practical designed controllers (described in Chapters 4 and 5) is compared with the performance of a passive suspension, optimal fully-active suspension controller (FAS LQR) and a clipped-optimal semi-active suspension controller (SAS LQR) for benchmarking. The practical controller configurations feature realistic actuator dynamics limitations as presented in chapters 6.2.1 and 6.2.2.

The comparison is carried out for two vertical dynamics test procedures – a *sine bump* procedure and a *sine sweep* procedure. Additionally, two handling procedures with stochastic road profiles are considered – a *lane change ISO 3888-1* procedure and *Hockenheim short lap* time simulation.

### 7.1. Vertical dynamics test procedures

The vertical dynamics KPIs defined in Subchapter 4.1 (based on a two degree-of freedom dynamic model) include variances of the vertical chassis acceleration, tyre deflection and suspension deflection. The seven degree-of-freedom full vehicle model gives the possibility to consider chassis pitch acceleration and roll acceleration as passenger comfort metrics. As the road excitation of left and right wheels is synchronized, vertical dynamics procedures do not include the roll acceleration KPI.

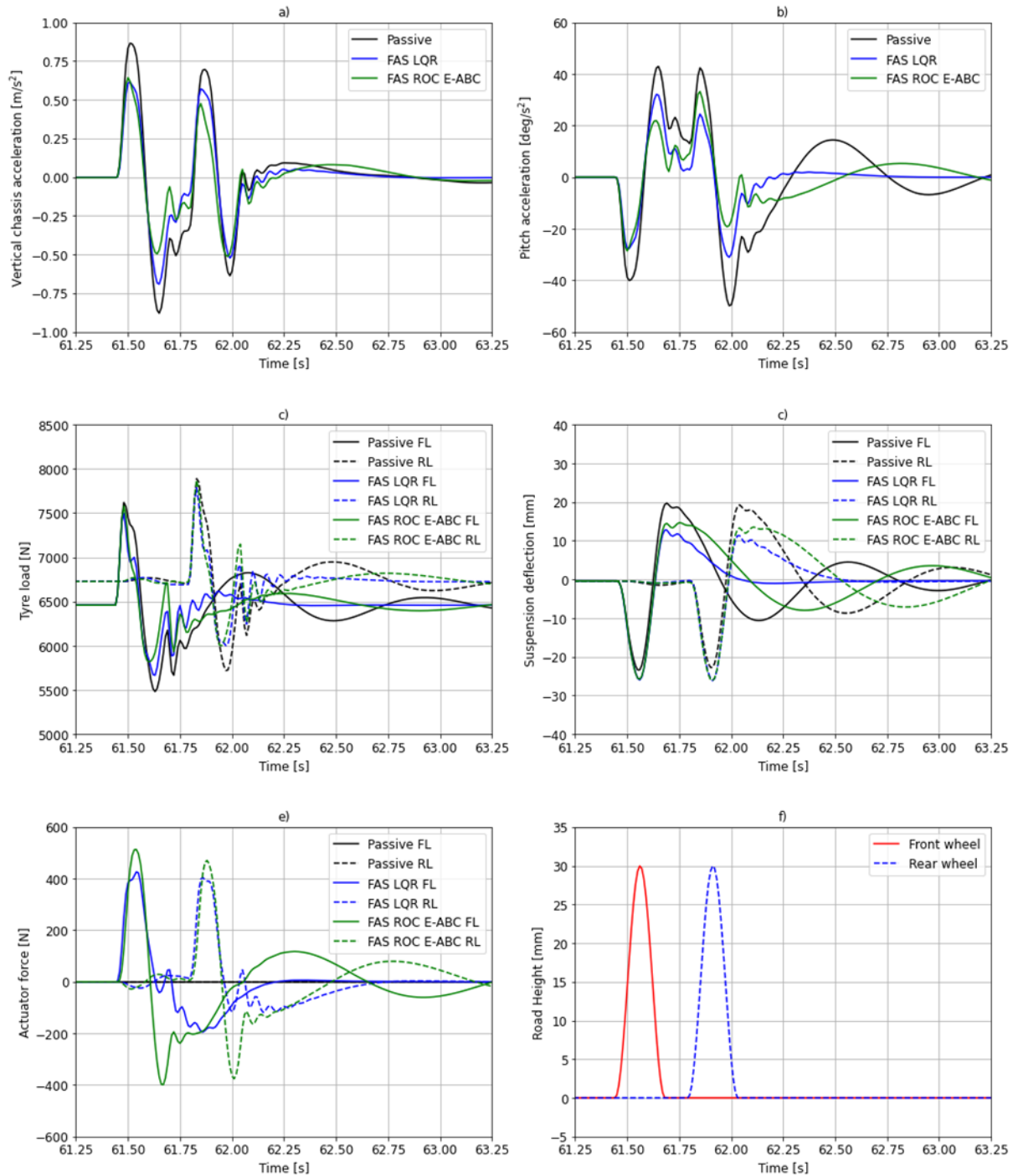
The comparisons illustrated in Figures are carried out for controllers in their comfort setups, while the KPIs of other considered setups (Table 4) are presented in corresponding Tables. In the case of *SH-Linear* controller, the comfort setting corresponds to the tuning parameter set to  $\alpha = 0,5$  – which resulted in better response than for lower  $\alpha$  values (proposed for improved comfort in [2]).

#### 7.1.1. Sine bump

The road profile in this procedure is modelled as a single sine bump (illustrated in Figure 20 f) and the vehicle travels at a predefined constant speed of 30 km/h. With an amplitude of 30 mm, the sine wave approximates a “speed bump”. Even though it is used for the drivers to reduce their driving speed, it provides significant discomfort even at lower vehicle speeds. In this specific case, a 2 m long sine wave at a vehicle speed of 30 km/h, results in the road excitation frequency of 4,2 Hz.

Figure 20 shows the time responses of a passive suspension and the comfort-oriented FAS LQR and FAS ROC, while Figure 21 shows time responses of a passive suspension and comfort-oriented SAS LQR and SAS *SH-Lin*. The KPIs of corresponding simulation results, and additional setups are given in Tables 6 and 7.

Figures 20 a and b show vertical chassis acceleration and chassis pitch acceleration, both of which are decreased in magnitude in FAS LQR and FAS ROC case, and which stabilize faster compared to passive suspension. Both controllers significantly decreased tyre load (Figure 20 c) and suspension deflection (Figure 20 d) variations, and dampen the oscillations faster than passive suspension. Out of the two, the FAS LQR decreases tyre load and suspension deflection, as well as pitch acceleration to a greater extent than the ROC, which is better in suppressing vertical acceleration. Additionally, the FAS LQR requires lower actuator forces, compared to the FAS ROC.



**Figure 20. Time responses of comfort-oriented fully-active suspension controllers and passive suspension for sine bump road excitation**

Key performance indices in Table 6 show that the comfort setups of both the FAS LQR and FAS ROC provide large improvements across all KPIs (up to 70%), except for suspension deflection variance for the FAS ROC – where oscillations occur for a prolonged period (Figure 20 d), but the second peak of deflection (in rebound) is reduced significantly. In terms of KPIs, other FAS LQR setups generally resulted with comfort and road holding improvements (up to 53%), except for chassis vertical acceleration in the handling setup, which degraded by 29,18%. Handling and balanced setups of the FAS ROC did not provide significant improvements of the response in this test procedure in terms of KPI values.

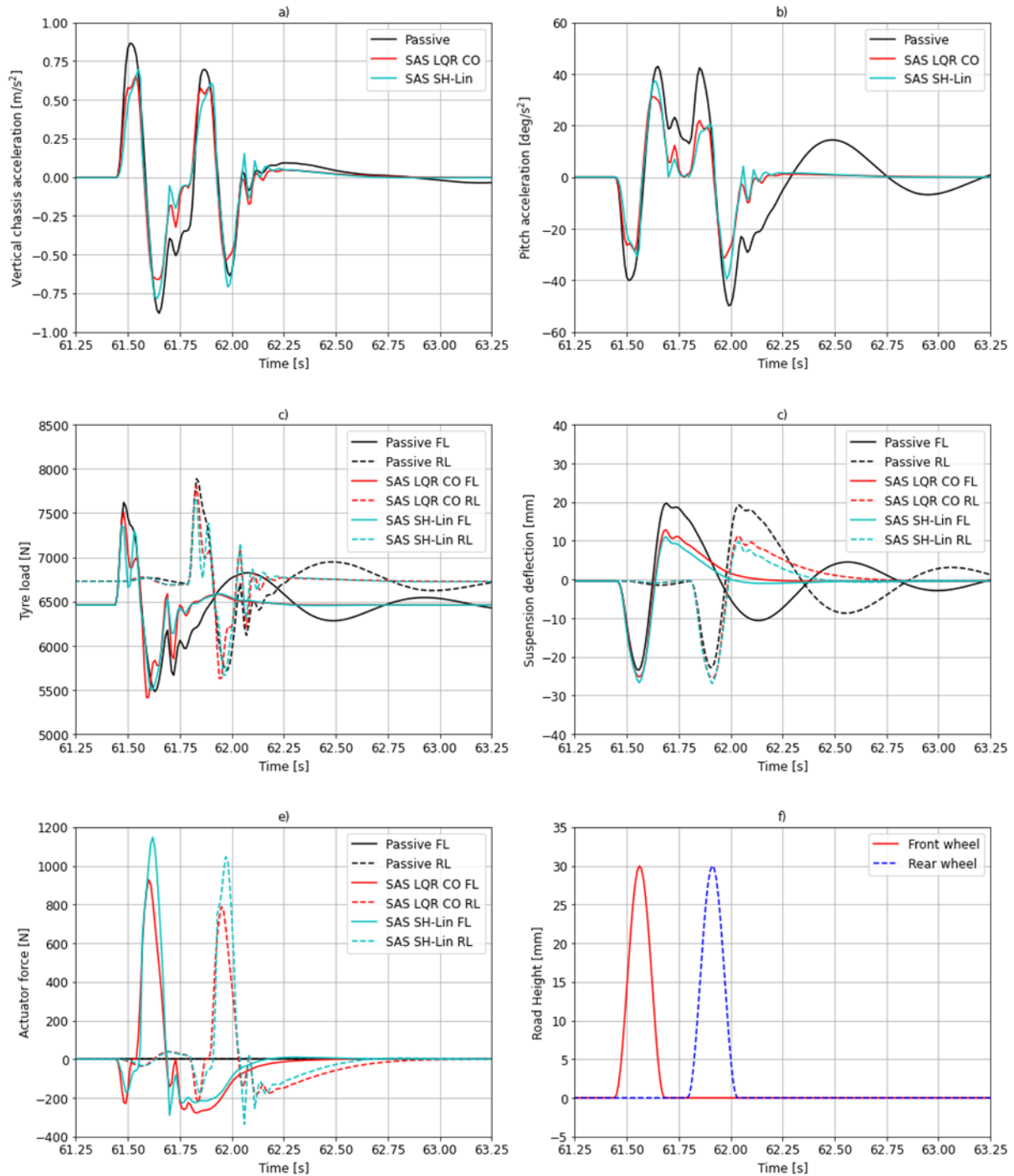
This results indicate that LQR is slightly superior to ROC controller for the particular excitation frequency. Note that the results may differ depending on the frequency of the bump excitation (defined by the combination of vehicle speed and bump length) and the amplitude of the bump, which is illustrated in the next procedure.

**Table 6. KPI comparison of fully-active suspension controllers and passive suspension for *sine bump* excitation**

| KPI [unit]   | Configuration         |                       |                       |                       |                               |                               |                              |
|--|-----------------------|-----------------------|-----------------------|-----------------------|-------------------------------|-------------------------------|------------------------------|
|  | Passive               | FAS LQR Handling      | FAS LQR Balanced      | FAS LQR Comfort       | FAS ROC <i>E-ABC</i> Handling | FAS ROC <i>E-ABC</i> Balanced | FAS ROC <i>E-ABC</i> Comfort |
| Chassis vertical accel. variance [m <sup>2</sup> /s <sup>4</sup> ] | 0,0369                | 0,0477                | 0,0326                | 0,0207                | 0,0366                        | 0,0380                        | 0,0155                       |
|  | -                     | 29,18%                | -11,76%               | -44,00%               | -0,90%                        | 2,87%                         | -57,97%                      |
| Pitch acceleration variance [° <sup>2</sup> /s <sup>4</sup> ]      | 143,46                | 92,43                 | 67,45                 | 46,35                 | 142,79                        | 149,53                        | 42,75                        |
|  | -                     | -35,57%               | -52,99%               | -67,69%               | -0,47%                        | 4,23%                         | -70,20%                      |
| Tyre deflection variance [m <sup>2</sup> ]                         | 3,93·10 <sup>4</sup>  | 3,66·10 <sup>4</sup>  | 2,64·10 <sup>4</sup>  | 1,87·10 <sup>4</sup>  | 3,86·10 <sup>4</sup>          | 4,05·10 <sup>4</sup>          | 1,94·10 <sup>4</sup>         |
|  | -                     | -6,67%                | -32,86%               | -52,34%               | -1,69%                        | 3,23%                         | -50,55%                      |
| Suspension deflection variance [m <sup>2</sup> ]                   | 2,65·10 <sup>-5</sup> | 1,41·10 <sup>-5</sup> | 1,50·10 <sup>-5</sup> | 1,59·10 <sup>-5</sup> | 2,67·10 <sup>-5</sup>         | 2,66·10 <sup>-5</sup>         | 2,70·10 <sup>-5</sup>        |
|  | -                     | -46,71%               | -43,64%               | -40,14%               | 0,65%                         | 0,14%                         | 1,54%                        |

The comfort-oriented SAS LQR and SAS *SH-Lin* controller's time responses are shown in Figure 21. The vertical chassis acceleration and chassis pitch acceleration are again decreased in amplitude and stabilization time compared to the passive suspension. Both SAS configurations improve the attenuation of tyre load and suspension deflection by a similar amount. As these controllers do not feature road preview and react to disturbances, they cannot significantly reduce the first disturbance peak (*jounce*), but the second peak amplitude (*rebound*) in terms of suspension deflection is significantly reduced.

The FAS LQR gives slightly improved performance compared to SAS LQR in terms of all analysed metrics. The FAS ROC clearly dampens chassis vertical acceleration and chassis pitch acceleration better than the *SH-Linear* controller, while also providing comparable tyre deflection, but it does not provide significant suspension deflection attenuation as the *SH-Linear* controller.



**Figure 21. Time responses of comfort-oriented semi-active suspension controllers and passive suspension for sine bump road excitation**

Improvements in all KPIs compared to passive suspension are noticeable for both SAS controllers (up to 67%), with a few exceptions occurring for the chassis vertical acceleration and the handling setup of the SAS LQR, which degraded only by 9,95%. Another exception is a marginal degradation of the tyre deflection variance KPI for the handling setup of the SAS SH-Lin controller. In other controller setups, the SAS LQR provides more consistent ride comfort improvements, but lacks in handling improvement in its handling setup, in comparison to the SAS LQR. The SAS ROC provides passenger comfort and handling improvements in its comfort setup, and the SAS SH-Lin in its comfort setup giving comparable improvements.

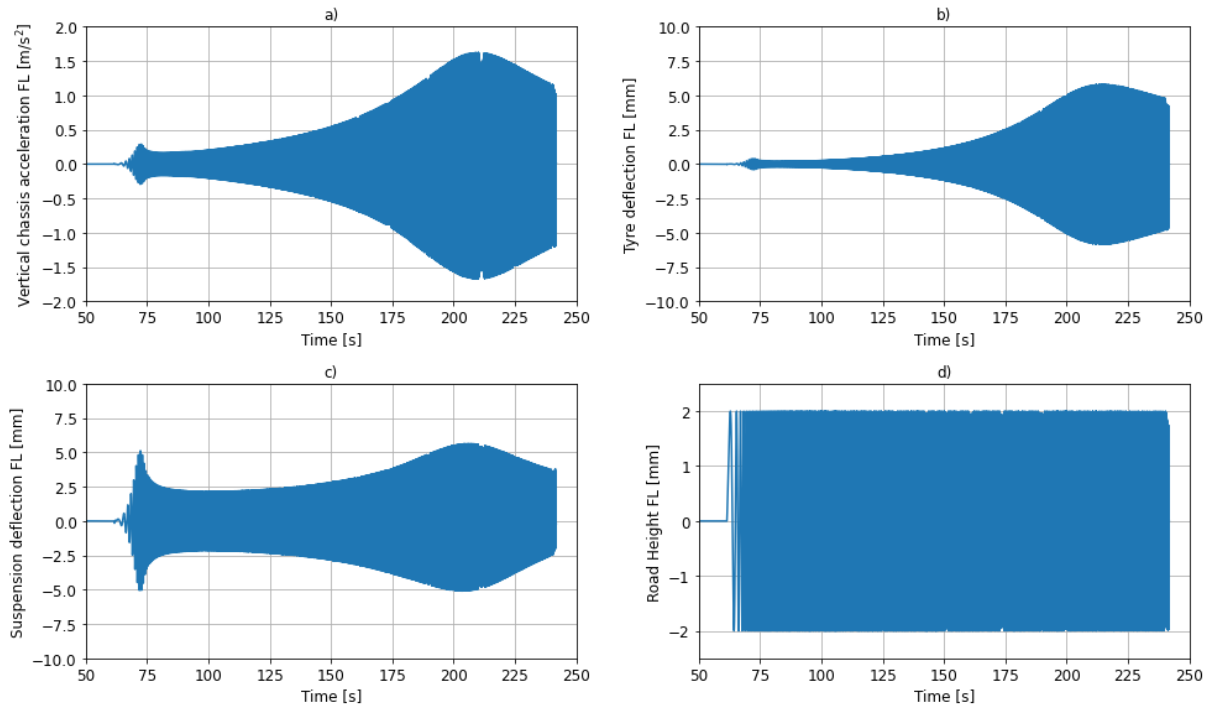
**Table 7. KPI comparison of semi-active suspension controllers and passive suspension for *sine bump* procedure**

| KPI [unit]   | Configuration        |                      |                      |                      |                                 |                                |                              |
|--|----------------------|----------------------|----------------------|----------------------|---------------------------------|--------------------------------|------------------------------|
|  | Passive              | SAS LQR Handling     | SAS LQR Balanced     | SAS LQR Comfort      | SAS SH-Linear ( $\alpha=0,25$ ) | SAS SH-Linear ( $\alpha=0,5$ ) | SAS SH-Linear ( $\alpha=1$ ) |
| Chassis vertical accel. variance [ $\text{m}^2/\text{s}^4$ ] | 0,0369               | 0,0406               | 0,0300               | 0,0230               | 0,0190                          | 0,0242                         | 0,0369                       |
|  | -                    | 9,95%                | -18,84%              | -37,58%              | -48,53%                         | -34,51%                        | -0,10%                       |
| Pitch acceleration variance [ $\text{°}^2/\text{s}^4$ ]      | 143,46               | 81,27                | 61,13                | 48,31                | 47,44                           | 53,33                          | 77,48                        |
|  | -                    | -43,35%              | -57,39%              | -66,32%              | -66,93%                         | -62,83%                        | -45,99%                      |
| Tyre deflection variance [ $\text{m}^2$ ]                    | $3,93 \cdot 10^4$    | $3,40 \cdot 10^4$    | $2,62 \cdot 10^4$    | $2,20 \cdot 10^4$    | $1,57 \cdot 10^4$               | $2,00 \cdot 10^4$              | $4,08 \cdot 10^4$            |
|  | -                    | -13,38%              | -33,24%              | -43,86%              | -60,03%                         | -49,05%                        | 3,82%                        |
| Suspension deflection variance [ $\text{m}^2$ ]              | $2,65 \cdot 10^{-5}$ | $1,40 \cdot 10^{-5}$ | $1,47 \cdot 10^{-5}$ | $1,57 \cdot 10^{-5}$ | $1,72 \cdot 10^{-5}$            | $1,45 \cdot 10^{-5}$           | $1,35 \cdot 10^{-5}$         |
|  | -                    | -47,40%              | -44,56%              | -40,83%              | -35,05%                         | -45,44%                        | -49,19%                      |

### 7.1.2. Sine sweep

To evaluate the vehicle response in the ride frequency range, which encompasses the sprung and unsprung mass natural frequencies, a *sine sweep* test procedure is carried out and the KPIs (presented in Subchapter 4.1) are calculated for a vertical road excitation from 0,1 to 20 Hz. This procedure was also used to tune the controller by optimizing the gains in its feedback loop (Chapter 4) – where the excitation was used on a two degree-of-freedom model.

Figure 22 shows the road excitation (d) and vehicle time responses (a - c) for a passive suspension vehicle corner. As the frequency increases, it is clearly visible that the response resonates at certain excitation frequencies – which are the sprung and unsprung mass natural frequencies, occurring at around 70 s and 210 s, respectively.



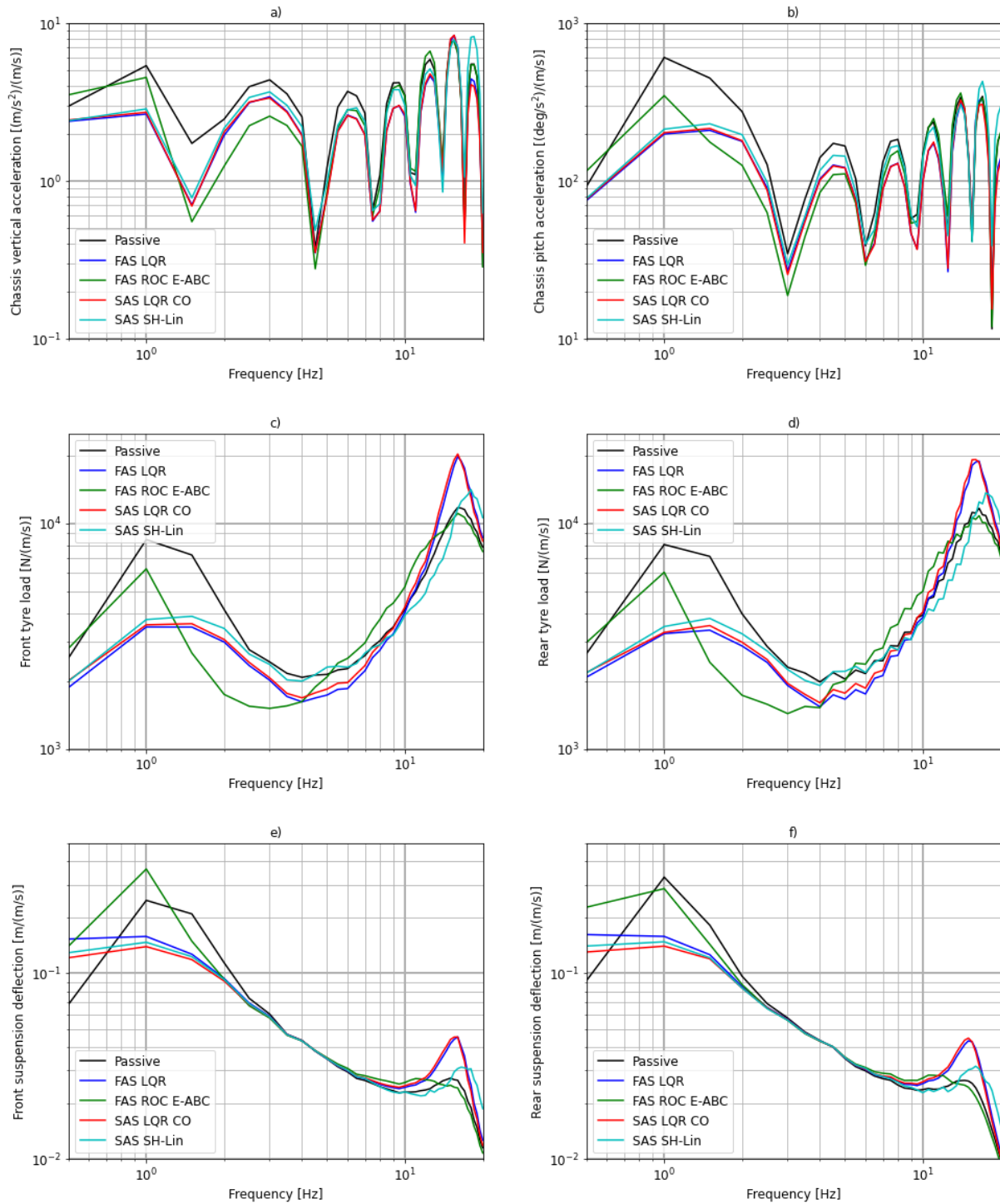
**Figure 22. Vehicle response (a, b, c) in time domain for a passive suspension in a *sine sweep* (d) test procedure**

The comfort-oriented active and semi-active suspension controller's frequency responses are shown in Figure 23. To calculate a smooth frequency response, the test procedure features a stepped increase in frequency (increasing by 0.5 Hz). The amplification for every discrete step is calculated on a 3 s window after a 3 s stabilization interval per frequency.

FAS LQR and FAS ROC provide improved attenuation of chassis accelerations (Figure 23 a and b) in low- and mid-frequency range (up to 10 Hz). These configurations also improve road holding (Figure 23 c and d). However, unlike FAS LQR, reduced-order controller FAS ROC barely attenuates tyre load at low frequencies (below sprung mass natural frequency). Similarly, FAS ROC has higher amplitude of suspension deflection at sprung mass natural frequency. At the unsprung mass natural frequency (around 15 Hz), the FAS LQR has increased peak tyre load and suspension deflection amplitude compared to passive suspension while the FAS ROC is comparable, and slightly better than passive suspension. This indicates that LQR may perform better when the road irregularity frequency is closer to sprung mass natural frequency, while ROC controller may be better at unsprung mass natural frequency.

The SAS controllers tuned for comfort show a consistently better response for chassis acceleration and tyre load in low- and mid-frequency ranges, compared to a passive suspension (Figure 23), with the SAS LQR being comparable to FAS LQR. For high-frequency road irregularities, the unsprung mass resonant peaks for the tyre load and suspension deflection amplification characteristic are larger for both the SAS LQR and SAS *SH-Lin* controller compared to a passive suspension and the FAS ROC.





**Figure 23. Frequency response amplification of comfort-oriented fully-active and semi-active suspension controllers and passive suspension**

The KPIs shown in Table 8 correspond to the *sine sweep* procedure. Since these KPIs comprise vehicle response over the entire considered frequency range (0,1 – 20 Hz), the observations may lead to different conclusion than those obtained from Figure 23. For example, the practical FAS ROC in comfort configuration does not provide any passenger comfort improvement in aggregate KPI due to larger amplifications of vertical chassis acceleration and chassis pitch acceleration at high-frequency excitation. However, as it is shown in Figure 23, this configuration improves ride comfort in the low- and mid-range frequencies which are most important for passenger comfort (Figure 1). The KPIs also show an improvement in tyre and



suspension deflection for the FAS ROC controller setup, illustrated in Figure 23. The KPIs in terms of the FAS LQR controller on the other hand, show clearly that the comfort setup resulted in consistent comfort improvement by up to 20%, combined with an increase of tyre and suspension deflection by up to 90%. The handling setup of the FAS LQR resulted in small handling KPI and mechanical limitation improvement (up to 2,4% and 7,9%), with accompanying negligible deterioration of ride comfort.

**Table 8. KPI comparison of fully-active suspension controllers and passive suspension for *sine sweep* excitation**

| KPI [unit]  | Configuration          |                        |                        |                        |                               |                               |                              |
|---|------------------------|------------------------|------------------------|------------------------|-------------------------------|-------------------------------|------------------------------|
|   | Passive                | FAS LQR Handling       | FAS LQR Balanced       | FAS LQR Comfort        | FAS ROC <i>E-ABC</i> Handling | FAS ROC <i>E-ABC</i> Balanced | FAS ROC <i>E-ABC</i> Comfort |
| Chassis vert. accel. variance [m <sup>2</sup> /s <sup>4</sup> ] | 0,1976                 | 0,2033                 | 0,1818                 | 0,1582                 | 0,1941                        | 0,1980                        | 0,2003                       |
|   | -                      | 2,92%                  | -7,96%                 | -19,92%                | -1,73%                        | 0,24%                         | 1,36%                        |
| Pitch accel. variance [° <sup>2</sup> /s <sup>4</sup> ]         | 432,15                 | 440,26                 | 397,83                 | 357,40                 | 425,08                        | 433,33                        | 441,07                       |
|   | -                      | 1,88%                  | -7,94%                 | -17,30%                | -1,64%                        | 0,27%                         | 2,06%                        |
| Tyre deflection variance [m <sup>2</sup> ]                      | 4,5 · 10 <sup>-6</sup> | 4,4 · 10 <sup>-6</sup> | 6,0 · 10 <sup>-6</sup> | 8,5 · 10 <sup>-6</sup> | 4,8 · 10 <sup>-6</sup>        | 4,5 · 10 <sup>-6</sup>        | 4,4 · 10 <sup>-6</sup>       |
|   | -                      | -2,42%                 | 33,38%                 | 89,56%                 | 6,95%                         | -0,58%                        | -2,74%                       |
| Susp. deflection variance [m <sup>2</sup> ]                     | 5,7 · 10 <sup>-6</sup> | 5,4 · 10 <sup>-6</sup> | 7,0 · 10 <sup>-6</sup> | 9,6 · 10 <sup>-6</sup> | 6,1 · 10 <sup>-6</sup>        | 5,7 · 10 <sup>-6</sup>        | 5,6 · 10 <sup>-6</sup>       |
|   | -                      | -5,90%                 | 22,75%                 | 67,32%                 | 6,22%                         | -0,32%                        | -2,03%                       |

The comfort setup of the SAS LQR provides the expected improvement in passenger comfort, with a deterioration of handling and suspension deflection KPIs (Table 9). The setups more directed towards handling provide a smaller improvement of comfort in terms of vertical chassis acceleration and pitch acceleration variance, while the deterioration of tyre and suspension deflection is of a lesser degree.

The SAS *SH-Lin* implementation results with gradually deteriorating overall vehicle response with a reduction of the tuning factor  $\alpha$ , which is contrary to the explanation given in literature [2] with respect to comfort. For the  $\alpha = 0,25$  semi-active practical controller setup, at high-frequency excitation, the vehicle response largely deteriorates causing worse KPIs value. The semi-active practical controller setup with  $\alpha = 0,5$  offers good comfort improvement in low- and mid-frequency ranges, as shown in Figure 23.

In its comfort setup, the SAS LQR follows the trend set by the FAS LQR, providing improved attenuation of chassis accelerations in combination with deterioration of tyre and suspension deflection variances. The FAS LQR trend is followed closely by the SAS LQR in the handling setup as well. The KPIs do not show an improvement for the FAS ROC in the handling or

balanced setup, while the SAS *SH-Linear* controller shows significant attenuation of tyre and suspension deflection in its handling setup (up to 55,5% and 40,8%), accompanied by passenger comfort deterioration by up to 56,3%.

**Table 9. KPI comparison of semi-active suspension controllers and passive suspension for *sine sweep* excitation**

| KPI [unit]  | Configuration       |                     |                     |                     |  |                                       |                                     |
|---|---------------------|---------------------|---------------------|---------------------|--|---------------------------------------|-------------------------------------|
|   | Passive             | SAS LQR Handling    | SAS LQR Balanced    | SAS LQR Comfort     | SAS <i>SH-Linear</i> ( $\alpha=0,25$ ) | SAS <i>SH-Linear</i> ( $\alpha=0,5$ ) | SAS <i>SH-Linear</i> ( $\alpha=1$ ) |
| Chassis vert. accel. variance [ $\text{m}^2/\text{s}^4$ ] | 0,1976              | 0,1967              | 0,1748              | 0,1514              | 0,7646                                 | 0,2730                                | 0,3089                              |
|   | -                   | -0,45%              | -11,53%             | -23,36%             | 287,01%                                | 38,16%                                | 56,34%                              |
| Pitch accel. variance [ $^\circ^2/\text{s}^4$ ]           | 432,15              | 427,48              | 386,13              | 349,26              | 1098,62                                | 594,38                                | 649,77                              |
|   | -                   | -1,08%              | -10,65%             | -19,18%             | 154,22%                                | 37,54%                                | 50,36%                              |
| Tyre deflection variance [ $\text{m}^2$ ]                 | $4,5 \cdot 10^{-6}$ | $4,6 \cdot 10^{-6}$ | $6,2 \cdot 10^{-6}$ | $8,7 \cdot 10^{-6}$ | $2,1 \cdot 10^{-6}$                    | $5,7 \cdot 10^{-6}$                   | $2,0 \cdot 10^{-6}$                 |
|   | -                   | 2,48%               | 38,45%              | 93,65%              | 356,69%                                | 26,67%                                | -55,54%                             |
| Susp. deflection variance [ $\text{m}^2$ ]                | $5,7 \cdot 10^{-6}$ | $5,5 \cdot 10^{-6}$ | $7,1 \cdot 10^{-6}$ | $9,6 \cdot 10^{-6}$ | $8,1 \cdot 10^{-5}$                    | $7,5 \cdot 10^{-6}$                   | $3,4 \cdot 10^{-6}$                 |
|   | -                   | -4,54%              | 23,92%              | 67,60%              | 1309,21%                               | 30,65%                                | -40,76%                             |

## 7.2. Lateral dynamics test procedures

In this subsection, the potential for performance improvement in terms of lateral dynamics is explored for the aforementioned controller designs. It presents the comparison of vehicle response for practical controllers (designed as presented in Chapters 4 and 5) versus optimal controllers and a passive suspension for the *lane change* and *Hockenheim short* lap time simulation lateral test procedures. The handling procedures are evaluated with the following KPIs: the maximum chassis roll angle and rear axle slip angle for the *lane change* procedure, and the full set of metrics defined in Subchapter 4.1, including chassis roll and pitch acceleration and the lap time for the *Hockenheim short* test procedure.

The comparisons given in Figures correspond to handling setups (Table 4). For the *SH-Linear* controller, the handling setup corresponds to the tuning parameter set to  $\alpha = 1$ .

### 7.2.1. Lane change with road roughness (ISO 3888-1)

The *lane change* procedure, illustrated in Figure 24, is a standard lateral test procedure as defined in ISO 3888-1 [32]. It primarily provides the information on vehicle stability and lateral chassis response while the driver tries to follow the predefined path at a certain entry speed, set to 100 km/h here.

A similar lateral test procedure – the *moose test* (ISO 3888-2) features a tighter layout in comparison to the *lane change* ISO 3888-1, with the goal of passing the track at a high-as-possible entry speed without braking, touching any cones or rolling over. This takes the stability test to an extreme and is an effective way of picking out vehicles which are unstable in this type of evasive manoeuvre [33].

The *VSM* internal *curvature controlled* driver model calculates the steering wheel angle based on a PI controller using lateral acceleration tracking error as a feedback. The lateral acceleration tracking error is defined by subtracting the demand lateral acceleration based on track curvature and the current vehicle lateral acceleration, and is used as the steering controller input:

$$a_{Y,err} = c \cdot v^2 - \dot{\gamma} \cdot v \quad (7.1)$$

where  $a_{Y,err}$  is the lateral acceleration error, the first term on the left-hand side is the reference lateral acceleration obtained from track curvature  $c$  and chassis speed  $v$ , and the second term on the right-hand side is measured lateral acceleration obtained as a product of chassis speed  $v$  and yaw rate  $\dot{\gamma}$ .

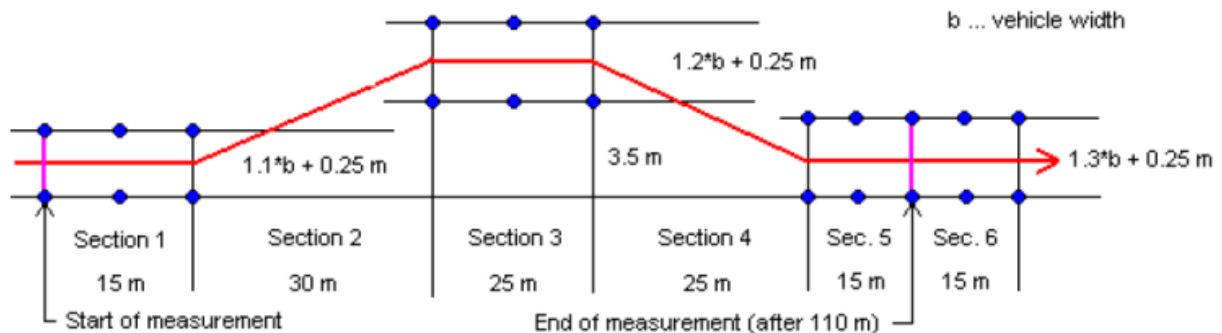
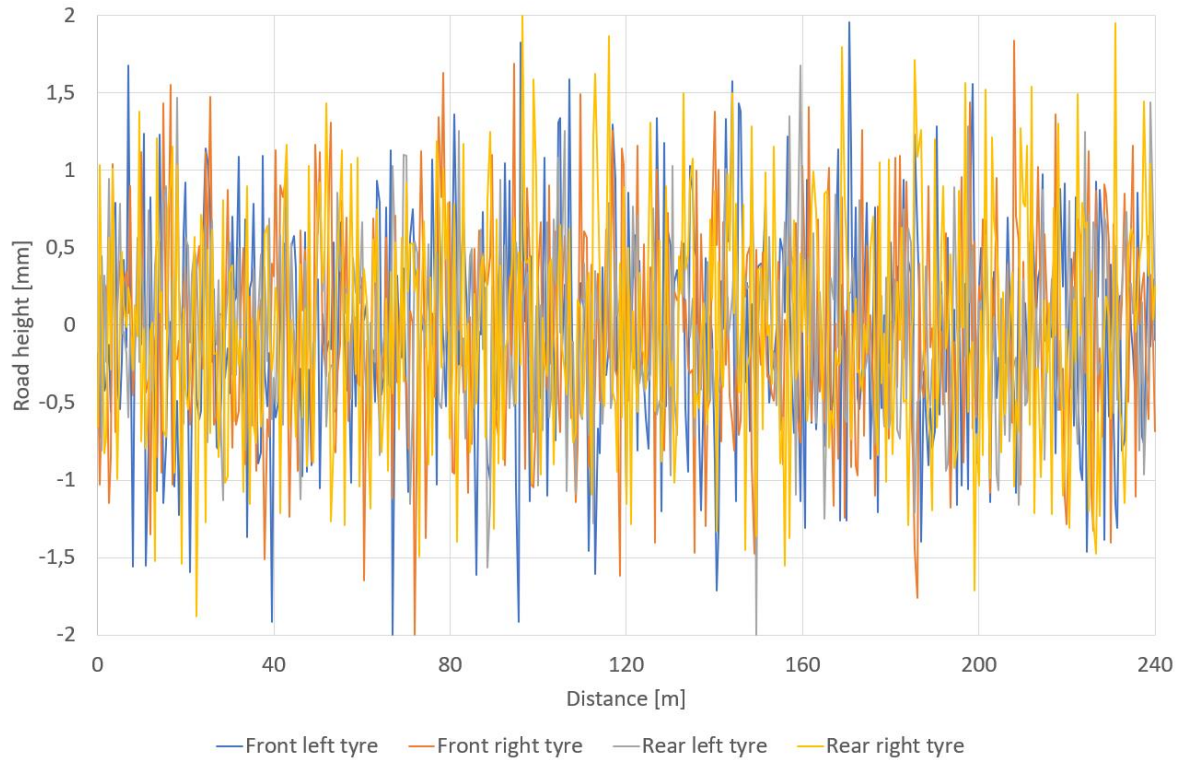


Figure 24. Lane change ISO 3888-1 test stage layout [30]

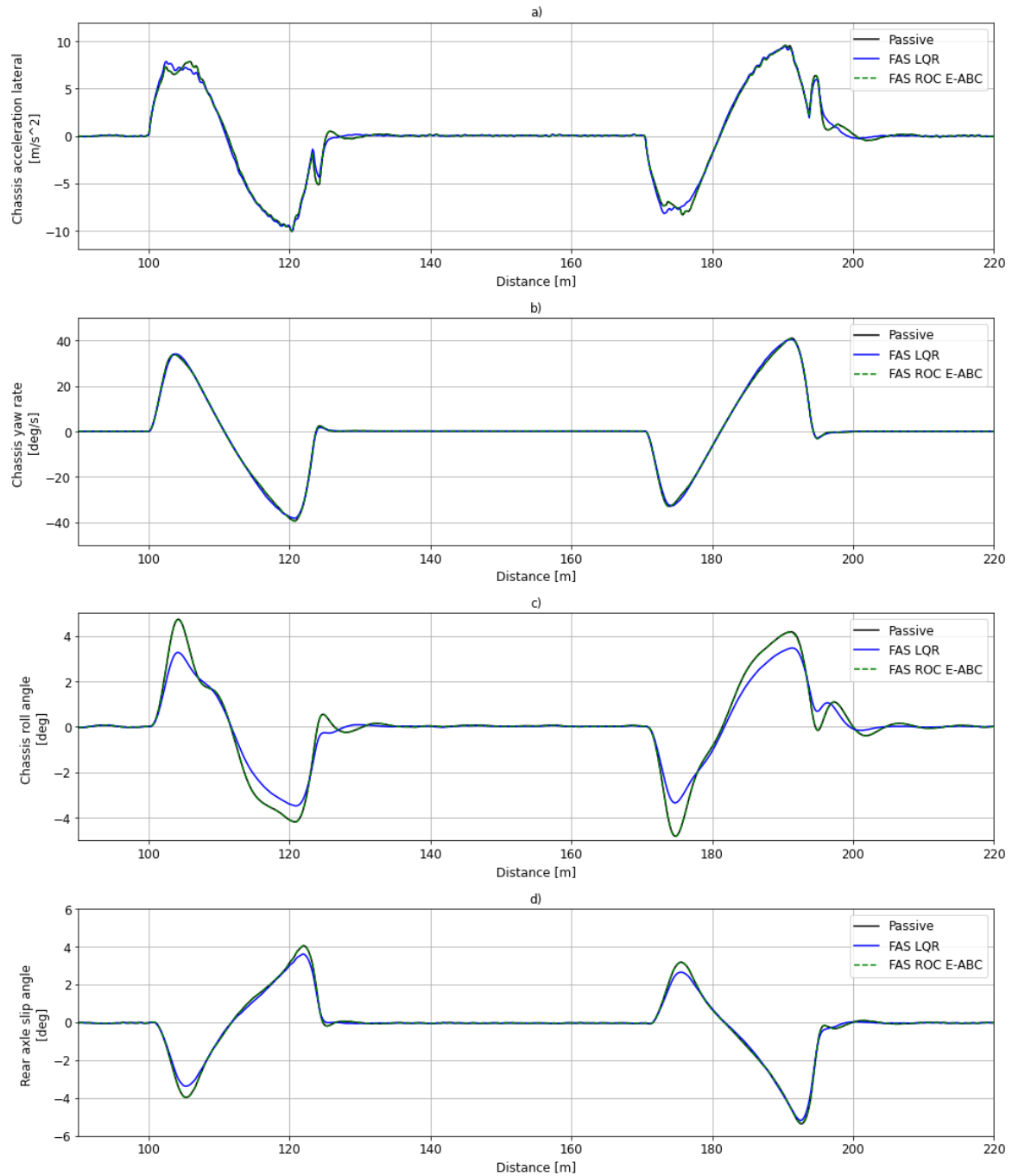
The track parametrization includes stochastic vertical road irregularities shown in Figure 25, of 2 mm maximum amplitude with normal distribution, which approximates the texture of a smooth test track.



**Figure 25. Lane change ISO 3888-1 test stage layout**

The maximum chassis roll angle and rear axle slip angle are used to compare the vehicle stability for different controller configurations. Excessive roll angle indicates a roll-over risk, especially in the case of coming onto a lateral obstacle while negotiating a significant curvature. A high rear axle slip angle can be translated as unresponsiveness of the vehicle regarding handling, as the tyres deform to a large amount due to contact patch lateral forces.

The FAS LQR and FAS ROC performance for the *lane change* procedure is compared in time domain in Figure 26. There is a noticeable reduction in roll angle and rear axle slip angle for the FAS LQR. On the other hand, the FAS ROC implementation does not provide any improvement of lateral dynamics performance as it results with identical performance as the passive suspension.



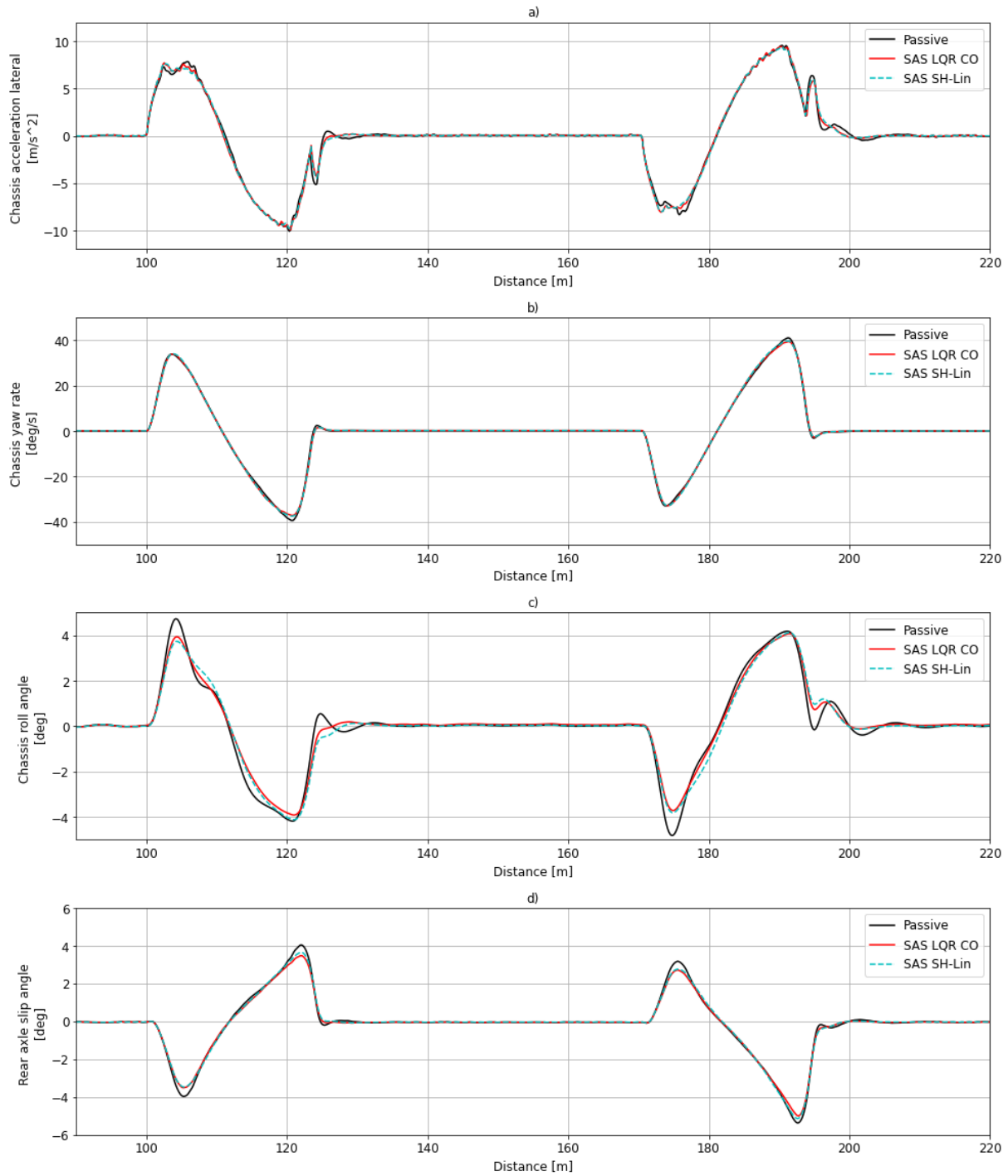
**Figure 26. Time responses of handling-oriented fully-active controllers and passive suspension for lane change procedure**

Comparing the other fully-active controller setups in terms of KPIs achieved for the *lane change* test procedure in Table 10, it is concluded that the FAS ROC provides no improvement for any controller setup. On the other hand, the FAS LQR provides a significant decrease in maximum chassis roll angle (up to 28%), which is the largest improvement for the handling-oriented setup. On the other hand, the maximum rear axle slip angle is decreased only slightly for all FAS LQR setups (up to 3,5%).

**Table 10. KPI comparison of fully-active suspension controllers and passive suspension for *lane change* procedure**

| KPI [unit]                       | Configuration |                  |                  |                 |                               |                               |                              |
|----------------------------------|---------------|------------------|------------------|-----------------|-------------------------------|-------------------------------|------------------------------|
|                                  | Passive       | FAS LQR Handling | FAS LQR Balanced | FAS LQR Comfort | FAS ROC <i>E-ABC</i> Handling | FAS ROC <i>E-ABC</i> Balanced | FAS ROC <i>E-ABC</i> Comfort |
| Maximum roll angle [°]           | 4,81          | 3,48             | 3,74             | 4,04            | 4,82                          | 4,82                          | 4,77                         |
|                                  | -             | -27,75%          | -22,33%          | -16,14%         | 0,14%                         | 0,13%                         | -0,93%                       |
| Maximum rear axle slip angle [°] | 5,37          | 5,18             | 5,20             | 5,21            | 5,33                          | 5,34                          | 5,02                         |
|                                  | -             | -3,46%           | -3,17%           | -2,95%          | -0,69%                        | -0,55%                        | -6,53%                       |

The lateral vehicle response that resulted by the application of the SAS LQR and SAS *SH-Lin* controller in the *lane change* procedure is shown in Figure 27. Both controllers result with a noticeable improvement in terms of maximum chassis roll angle and rear axle slip angle, similarly to FAS LQR. The SAS LQR results with slightly better response than the SAS *SH-Lin* controller in terms of both considered metrics.



**Figure 27. Time responses of handling-oriented semi-active controllers and passive suspension for *lane change* procedure**

The *KPIs* calculated for the SAS controllers for the *lane change* test procedure are presented in Table 11. Generally, all SAS controller setups provide improvements in terms of all *KPIs*. The handling setups provide better lateral stability by reducing the maximum chassis roll angle by 15,3% for the handling setup of the SAS LQR, in comparison with the comfort setup which reduces the maximum chassis roll angle by 14,4%. On the other hand, the SAS *SH-Lin* controller reduces the maximum chassis roll angle by 14,5% in its handling setup – which is comparable to the same setup for the optimal FAS LQR controller.

The rear axle slip angle is reduced by around 7% for all SAS LQR setups, with negligible difference between setups. The SAS *SH-Lin* controller in its handling configuration reduces the maximum rear axle slip angle by 4,4% in its handling setup, which is slightly better than its comfort setup ( $\alpha = 0,25$ ) which reduces it by 3,1%.

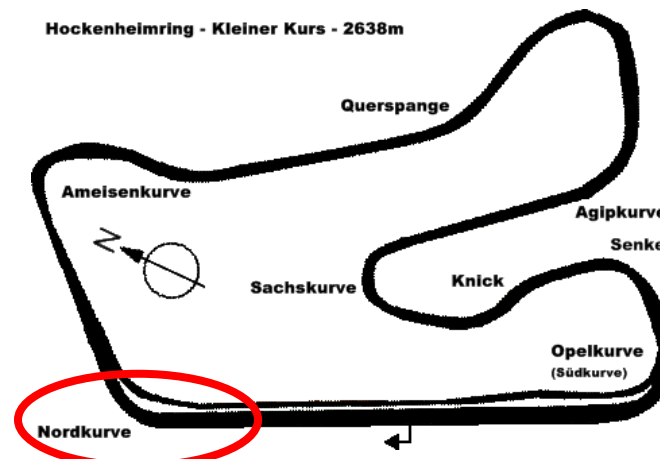
This comparative analysis proved that an active suspension primarily designed and optimized for vertical dynamics metrics, can also provide improvements in lateral dynamics aspects.

**Table 11. KPI comparison of semi-active suspension controllers and passive suspension for lane change procedure**

| KPI [unit]                       | Configuration |                  |                  |                 |  |                                       |                                     |
|----------------------------------|---------------|------------------|------------------|-----------------|--|---------------------------------------|-------------------------------------|
|                                  | Passive       | SAS LQR Handling | SAS LQR Balanced | SAS LQR Comfort | SAS <i>SH-Linear</i> ( $\alpha=0,25$ ) | SAS <i>SH-Linear</i> ( $\alpha=0,5$ ) | SAS <i>SH-Linear</i> ( $\alpha=1$ ) |
| Maximum roll angle [°]           | 4,81          | 4,08             | 4,10             | 4,12            | 4,36                                   | 4,16                                  | 4,12                                |
|                                  | -             | -15,33%          | -14,92%          | -14,35%         | -9,54%                                 | -13,65%                               | -14,50%                             |
| Maximum rear axle slip angle [°] | 5,37          | 4,99             | 5,00             | 4,99            | 5,20                                   | 5,17                                  | 5,13                                |
|                                  | -             | -6,95%           | -6,88%           | -7,05%          | -3,11%                                 | -3,71%                                | -4,35%                              |

### 7.2.2. Hockenheim short lap time simulation with road roughness

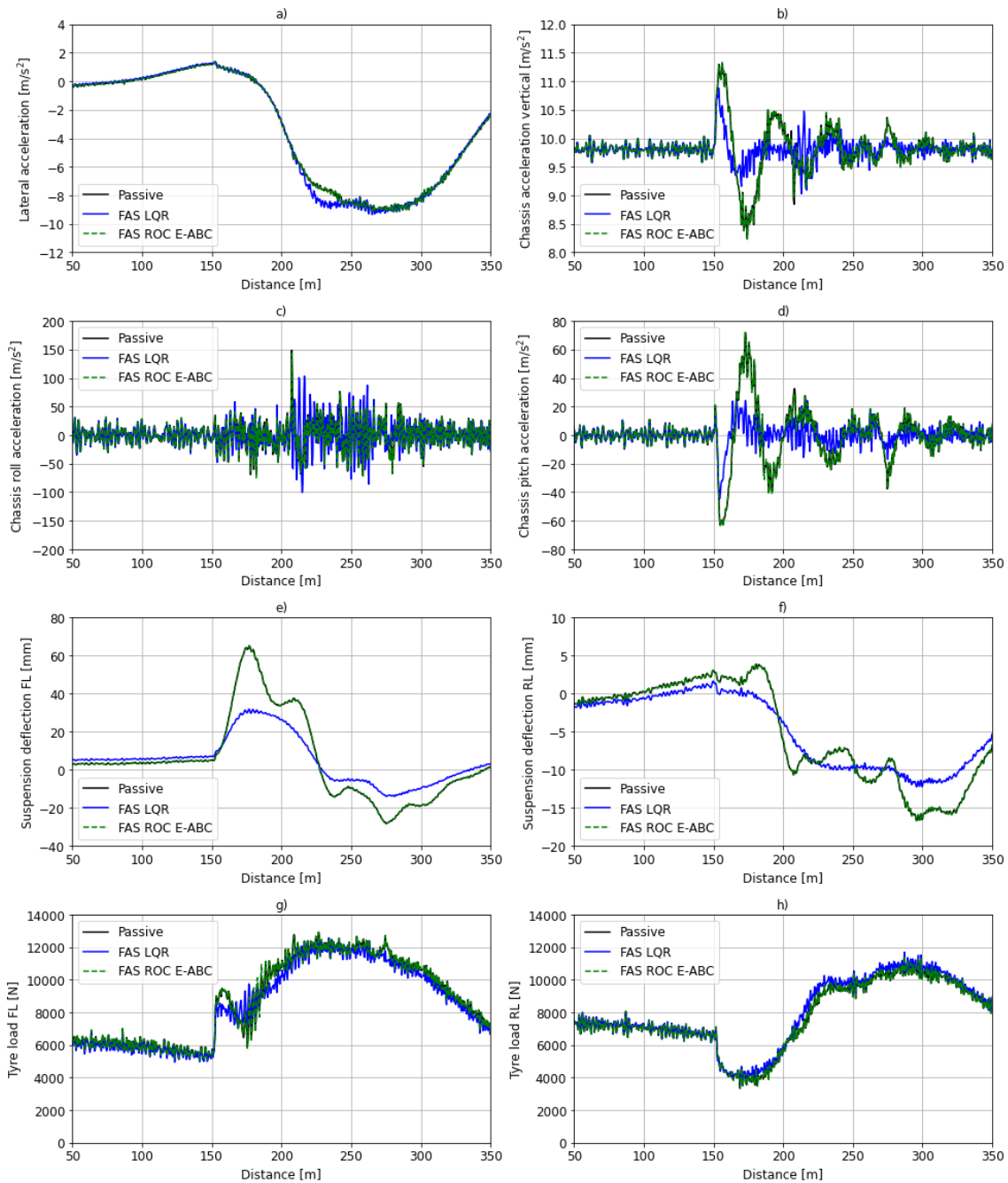
The goal of the lap time simulation comparative analysis conducted on the *Hockenheim short* track (Figure 28) is to explore whether implementing vertical dynamics controllers on a full vehicle model results in perceived performance improvement in a racetrack lap time simulation scenario. The metrics used to compare different controllers are: achieved lap time, KPIs related to passenger comfort (vertical chassis acceleration, chassis pitch and roll acceleration variances), road holding (tyre deflection variance) and suspension mechanical limitation (suspension deflection variance). A stochastic road height vertical oscillation (illustrated in Figure 25) is used to approximate the texture of a smooth test track. Using the *VSM curvature controlled* driver model (described in Chapter 7.2.1) the vehicle steering inputs are controlled by a PI regulator in the lap simulation.



**Figure 28. Hockenheim Short track – Analysed track corner in Figures 29 and 30, circled in red**



The FAS controller performance in handling setup is compared in Figure 29 for the first corner of the *Hockenheim Short* lap time simulation – *Nordkurve*. Clearly, the FAS LQR shows improvements in vertical chassis acceleration amplitude and oscillation duration. The suspension deflection is more than halved and there is a noticeable reduction in tyre load initial peak after the braking point at 150 m distance. The peak longitudinal and lateral accelerations are equal, which indicates that the FAS LQR only provides improvement in transient events. In the *lane change* test procedure, the FAS ROC does not provide improvements in vehicle handling characteristics, which is reflected here as well, as its response follows the passive suspension closely. This may be explained by the fact that both of these controllers react to changes in suspension state variables, which occur here primarily due to load shifting upon braking or cornering.



**Figure 29. Time responses of handling-oriented fully-active suspension controllers and passive suspension for *Hockenheim short* lap time simulation**

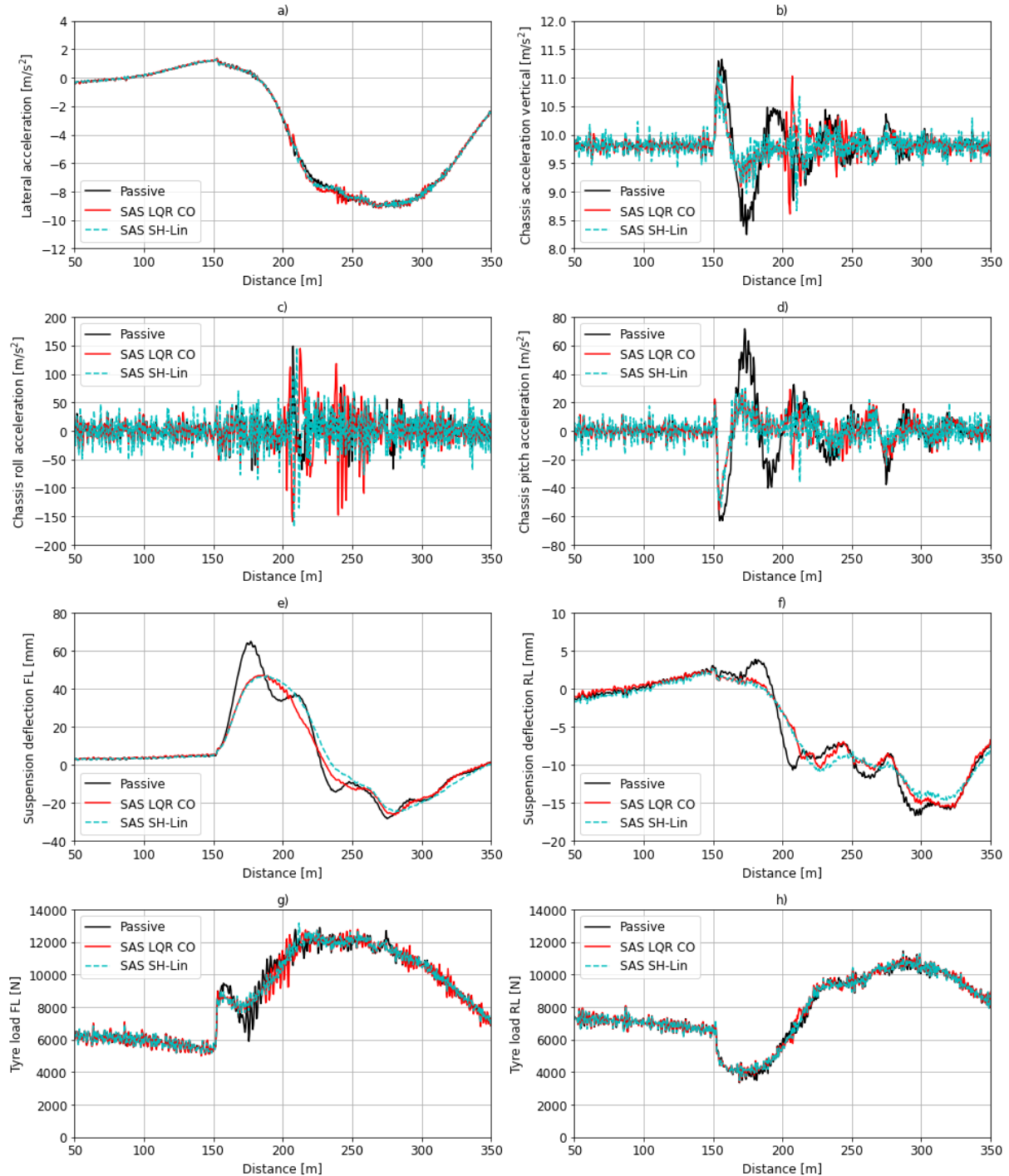
The KPIs calculated for the *Hockenheim short* lap time simulation show that the lap time is slightly improved for the FAS LQR. The best result is accomplished by using its handling configuration, with a lap time improvement of 0,12% in comparison with the passive suspension. It is interesting that for this setup the comfort is improved as well – which is reflected in chassis vertical acceleration reduction by 65,1% and chassis pitch acceleration reduction by 70,5%. The suspension deflection variance is improved as well by 53,2%. On the other hand, the FAS ROC does not provide a lap time improvement in any configuration. Significant improvements in terms of passenger comfort are achieved for the FAS ROC in its comfort configuration, for which the chassis vertical acceleration is reduced by 38,3% and the chassis pitch acceleration by 43,1%. The comfort-oriented setup of the FAS LQR results with significant oscillations of chassis vertical acceleration and roll acceleration, which leads to large variances in terms of passenger comfort.

**Table 12. KPI comparison of fully-active suspension controllers and passive suspension for *Hockenheim short* lap time procedure**

| KPI [unit]  | Configuration         |                       |                       |                       |                               |                               |                              |
|---|-----------------------|-----------------------|-----------------------|-----------------------|-------------------------------|-------------------------------|------------------------------|
|   | Passive               | FAS LQR Handling      | FAS LQR Balanced      | FAS LQR Comfort       | FAS ROC <i>E-ABC</i> Handling | FAS ROC <i>E-ABC</i> Balanced | FAS ROC <i>E-ABC</i> Comfort |
| Lap time [s]  | 75,04                 | 74,95                 | 74,98                 | 75,02                 | 75,04                         | 75,04                         | 75,04                        |
|   | -                     | -0,12%                | -0,08%                | -0,03%                | 0,00%                         | 0,00%                         | 0,00%                        |
| Chassis vert. accel. variance [m <sup>2</sup> /s <sup>4</sup> ] | 0,0578                | 0,0202                | 0,0249                | 0,1219                | 0,0580                        | 0,0592                        | 0,0357                       |
|   | -                     | -65,08%               | -56,93%               | 110,88%               | 0,41%                         | 2,50%                         | -38,30%                      |
| Pitch accel. variance [° <sup>2</sup> /s <sup>4</sup> ]         | 105,51                | 31,12                 | 35,39                 | 85,64                 | 105,44                        | 108,34                        | 59,97                        |
|   | -                     | -70,50%               | -66,46%               | -18,84%               | -0,07%                        | 2,68%                         | -43,16%                      |
| Roll accel. variance [° <sup>2</sup> /s <sup>4</sup> ]          | 461,82                | 463,15                | 525,78                | 1386,13               | 474,89                        | 465,16                        | 387,88                       |
|   | -                     | 0,29%                 | 13,85%                | 200,15%               | 2,83%                         | 0,72%                         | -16,01%                      |
| Tyre deflection variance [m <sup>2</sup> ]                      | 8,97·10 <sup>6</sup>  | 8,91·10 <sup>6</sup>  | 8,95·10 <sup>6</sup>  | 9,42·10 <sup>6</sup>  | 8,97·10 <sup>6</sup>          | 8,96·10 <sup>6</sup>          | 8,97·10 <sup>6</sup>         |
|   | -                     | -0,64%                | -0,21%                | 5,09%                 | 0,02%                         | -0,05%                        | 0,07%                        |
| Suspension deflection variance [m <sup>2</sup> ]                | 1,38·10 <sup>-3</sup> | 6,47·10 <sup>-4</sup> | 8,46·10 <sup>-4</sup> | 1,19·10 <sup>-3</sup> | 1,39·10 <sup>-3</sup>         | 1,38·10 <sup>-3</sup>         | 1,41·10 <sup>-3</sup>        |
|   | -                     | -53,23%               | -38,79%               | -14,10%               | 0,72%                         | 0,10%                         | 1,70%                        |

Figure 30 shows a vehicle response comparison of SAS controllers in their handling setups for the *Hockenheim Short* lap time simulation. Both controllers provide a decrease in vertical

chassis acceleration amplitude after the braking point (at 150 m distance) and a quicker stabilization. Suspension deflection amplitude is reduced in the application of both SAS controllers as well, along with the tyre load initial peak. The SAS *SH-Lin* controller reduces the amplitude of tyre load oscillations throughout the cornering manoeuvre, compared to both passive suspension and SAS LQR.



**Figure 30. Time responses of handling-oriented semi-active suspension controllers and passive suspension for Hockenheim short lap time simulation**

By comparing the KPIs given in Table 13, we can conclude that none of the analysed SAS controllers provide a lap time improvement in this *Hockenheim Short* lap time simulation comparison with the passive suspension, mainly due to unimproved tyre deflection KPI. All

SAS LQR setups provide significant comfort improvement in terms of reduced chassis vertical acceleration and chassis pitch acceleration (~50%), while deteriorating the chassis roll acceleration by a small amount (~20%). The SAS *SH-Linear* controller gives a similar response as the SAS LQR, but results with smaller improvements in vertical and pitch acceleration (~45%) and deteriorates the roll acceleration by a larger value (37,3%). Other SAS *SH-Linear* controller setups provide deterioration of most KPIs. Similarly to the comfort setup FAS LQR, the SAS *SH-Linear* controller with  $\alpha = 0,25$  results with large oscillations of chassis vertical acceleration and roll acceleration, which causes deterioration of passenger comfort metrics.

**Table 13. KPI comparison of semi-active suspension controllers and passive suspension for a *Hockenheim* short lap time procedure**

| KPI [unit]  | Configuration        |                      |                      |                      |  |                                       |                                     |
|---|----------------------|----------------------|----------------------|----------------------|--|---------------------------------------|-------------------------------------|
|   | Passive              | SAS LQR Handling     | SAS LQR Balanced     | SAS LQR Comfort      | SAS <i>SH-Linear</i> ( $\alpha=0,25$ ) | SAS <i>SH-Linear</i> ( $\alpha=0,5$ ) | SAS <i>SH-Linear</i> ( $\alpha=1$ ) |
| Lap time [s]  | 75,04                | 75,03                | 75,03                | 75,03                | 75,05                                  | 75,05                                 | 75,04                               |
|   | -                    | -0,01%               | -0,01%               | -0,01%               | 0,01%                                  | 0,01%                                 | 0,00%                               |
| Chassis vert. accel. variance [m <sup>2</sup> /s <sup>4</sup> ] | 0,0578               | 0,0319               | 0,0306               | 0,0300               | 0,1280                                 | 0,0675                                | 0,0313                              |
|   | -                    | -44,84%              | -46,99%              | -48,04%              | 121,49%                                | 16,83%                                | -45,75%                             |
| Pitch accel. variance [° <sup>2</sup> /s <sup>4</sup> ]         | 105,51               | 49,10                | 47,20                | 44,27                | 94,51                                  | 71,37                                 | 58,64                               |
|   | -                    | -53,47%              | -55,26%              | -58,04%              | -10,43%                                | -32,36%                               | -44,42%                             |
| Roll accel. variance [° <sup>2</sup> /s <sup>4</sup> ]          | 461,82               | 580,61               | 543,35               | 557,39               | 1987,39                                | 954,17                                | 634,21                              |
|   | -                    | 25,72%               | 17,65%               | 20,69%               | 330,34%                                | 106,61%                               | 37,33%                              |
| Tyre deflection variance [m <sup>2</sup> ]                      | $8,97 \cdot 10^6$    | $8,96 \cdot 10^6$    | $8,96 \cdot 10^6$    | $8,99 \cdot 10^6$    | $9,64 \cdot 10^6$                      | $9,13 \cdot 10^6$                     | $8,95 \cdot 10^6$                   |
|   | -                    | -0,07%               | -0,06%               | 0,27%                | 7,51%                                  | 1,84%                                 | -0,18%                              |
| Susp. deflection variance [m <sup>2</sup> ]                     | $1,38 \cdot 10^{-3}$ | $1,23 \cdot 10^{-3}$ | $1,24 \cdot 10^{-3}$ | $1,28 \cdot 10^{-3}$ | $1,39 \cdot 10^{-3}$                   | $1,38 \cdot 10^{-3}$                  | $1,32 \cdot 10^{-3}$                |
|   | -                    | -10,89%              | -10,34%              | -7,28%               | 0,17%                                  | -0,49%                                | -4,63%                              |

### 7.3. Robustness analysis

The active suspension controller performance is primarily defined by its design and actuator dynamics, but other effects influence its performance – such as disturbances in terms of vehicle loading change, noise and offset in measurement signals, etc. The controller must be sufficiently robust with respect to these uncertainties to meet the design requirements.

The co-simulation environment described in Chapter 6.1 is used to run a full vehicle simulation model (Chapter 6.2) in a *sine sweep* procedure (Chapter 7.1.2). This robustness analysis is carried out for the FAS ROC *E-Active Body Control* controller, for which the design was presented in Chapter 4. The controller is set to its comfort setup.

### 7.3.1. Actuator dynamics

In this subsection, the actuator dynamics aspects which are most influential on controller performance are varied and these include actuator lag time constant and actuator force gradient. The performance is compared in terms of key performance indices defined in Chapter 2.

#### 7.3.1.1. Actuator lag time constant

The actuator force response is modelled as a first order lag (Equation 6.2). The time constant is calculated from the actuator bandwidth. For a low bandwidth, the actuator force response changes slowly which means that the controller cannot react in a prompt manner to high frequency force demand.

As shown in Table 14, decreasing the actuator bandwidth results with increased comfort KPI values (worse comfort) and lower tyre deflection and suspension deflection. As this analysis is carried out using a comfort controller setup, the KPIs which are targeted for improvement generally deteriorate, compared to the infinite bandwidth setup. The FAS ROC *E-ABC* controller with 5 Hz actuator bandwidth results with ~30% deterioration of comfort and a reduction of tyre and suspension deflection by 31% and 25%, compared to an infinite bandwidth case. This improvement in handling and mechanical limitation metrics is expected as the comfort-oriented controller setup generally causes a deterioration of the opposing criteria.

**Table 14. FAS ROC *E-ABC* performance for varying actuator bandwidth**

| KPI<br>[Unit]           | Comfort KPI |  |        |  |        | Handling KPI                                  |         | Mechanical<br>limitation KPI                           |         |
|-------------------------|-------------|--|--------|--|--------|---|---------|--|---------|
|                         |             | Chassis vertical<br>accel. variance<br>[m <sup>2</sup> /s <sup>4</sup> ] |        | Pitch acceleration<br>variance [° <sup>2</sup> /s <sup>4</sup> ] |        | Tyre deflection<br>variance [m <sup>2</sup> ] |         | Suspension<br>deflection variance<br>[m <sup>2</sup> ] |         |
| Actuator bandwidth [Hz] | 3           | 0,2014   | 28,26% | 441,53   | 33,35% | 4,40 · 10 <sup>-6</sup>                       | -30,60% | 5,58 · 10 <sup>-6</sup>                                | -25,57% |
|                         | 5           | 0,2003   | 27,51% | 441,07   | 33,21% | 4,38 · 10 <sup>-6</sup>                       | -30,78% | 5,62 · 10 <sup>-6</sup>                                | -25,08% |
|                         | 8           | 0,1959   | 24,72% | 435,57   | 31,55% | 4,44 · 10 <sup>-6</sup>                       | -29,86% | 5,69 · 10 <sup>-6</sup>                                | -24,13% |
|                         | 10          | 0,1924   | 22,53% | 429,77   | 29,80% | 4,52 · 10 <sup>-6</sup>                       | -28,65% | 5,75 · 10 <sup>-6</sup>                                | -23,23% |
|                         | 12          | 0,1891   | 20,38% | 422,87   | 27,72% | 4,61 · 10 <sup>-6</sup>                       | -27,15% | 5,84 · 10 <sup>-6</sup>                                | -22,15% |
|                         | 15          | 0,1845   | 17,47% | 411,88   | 24,40% | 4,77 · 10 <sup>-6</sup>                       | -24,70% | 5,97 · 10 <sup>-6</sup>                                | -20,36% |
|                         | 20          | 0,1784   | 13,59% | 394,94   | 19,28% | 5,02 · 10 <sup>-6</sup>                       | -20,73% | 6,19 · 10 <sup>-6</sup>                                | -17,41% |
|                         | ∞           | 0,1571   | -      | 331,10   | -      | 6,33 · 10 <sup>-6</sup>                       | -       | 7,50 · 10 <sup>-6</sup>                                | -       |

\* percentile KPI difference calculated with respect to infinite bandwidth

### 7.3.1.2. Actuator force gradient

An influential limiting factor for the actuator force is its maximum force gradient limit. This primarily influences the response to demanded actuator forces of high amplitudes or high frequencies.

The parameter sensitivity analysis is carried out for a *sine sweep* test procedure and the results are presented in Table 15. With a lower actuator force gradient limit, the comfort controller setup provides worse comfort metrics than with an infinite actuator force gradient limit. The passenger comfort only deteriorates by a small amount (~2,5%). On the other hand, improvements are visible in handling and mechanical limitation KPI values (3% and 2,6% respectively). Similarly to the actuator time lag constant sensitivity, this analysis also proved that a comfort-oriented controller with slower actuator dynamics will show deterioration of passenger comfort. The conflicting criteria (which are not prioritized in the controller setup) that would deteriorate at high frequencies if the actuator had faster response, are less affected by a controller with slower actuator dynamics.

**Table 15. FAS ROC E-ABC performance for varying actuator force gradient limit**

| KPI<br>[Unit]                  |    | Comfort KPI  |        |   |        | Handling KPI                               |        | Mechanical limitation KPI                        |        |
|--------------------------------|----|--|--------|---|--------|--|--------|--|--------|
|                                |    | Chassis vertical accel. variance [m <sup>2</sup> /s <sup>4</sup> ] |        | Pitch acceleration variance [° <sup>2</sup> /s <sup>4</sup> ] |        | Tyre deflection variance [m <sup>2</sup> ] |        | Suspension deflection variance [m <sup>2</sup> ] |        |
| Actuator force gradient [kN/s] | 12 | 0,2021   | 2,29%  | 443,29  | 2,58%  | 4,37·10 <sup>-6</sup>                      | -3,07% | 5,58·10 <sup>-6</sup>                            | -2,57% |
|                                | 18 | 0,2019   | 2,22%  | 440,89  | 2,02%  | 4,36·10 <sup>-6</sup>                      | -3,27% | 5,60·10 <sup>-6</sup>                            | -2,35% |
|                                | 24 | 0,2003   | 1,36%  | 441,07  | 2,06%  | 4,38·10 <sup>-6</sup>                      | -2,74% | 5,62·10 <sup>-6</sup>                            | -2,03% |
|                                | 30 | 0,1991   | 0,77%  | 438,20  | 1,40%  | 4,46·10 <sup>-6</sup>                      | -1,06% | 5,67·10 <sup>-6</sup>                            | -1,04% |
|                                | 36 | 0,1972   | -0,19% | 431,50  | -0,15% | 4,60·10 <sup>-6</sup>                      | 2,07%  | 5,79·10 <sup>-6</sup>                            | 1,01%  |
|                                | ∞  | 0,1976   | -      | 432,15  | -      | 4,51·10 <sup>-6</sup>                      | -      | 5,73·10 <sup>-6</sup>                            | -      |

\* percentile KPI difference calculated with respect to infinite force gradient limit

### 7.3.2. Axle load change uncertainty

The vehicle rarely encounters constant vertical load on a certain wheel. This is specially accentuated in the case of loading the trunk with heavy payload and carrying passengers on the rear seats. The sensitivity analysis of the controller to rear axle loading is carried out, while the front axle load is kept equal. The considered SUV BEV vehicle kerb (unladen) mass is 2565 kg. Including a 65 kg driver, the vehicle mass is 2630 kg, 1313 kg of which is distributed onto the rear axle – which is the nominal rear axle load used in this sensitivity analysis. The maximum laden vehicle weight is 3130 kg, which leads to a maximum rear axle load of 1813 kg.

Table 16 shows parameter sensitivity analysis results for the rear axle load change. The increase of rear axle load shows an improvement of comfort in terms of vertical chassis acceleration (up to 30,5% for the maximum vehicle laden weight) in combination with the deterioration of pitch acceleration response (up to only 3,2% for the maximum vehicle laden weight). Due to a small variation of pitch acceleration variance in comparison with the vertical chassis acceleration, it



can be concluded that the comfort KPIs have improved. The handling and mechanical limitation show a negligible improvement in terms of KPI values. The results show a logical trend, as for a passive suspension, the increase in sprung mass causes an increase of suspension damping ratio and consequently improved comfort.

**Table 16. FAS ROC E-ABC performance for varying rear axle load**

| KPI [Unit]          |      | Comfort KPI  |         |   |       | Handling KPI                               |        | Mechanical limitation KPI                        |        |
|---------------------|------|--|---------|---|-------|--|--------|--|--------|
|                     |      | Chassis vertical accel. variance [m <sup>2</sup> /s <sup>4</sup> ] |         | Pitch acceleration variance [° <sup>2</sup> /s <sup>4</sup> ] |       | Tyre deflection variance [m <sup>2</sup> ] |        | Suspension deflection variance [m <sup>2</sup> ] |        |
| Rear axle load [kg] | 1313 | 0,2036   | -       | 431,86  | -     | 4,51·10 <sup>-6</sup>                      | -      | 5,74·10 <sup>-6</sup>                            | -      |
|                     | 1413 | 0,1880   | -7,64%  | 433,04  | 0,27% | 4,51·10 <sup>-6</sup>                      | -0,13% | 5,73·10 <sup>-6</sup>                            | -0,21% |
|                     | 1513 | 0,1743   | -14,39% | 435,21  | 0,78% | 4,50·10 <sup>-6</sup>                      | -0,27% | 5,71·10 <sup>-6</sup>                            | -0,40% |
|                     | 1613 | 0,1621   | -20,38% | 438,14  | 1,45% | 4,50·10 <sup>-6</sup>                      | -0,39% | 5,70·10 <sup>-6</sup>                            | -0,66% |
|                     | 1713 | 0,1512   | -25,73% | 441,68  | 2,27% | 4,49·10 <sup>-6</sup>                      | -0,50% | 5,69·10 <sup>-6</sup>                            | -0,81% |
|                     | 1813 | 0,1414   | -30,54% | 445,57  | 3,17% | 4,49·10 <sup>-6</sup>                      | -0,58% | 5,69·10 <sup>-6</sup>                            | -0,81% |

\* percentile KPI difference calculated with respect to nominal wheel load

### 7.3.3. Measurement noise and offset

Due to imperfections in the road profile, sensor inaccuracies and compliance in the suspension system or chassis, sensors rarely measure smooth signals. This could be the case if the measured signals are adequately discretized, but more accuracy can be achieved by filtering a noisy signal. By evaluating the sensitivity of controller performance on measured signal noise power, sensor requirements in terms of expected noise can be defined – this helps with sensor selection, as the expected noise is declared in the specifications sheet.

With age, sensor measurement signals can “drift” from their nominal position. This is expected and the sensitivity of controller performance on the measurement offset must be evaluated.

The noise and offset are applied to suspension deflection and vertical chassis acceleration measurement signals, while the vertical wheel acceleration is estimated from a combination of the measurement signals (Equation 4.16). The percentile differences in KPIs are calculated in relation to a vehicle response with no noise added to the measurement signals. The noise is added by using a Band-limited white noise source block in *Simulink*<sup>®</sup>, resulting in stochastic noise illustrated in Figure 31. The signal noise is quantified by the defined noise power, which is given as signal noise variance divided by time.

Table 17 presents the sensitivity analysis of the controller performance to measurement signal noise. The suspension deflection noise shows little influence on performance for a noise power of 10<sup>-12</sup>, but a suspension deflection variance increase by 108% for a noise power of 10<sup>-11</sup>. Complete response deterioration occurs for a noise power of 10<sup>-9</sup>, where the comfort and handling KPIs increase significantly as well.

Noise added to sprung mass vertical acceleration measurement signals causes a gradual deterioration of the comfort KPIs, up to ~3% for a noise power of 5·10<sup>-5</sup>. The influence is small for the handling KPI, while the mechanical limitation KPI improves by a similar amount as the comfort KPIs deteriorate.

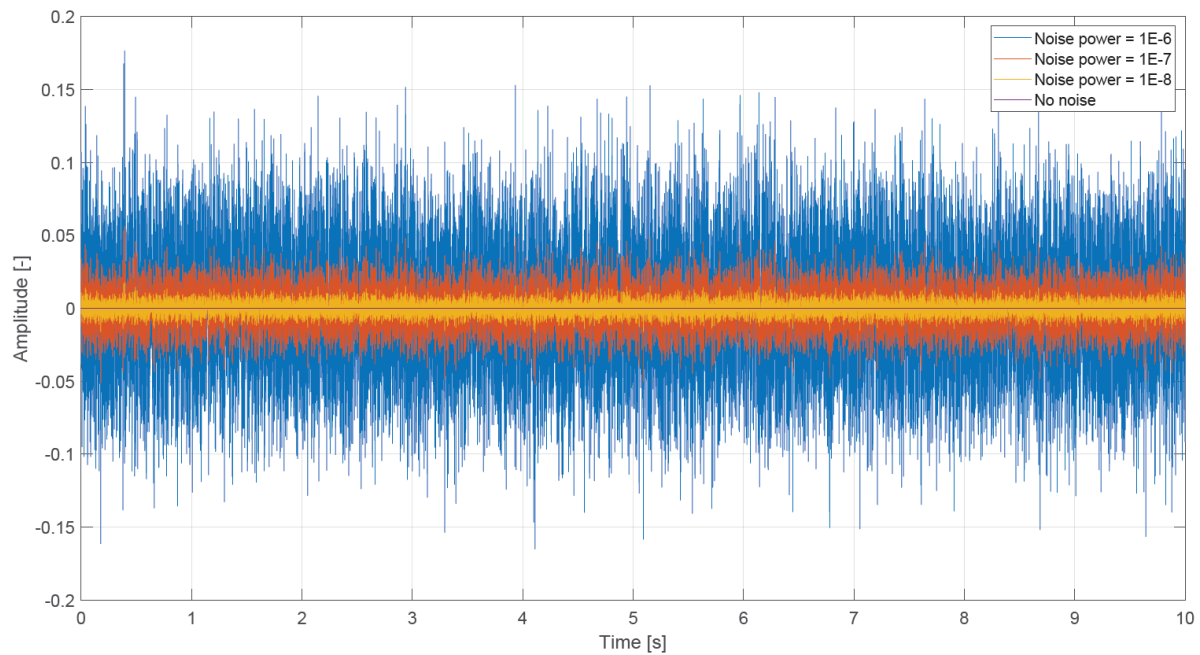


Figure 31. Signal noise in dependence of noise power

Table 17. FAS ROC E-ABC performance for varying measurement signal noise power

| KPI [Unit]  |                      | Comfort KPI  |        |   |       | Handling KPI                               |       | Mechanical limitation KPI  |         |
|---|----------------------|--|--------|---|-------|--|-------|--|---------|
|   |                      | Chassis vertical accel. variance [m <sup>2</sup> /s <sup>4</sup> ] |        | Pitch accel. variance [° <sup>2</sup> /s <sup>4</sup> ] |       | Tyre deflection variance [m <sup>2</sup> ] |       | Chassis vertical accel. variance [m <sup>2</sup> /s <sup>4</sup> ] |         |
| No noise  |                      | 0,2003   | -      | 441,07  | -     | 4,4 · 10 <sup>-6</sup>                     | -     | 5,6 · 10 <sup>-6</sup>   | -       |
| Suspension deflection meas. noise power [m <sup>2</sup> /Hz]                | 10 <sup>-12</sup>    | 0,2063   | 3,00   | 449,94  | 2,01  | 4,3 · 10 <sup>-6</sup>                     | -1,43 | 6,9 · 10 <sup>-6</sup>   | 23,45   |
|   | 10 <sup>-11</sup>    | 0,2070   | 3,36   | 438,43  | -0,60 | 4,5 · 10 <sup>-6</sup>                     | 3,01  | 1,2 · 10 <sup>-6</sup>   | 107,99  |
|   | 10 <sup>-10</sup>    | 0,2006   | 0,18   | 415,83  | -5,72 | 5,7 · 10 <sup>-6</sup>                     | 30,63 | 1,2 · 10 <sup>-6</sup>   | 2037,87 |
|   | 10 <sup>-9</sup>     | 0,5704   | 184,85 | 502,71  | 13,98 | 5,6 · 10 <sup>-6</sup>                     | 26,69 | 7,7 · 10 <sup>-6</sup>   | 1263,45 |
| Acceleration measurement noise power [(m <sup>2</sup> /s <sup>4</sup> )/Hz] | 5 · 10 <sup>-8</sup> | 0,2005   | 0,10   | 441,31  | 0,05  | 4,4 · 10 <sup>-6</sup>                     | 0,01  | 5,6 · 10 <sup>-6</sup>   | 0,03    |
|   | 5 · 10 <sup>-7</sup> | 0,2012   | 0,46   | 442,39  | 0,30  | 4,4 · 10 <sup>-6</sup>                     | 0,01  | 5,6 · 10 <sup>-6</sup>   | 0,19    |
|   | 5 · 10 <sup>-6</sup> | 0,2033   | 1,52   | 446,01  | 1,12  | 4,4 · 10 <sup>-6</sup>                     | -0,11 | 5,7 · 10 <sup>-6</sup>   | 0,63    |
|   | 5 · 10 <sup>-5</sup> | 0,2076   | 3,66   | 454,66  | 3,08  | 4,3 · 10 <sup>-6</sup>                     | -0,86 | 5,8 · 10 <sup>-6</sup>   | 3,15    |

\* percentile KPI difference calculated with respect to no measurement signal noise



The parameter sensitivity analysis in terms of measurement signal offset is presented in Table 18. The offset of suspension displacement signal of up to 0,1 m results with very little influence on controller performance. It's unlikely that signal offsets larger than 0,1 m would ever be encountered. A vertical chassis acceleration measurement signal offset of  $1 \text{ m/s}^2$  provides satisfactory controller performance barely distinguishable from a performance with no offset added. A vertical chassis acceleration measurement signal offset of  $10 \text{ m/s}^2$  causes a mechanical limitation KPI deterioration by 43,91% and handling KPI deterioration by 11,82%. Comfort KPIs vary by a small margin for this case.

For the ROC, the offset does not affect the suspension performance in a significant way. The feedback signal offset causes a change in ride height, due to the actuator providing an additional static force parallel to the suspension spring for given static offset. The change in ride height is dependent on gain magnitude, as well as the measurement signal offset. This scenario can be prevented by implementing high-pass filters, as suggested in [6]. High-pass filtering of signals, for example suspension deflection, may also mitigate the impact of low-frequency excitations such as road undulations, beside mitigating the offsets.

**Table 18. FAS ROC E-ABC performance for varying measurement signal offset**

| KPI [Unit]                             |           | Comfort KPI  |       |   |       | Handling KPI                              |        | Mechanical limitation KPI                       |        |
|--|-----------|--|-------|---|-------|---|--------|---|--------|
|  |           | Chassis vertical accel. variance [ $\text{m}^2/\text{s}^4$ ] |       | Pitch accel. variance [ $^\circ^2/\text{s}^4$ ] |       | Tyre deflection variance [ $\text{m}^2$ ] |        | Suspension deflection variance [ $\text{m}^2$ ] |        |
| No offset                              |           | 0,2172   | -     | 441,82  | -     | $4,3 \cdot 10^{-6}$                       | -      | $5,6 \cdot 10^{-6}$                             | -      |
| Suspension deflection offset [m]       | $10^{-5}$ | 0,2172   | 0,00% | 441,82  | 0,00% | $4,3 \cdot 10^{-6}$                       | 0,00%  | $5,6 \cdot 10^{-6}$                             | 0,00%  |
|  | $10^{-4}$ | 0,2172   | 0,00% | 441,82  | 0,00% | $4,3 \cdot 10^{-6}$                       | 0,00%  | $5,6 \cdot 10^{-6}$                             | 0,00%  |
|  | $10^{-3}$ | 0,2172   | 0,00% | 441,82  | 0,00% | $4,3 \cdot 10^{-6}$                       | 0,00%  | $5,6 \cdot 10^{-6}$                             | 0,00%  |
|  | $10^{-2}$ | 0,2172   | 0,00% | 441,82  | 0,00% | $4,3 \cdot 10^{-6}$                       | 0,00%  | $5,6 \cdot 10^{-6}$                             | 0,00%  |
|  | $10^{-1}$ | 0,2172   | 0,00% | 441,82  | 0,00% | $4,3 \cdot 10^{-6}$                       | 0,00%  | $5,6 \cdot 10^{-6}$                             | 0,00%  |
| Accel. meas. offset [ $\text{m/s}^2$ ] | $10^{-2}$ | 0,2172   | 0,00% | 441,83  | 0,00% | $4,3 \cdot 10^{-6}$                       | 0,00%  | $5,6 \cdot 10^{-6}$                             | 0,00%  |
|  | $10^{-1}$ | 0,2172   | 0,01% | 441,88  | 0,01% | $4,3 \cdot 10^{-6}$                       | -0,01% | $5,6 \cdot 10^{-6}$                             | 0,00%  |
|  | 10        | 0,2142   | 0,06% | 442,40  | 0,13% | $4,3 \cdot 10^{-6}$                       | -0,07% | $5,6 \cdot 10^{-6}$                             | 0,04%  |
|  | $10^1$    | 0,2172   | 0,35% | 448,11  | 1,42% | $4,3 \cdot 10^{-6}$                       | -1,78% | $6,5 \cdot 10^{-6}$                             | 15,69% |

\* percentile KPI difference calculated with respect to no measurement signal offset

## 8. CONCLUSION

This thesis presented the design of optimal and practical fully-active and semi-active suspension controllers and their implementation within an advanced simulation environment. The design of active suspension control systems is based on the quarter vehicle model. The optimal, linear quadratic regulator of a fully-active suspension (FAS LQR) serves as a benchmark for a reduced order controller (FAS ROC), which relies on easily measurable signals. A practical *Skyhook-Linear* logic is used as a base for a semi-active practical suspension controller (SAS *SH-Lin*) design, an alternative to a clipped-optimal linear quadratic regulator (SAS LQR).

A controller feedback gain optimization procedure is presented and carried out for three characteristic setups: handling-oriented, balanced and comfort-oriented. The optimization is based on a gradient-free linear constrained optimization method (*COBYLA*).

The performance of the designed practical controllers is compared to optimal controllers and a passive suspension in a full vehicle simulation environment for two vertical dynamics test procedures and two handling test procedures. In the *sine bump* test procedure both practical controller designs result in performance improvements in their comfort setup, which is comparable to optimal controllers. The fully-active suspension controller consistently performs better by 4% to 10% than the semi-practical active controller in terms of comfort and road-holding. *Sine sweep* frequency responses showed significantly improved ride comfort and road holding performance of the FAS-ROC from 1,5 Hz to 5 Hz, but due to the relatively low actuator bandwidth (5 Hz), its performance improves only slightly in the mid- to high-frequency range, compared to the passive suspension. The SAS *SH-Lin* shows improved comfort KPIs up to high-frequency range compared to passive suspension, which are still slightly worse than the FAS ROC. However, SAS *SH-Lin* did provide consistent tyre deflection attenuation throughout the analysed frequency range, which is not the case for any other controller. Both practical controllers resonate with significantly lower amplifications at the unsprung mass resonant frequency, compared to the optimal controllers.

In the *lane change* test procedure, the FAS and SAS LQR showed significant improvements in maximum roll angle and rear axle slip angle – the FAS LQR aiding more to stability and the SAS LQR more to handling performance. The FAS ROC did not result with improved stability or handling performance, while the SAS *SH-Lin* exhibited improvements comparable to the SAS LQR in their handling setups. In the *Hockenheim short* lap time simulations, a noticeable improvement of 0,1 s in lap time was achieved only by the FAS LQR in its handling setup. Both SAS and FAS LQR in their handling setups significantly improved comfort and suspension deflection KPIs, while only slightly improving handling KPI values. Handling-oriented practical controller setups were not effective in this procedure, as only the SAS *SH-Lin* results in comfort improvement. The full vehicle simulation takeaway is that suspension controller design and tuning purely based on a quarter car model shows great potential in terms of vertical dynamics, noticeable improvements in standard lateral procedures such as the *lane change* in terms of chassis stability, but they are ineffective in terms of lap time improvement.

The FAS ROC robustness analysis showed that actuator dynamics limitations gradually degrade the controller performance. Lower actuator bandwidth or force gradient limit results with worse passenger comfort for a controller in its comfort setup. When considering the parameter disturbance case of increased rear axle load, the improved passenger comfort, which holds for a passive suspension as well, is due to the decrease in damping ratio. The robustness with respect to noise power of measurement signals up to  $10^{-12} \text{ m}^2/\text{Hz}$  in terms of suspension deflection measurement and up to  $5 \cdot 10^{-6} (\text{m}^2/\text{s}^4)/\text{Hz}$  in terms of vertical acceleration

measurement has been verified. Offset of suspension deflection measurement signals does not affect the controller performance in a significant way, and on the other hand, “drift” of vertical chassis acceleration measurement signals over  $1\text{ m/s}^2$  can cause controller performance deterioration. This is of course highly-dependent on the controller gains.

Since negligible improvements of handling performance were achieved by the implementation of a quarter-car model-based fully-active suspension controller which controls vehicle suspension corners individually, future work may be directed towards designing a coupled FAS controller using a full vehicle model. Such controller may also include lateral and longitudinal load transfer compensation, or feedforward terms targeted for improved cornering or braking performance. Alternatively, vertical dynamics control may be integrated with lateral dynamics control in a centralized chassis controller. These control systems can easily be implemented and verified in an advanced simulation environment, as illustrated in this thesis.

Beside using constant vehicle setups, an adaptive control scheme should be developed to improve robustness with respect to parameter changes or to actively change the performance in cornering and straight driving. For example, an approach to online adaptive control is presented in [4] where the Lyapunov stability principle is applied to tune the optimal controller online.

The optimization procedure presented in this thesis may be improved by including the suspension stiffness and damping into the optimization parameter set. Besides using the *COBYLA* algorithm [26], the overall optimization problem could be solved with alternative algorithms, such as global optimization or genetic algorithm-based optimization [3].

Finally, road preview could be implemented into the simulation environment to achieve an ultimate fully-active suspension control system, using the model predictive control approach or LQR-based road preview control approach.

## REFERENCES

- [1] Mastinu, G., & Ploechl, M.: Road and Off-Road Vehicle System Dynamics Handbook, CRC Press, 2014.
- [2] Savaresi, S., Poussot-Vassal, C., Spelta, C., Sename, O., Dugard, L.: Semi-Active Suspension Control Design for Vehicles. Semi-Active Suspension Control Design for Vehicles, 2010.
- [3] Cvok, I.: Design and comparative analysis of vertical vehicle dynamics control systems based on active and semi-active suspension, FSB Zagreb, 2018.
- [4] Esmailzadeh, E., Fahimi, F.: Optimal Adaptive Active Suspensions for a Full Car Model, Vehicle System Dynamics 27(2):89-107, 1997.
- [5] BMW of Freeport: How Does BMW Adaptive Suspension Work?, 2017., access date: 18.06.2021., <https://www.bmwoffreeport.com/blogs/827/how-does-bmw-adaptive-suspension-work/>
- [6] Arat, M., Taheri, S., Holweg, E.: Road Profile Estimation for Active Suspension Applications, SAE International Journal of Passenger Cars - Mechanical Systems 8(2):492-500, 2015.
- [7] Theunissen, J.: Regionless Explicit Model Predictive Control of Active Suspension Systems With Preview, IEEE Transactions on Industrial Electronics 67(6):4877-4888, 2020.
- [8] Tseng, H.E., Hrovat, D.: State of the art survey: active and semi-active suspension control, Vehicle System Dynamics 53(7):1-29, 2015.
- [9] F1 Technical: Williams FW14B Renault, access date: 03.06.2021., <https://www.f1technical.net/f1db/cars/729/williams-fw14b>
- [10] Wikipedia: Active Body Control, access date: 05.06.2021., [https://en.wikipedia.org/wiki/Active\\_Body\\_Control](https://en.wikipedia.org/wiki/Active_Body_Control)
- [11] Bascombe, K.: The Definitive Guide To The Mercedes-Benz AIRMATIC Suspension System, FCP euro, 2019., access date: 06.06.2021., <https://blog.fcpeuro.com/the-definitive-guide-to-the-mercedes-benz-airmatic-suspension-system>
- [12] Honda Manual: Adaptive Damper System Description - Components, access date: 08.06.2021., <https://hondamanual.org/products/6316>
- [13] Smith, M., Hoult, W., Brezas, P.: McLaren 720S semi-active suspension, SAE, 2018., access date: 10.06.2021., <https://www.sae.org/news/2018/07/mclaren-720s-semi-active-suspension>
- [14] Sherman, D.: McLaren Proactive Chassis Control, Car and Driver, 2011., access date: 10.06.2021., <https://www.caranddriver.com/features/a15123918/the-anti-anti-roll-bar-tennecos-kinetic-suspension-explained-feature/>
- [15] Wikipedia: MagneRide, access date: 10.06.2021., <https://en.wikipedia.org/wiki/MagneRide>
- [16] Mangal, S., Ashwani K.: Experimental and Numerical Studies of Magnetorheological (MR) Damper, Chinese journal of engineering 2014(1):1-7, 2014.

- [17] Soliman, A.M.A., Kaldas, M.M.S.: Semi-active suspension systems from research to mass-market – A review, *Journal of Low Frequency Noise, Vibration & Active Control* 40(2): 1005-1023, 2019.
- [18] Adcock, I.: Audi details new A8 active suspension, SAE, 2017., access date: 12.06.2021., <https://www.sae.org/news/2017/07/audi-details-new-a8-active-suspension>
- [19] Audi Magazine: Audi A8 – Active chassis, access date: 12.06.2021., <http://audi-magazine.otterbach.de/magazine/5/cars/44-more-personal-comfort.html>
- [20] Cytrynski, S., Neerpasch, U., Bellmann, R.: The Active Suspension of the New Mercedes-Benz GLE, *ATZ Worldwide*, 2018.
- [21] Gohrle, C., Schindler, A., Wagner, A., Sawodny, O.: Road Profile Estimation and Preview Control For Low-Bandwidth Active Suspension Systems, *IEEE/ASME Transactions - Mechatronics* 20(5):2299-2310, 2015.
- [22] Giua, A., Melas, M., Seatzu, C.: Design of a predictive semi-active suspension system, *Vehicle System Dynamics* April(4):277-300 , 2004.
- [23] Castrillo, J.L., Gastón, E., Reyero, M.: Application of fuzzy logic control to the design of semi-active suspension systems, *Proceedings of the sixth IEEE* 2(1):987-993, 1997.
- [24] Wikipedia: Linear quadratic regulator, access date: 02.06.2021., [https://en.wikipedia.org/wiki/Linear%E2%80%93quadratic\\_regulator](https://en.wikipedia.org/wiki/Linear%E2%80%93quadratic_regulator)
- [25] SciPy documentation: `scipy.integrate.odeint`, access date: 21.05.2021., <https://docs.scipy.org/doc/scipy/reference/generated/scipy.integrate.odeint.html>
- [26] SciPy documentation: `scipy.optimize.minimize`, access date: 23.05.2021., <https://docs.scipy.org/doc/scipy/reference/generated/scipy.optimize.minimize.html#scipy.optimize.minimize>
- [27] Heiing, B., Ersoy, M.: Chassis Handbook: Fundamentals, Driving Dynamics, Components, Mechatronics, Perspectives, Springer, 2011.
- [28] Causemann, P.: *Moderne Schwingungsdmpfung*, ATZ, 2003.
- [29] Qin, Z., Mitsunaka I.: Chaotic vibration of a nonlinear full-vehicle model, *International Journal of Solids and Structures*, Volume 43(3):747-759, 2006.
- [30] AVL List GmbH: *AVL VSM 4 User's Guide*, 2018.
- [31] Wikipedia: Nyquist frequency, access date: 28.06.2021., [https://en.wikipedia.org/wiki/Nyquist\\_frequency](https://en.wikipedia.org/wiki/Nyquist_frequency)
- [32] ISO: Test track for a severe lane-change manoeuvre, 2018., access date: 18.06.2021., <https://www.iso.org/standard/67973.html>
- [33] Constant, C.: The moose test (or VDA test), *Car-Engineer*, access date: 15.06.2021., <https://www.car-engineer.com/the-moose-test-or-vda-test/>

## **APPENDIX**

### **I. CD-R**